Study on molecular mechanisms and morphological characteristics of collective cancer cell invasion

がん細胞の集団浸潤における分子機構と形態学的特徴に関する研究

Yuji Kumagai

September 2022

Doctoral Dissertation

Division of Soft Matter
Graduate School of Life Science
Hokkaido University

Table of Contents

Chapter 1

General Introduction

1-1. Cancer

Cancer, a disease in which cells grow uncontrollably and spread to other parts of the body, is a leading cause of death worldwide [1]. American Cancer Society estimated 19.3 million new cases and 10 million cancer deaths worldwide in 2020 [2]. In Japan, cancer accounted for 27.6% of deaths in 2020 and is most common cause of death since 1981 [3]. There are various causes of death from cancer. Respiratory failure due to destruction of lung tissue, excessive calcium levels in the blood due to bone metastasis, and embolisms due to cancer cells clogging blood vessels in the brain, heart, and lungs [1] [4]. There are several other symptoms, and multiple organ failure also causes death [4]. Survival rates for cancer patients differ greatly depending on the stage of the disease at diagnosis [1] . According to the Japanese Association of Clinical Cancer Center (https://www.zengankyo.ncc.go.jp/etc/), the five-year survival rate for lung cancer patients diagnosed between 2009 and 2013 is 84.5% for stage I, 51.6% for stage II, 25.0% for stage III, and 6.5% for stage IV. Thus, survival rates are greatly reduced in stage IV not only for lung cancer but also for other cancers. In most cancers, the definition of stage IV is whether distant metastasis has occurred. Therefore, the approach to reduce deaths from cancer is to (1) detect cancer before the stage progresses (2) prevent cancer from metastasizing. Here I focused on (2) an approach to prevent cancer metastasis.

1-1-2. Cancer Metastasis

Metastasis, in which cancer cells translocate to distant organs away from the primary tumor, is an important cause of cancer-related deaths [5]. In early stages, the cancer is often cured by surgical procedures because the cancer is localized. On the other hand, in stage IV, the cancer has spread throughout the body, therefore, the effectiveness of surgical procedures is limited. This is directly related to the low survival rate in stage IV. Thus, it is very important to prevent the cancer from progressing to stage IV, or in other words, to prevent the cancer from distant metastasis.

There are two main ways to form metastatic tumor: (1) Angiogenesis (2) Invasion [5-7]. Both are important for metastasis; only one can cause metastasis, or both occur simultaneously in metastasis. (1) Angiogenesis is known to be induced by growth factors such as VEGF and FGF, secreted by cancer cells and cancer-associated fibroblasts (CAF). Growth factors promote neovascularization toward tumor mass by stimulating endothelial cell proliferation and migration [8-10]. Intratumor cancer cells are limited in the nutrients and oxygen that they receive by the tumor size and the accumulation of surrounding extracellular matrices [11, 12]. However, neovascularization contributes to cancer growth by solving these problems [13]. Furthermore, neovessels provide not only nutrients for the tumor to grow but also an escape route for the tumor cells to enter the circulation; therefore, cancer cells are transported to distant organs [13].

Lymphangiogenesis is also involved in distant metastasis via metastasizing to regional lymph nodes (LNs). Some types of cancer spread via the vascular and lymphatic systems simultaneously, while others metastasize in a metachronous manner with a tumor in LNs preceding those metastases in distant organs [14]. In these sequential cases, lymphadenectomy can be curative [15]. The classification using TNM scores assumes that cancer metastases progress sequentially from primary tumor to LN metastasis and then to distant metastasis.

(2) During metastasis, cancer cells undergo invasion, in which these cells disseminate into the normal surrounding tissues (Fig. 1.1) [5, 16, 17]. Most cancers have intercellular adhesion because of their epithelial origin, and loss of intercellular adhesion often triggers cancer invasion [18, 19]. In this case, the cancer cells invade individually. Such individual invasion may have an amoeboid- or mesenchymal-like morphology [7, 20]. These have plasticity, including epithelial-like morphology [21]. When individual cancer cells reach distant tissues and form metastases there, they are proposed to revert to epithelial-like morphology to increase cell proliferation and viability [22, 23]. The mechanisms of individual invasion have been investigated by numerous studies, particularly EMT [24]. In addition to these mode of invasion, cancer cells have a variety of invasive patterns , and one of which, collective invasion, has recently come to light (Fig.1.2) [25-27].

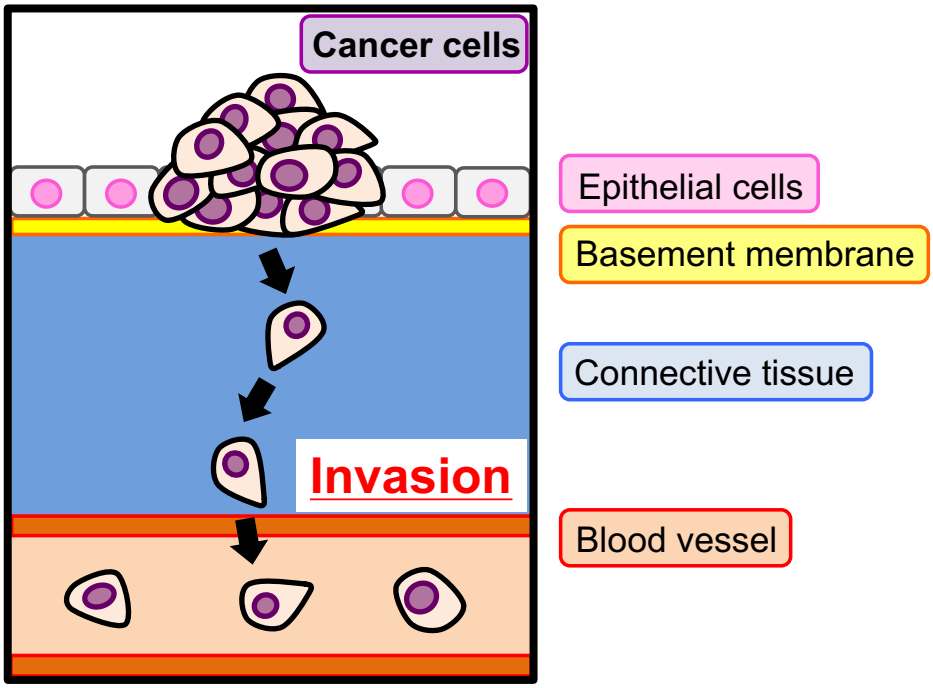

Fig. 1.1 Schematic illustration of cancer cell invasion

Epithelial tissue with carcinoma. Cancer cells break down basement membrane and migrate into surrounding normal tissues and blood vessels.

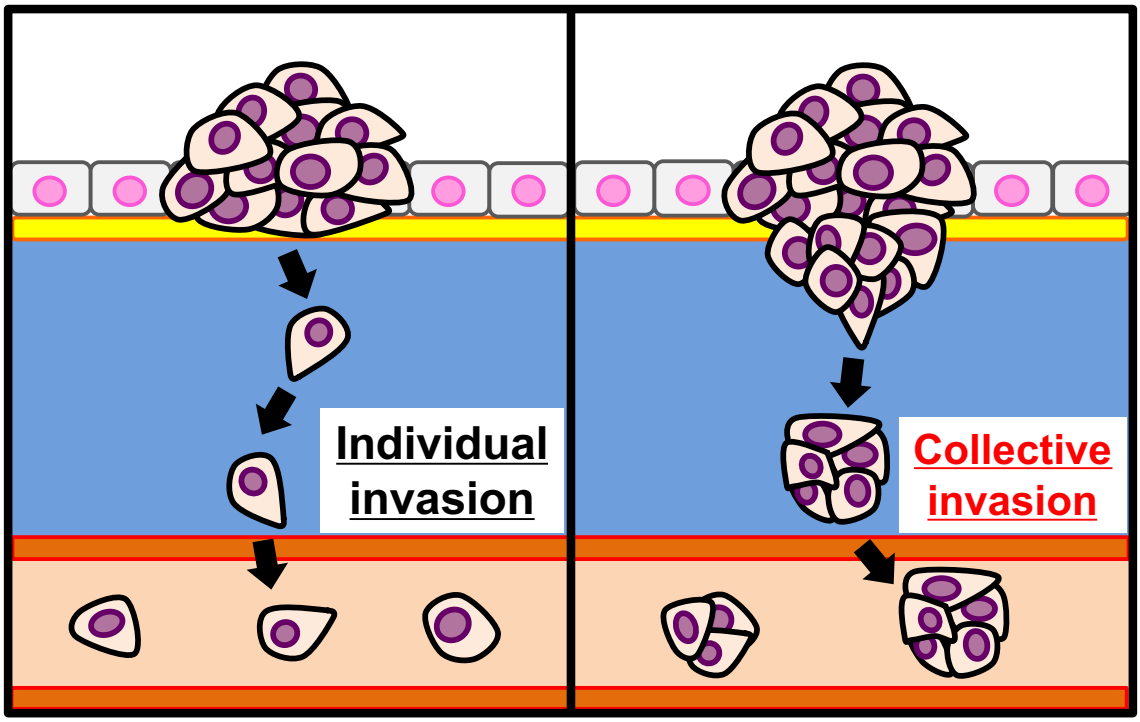

Fig. 1.2 Schematic illustration of individual invasion and collective invasion

Cancer cells can invade normal tissues not only individually but also collectively.

1-1-3. Collective Invasion

The process of collective invasion, during which cancer cell clusters retaining their epithelial characteristics invade the surrounding stroma and penetrate the circulatory system, such as blood and lymphatic vessels [28-30]. Although it has been known that cancer cell groups exist in the invasive areas of various cancers, the possibility that individually invaded cancer cells have grown there could not be denied. Therefore, it was unclear whether collective invasion actually occurs. One innovative study proved that the phenomenon of collective invasion actually occurs *in vivo* and *in vitro* [26]. In this study, cancer cells derived from MMTV-PyMT mice, mammary cancer spontaneous generation model, were multicolored and tracked in the process of invasion and metastasis. The cancer cell groups in the invasive area and in micrometastases in lungs were composed of multicolored cells. In addition, circulating tumor cell (CTC) clusters in blood also multicolored, indicating cancer metastasis is caused by collective invasion of genetically distinct cells (Fig. 1.3) [31].

Next agenda is whether individual invasion or collective invasion is more conducive to metastasis. One study assessed their capacity of invasion and metastasis using control or E-cadherin targeted sgRNA introduced MMTV-PyMT mice [30]. E-cadherin KO resulted in almost no collective invasion and a marked increase in the frequency of individual invasion, and higher dissemination score than control. However, metastasis in the control occurred more frequently than E-cadherin KO condition. These data indicate that cancer cells have higher invasive potential when they invade individually, but higher metastatic potential when they invade collectively. Another study showed that more metastases occur when the same number of cells are injected into a tail vein of mice as CTC clusters rather than as single CTCs [26, 32]. These findings suggest that metastasis is not determined simply by the strength of invasion, but rather by whether it is single or collective when it invades blood vessels. Furthermore, in clinical practice, increased CTC clusters in the blood stream is associated with a worse prognosis in breast cancer patients [33, 34]. It is suggested that collective invasion is considered a critical mode of cancer cell invasion for determining the prognosis of patients; therefore, inhibition of collective invasion is considered to improve cancer treatment. However, no significant target molecules have been found to inhibit collective invasion. In this study, we analyzed the mechanism of collective invasion in order to propose therapeutic target molecules.

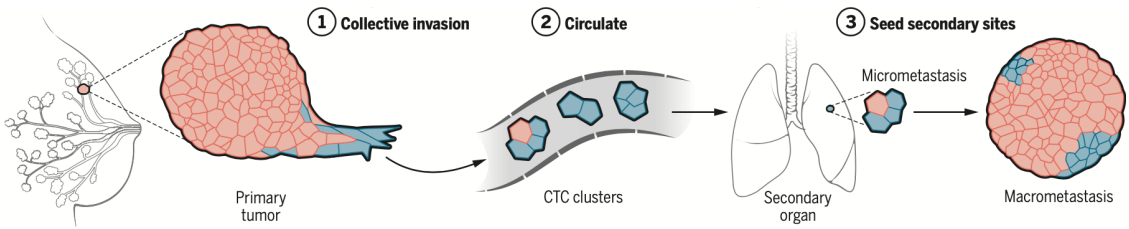

Fig. 1.3 A model for metastatic spread that is based on collective invasion of epithelial tumor cell clusters [31].

Chapter 2

Materials and Methods

2-1. Reagent

Product	Dilution rate	Source	Identifier
Antibodies for Immunofluorescent staining			
Rat anti-integrin-β1	1:200	DSHB	AIIB2
Mouse anti-integrin-α2	1:200	DSHB	P1E6
Mouse anti-integrin-α3	1:200	DSHB	P1B5
Mouse anti-integrin-α5	1:200	DSHB	BIIG2
Mouse anti-integrin-α6	1:200	DSHB	P5G10
Rabbit anti-COL17	1:500	Abcam	ab184996
Mouse anti-laminin-α3	1:100	DSHB	P3H9
Mouse anti-laminin-β3	1:500	Abcam	610423
Mouse anti-collagen I	1:500	Sigma	C2456
Rabbit anti-collagen IV	1:500	Abcam	ab6586
Mouse anti-laminin-α1	1:200	DSHB	L9393
Mouse anti-laminin-γ1	1:200	DSHB	2E8
Mouse anti-fibronectin	1:100	DSHB	13G3B7
Rabbit anti-interferon-β	1:500	Proteintech	27506-1-AP
Rabbit anti-STAT1	1:200	CST	14994
Goat anti-Rabbit IgG Alexa Fluor 405	1:200	Invitrogen	A-31556
Goat anti-Rabbit IgG Alexa Fluor 488	1:500	Invitrogen	A27034
Goat anti-Mouse IgG Alexa Fluor 488	1:500	Invitrogen	A28175
Antibodies for Immunoelectron microscopy			
Rat anti-integrin-β1	1:200	DSHB	AIIB2
Rabbit anti-interferon-β	1:200	Proteintech	27506-1-AP
Goat nanogold-anti-Rat IgG	1:100	Nanoprobes	2007
Goat nanogold-anti-Rabbit IgG	1:200	Nanoprobes	2003
Antibodies for Immunohistochemistry			
Rabbit anti-STAT1	1:3200	CST	14994
Antibodies for western blotting			
Mouse anti-integrin-β1	1:2,000	BD Biosciences	610467
Rabbit anti-COL17	1:1,000	Abcam	ab184996
Mouse anti-laminin-β3	1:1,000	BD Biosciences	610423
Rabbit anti-STAT1	1:2,000	CST	14994
Rabbit anti-pSTAT1 Y701	1:1,000	CST	9167

Rabbit anti-pSTAT1 S727	1:1,000	CST	9177
Rabbit anti-pJAK1 Y1034/1035	1:1,000	CST	3331
Mouse anti-beta actin	1:100,000	Abcam	ab6276
Mouse anti-GAPDH	1:100,000	Thermo	AM4300
Goat anti-Rabbit IgG, HRP linked	1:4,000	CST	7074
Goat anti-Mouse IgG, HRP linked	1:100,000	CST	7076
Antibodies for functional inhibition			
Rat anti-integrin-β1	2 μg/mL	DSHB	AIIB2
Mouse anti-integrinb-α2	2 μg/mL	DSHB	P1E6
Mouse anti-integrinb-α3	2 μg/mL	DSHB	P1B5
Mouse anti-integrinb-α5	2 μg/mL	DSHB	BIIG2
Mouse anti-integrinb-α6	2 μg/mL	DSHB	P5G10
Rat control IgG	2 μg/mL	Wako	147-09521
Antibodies for immunoprecipitation			
Rabbit anti-COL17	15 μg/mL	Abcam	ab184996
Rabbit control IgG	15 μg/mL	Wako	148-09551
Phalloidins for fluorescent observation			
Alexa Fluor 405 Phalloidin	1:500	Invitrogen	A30104
Alexa Fluor 488 Phalloidin	1:500	Invitrogen	A12379
Alexa Fluor 546 Phalloidin	1:200	Invitrogen	A22283

Primers for quantitative PCR		
Target gene symbol	**Forward/Reverse**	**Sequences (5' to 3')**
LAMA3	Forward	TGGGATGGCTGTGGATCTTTGG
	Reverse	CACCCTTTGCTGCTGTGAACTG
OAS1	Forward	GTGTCCAAGGTGGTAAAGGGTG
	Reverse	AAGACAACCAGGTCAGCGTC
OAS2	Forward	TGGCTCCTATGGACGGAAAAC
	Reverse	AGGATGTCACGTTGGCTTCTC
IFI6	Forward	TGCTGTGCCCATCTATCAGC
	Reverse	TTTTTCTTACCTGCCTCCACCC
IFI44L	Forward	GGCCACCGTCAGTATTTGGAATG
	Reverse	AGCCTATTTCTGTGCTCTCTGGC
IFNAR1	Forward	AGCGATGAGTCTGTCGGGAATG
	Reverse	GAGGACCAATCTGAGCTTTGCG
IFNAR2	Forward	AGATGCTTTTGAGCCAGAATGCC
	Reverse	ACACGAGGCTGATATACACCATGAG
IFNB1	Forward	AAGCCTTTGCTCTGGCACAAC
	Reverse	TGGAGAAGCACAACAGGAGAGC
KRT1	Forward	GAGGGAGAAGAAAGCAGGATGTC
	Reverse	ACTGATGGTGGTGTGGCTTG
KRT10	Forward	ACCACGAGGAGGAAATGAAAGACC
	Reverse	AACCAGGCTTCAGCATCTTTGC
KRT14	Forward	AGCAGCAGAACCAGGAGTACAAG
	Reverse	GAGGAGGTCACATCTCTGGATGAC
GAPDH	Forward	TCCTGTTCGACAGTCAGCCGC
	Reverse	TGACCAGGCGCCCAATACGAC
ACTB	Forward	TGGGACGACATGGAGAAAATCTG
	Reverse	AGGTCTCAAACATGATCTGGGTC

siRNAs	
Target gene symbol	**Target Sequences (5' to 3')**
COL17A1	TGGATGTAACCAAGAAAAACAAA
LAMA3	CAGTGATAAACTGTTAAATGAAG
LAMB3	CACAAACTTGAGAGTCAATTTCA
STAT1#1	AAGATGAATATGACTTCAAATGC
STAT1#2	TGACATCATTCGCAATTACAAAG
IFNAR1	TGGCTTATAGTTGGAATTTGTAT
IFNAR2	GTGGAAATTTCACCTATATCATT
IFNB1	GGCTAATGTACTGCATATGAAAG
KRT1	GAGAAATTCAAAGATAGAAATCC
KRT10	TACAGAAATTGATAATAACATCC
KRT14	ATCAATACAGCTTCATTATCTCC
Control (Guide)	AAACTACATGTCACATCACGG
Control (Passenger)	AACCGTGATGTGACATGTAGT

2-2. Cell Culture

2-2-1. Cell Passage

The human skin squamous carcinoma cell line, A431cells (American Type Culture Collection, Manassas, VA), were cultured in Dulbecco's Modified Eagle Medium (Sigma-Aldrich Co. LLC, St Louis, MO, USA) supplemented with 10% fetal bovine serum (Sigma-Aldrich Co. LLC) and 1% antibiotic/anti-mycotic solution (Sigma-Aldrich Co. LLC). The cells were cultured in a humidified incubator at 37℃ and 5% CO2. Ninety percent confluent cells were detached from the culture dish by treatment with 0.25% trypsin-EDTA (Thermo Fisher Scientific, Inc. Waltham, MA, USA) for 8 minutes. Twenty percent of the cell suspension was seeded in a new culture dish.

2-2-2. Establishment of A431 Subclones

A431 subclones were established using limited dilution method. Parental A431 cells were seeded in 96-well cell culture plates (Corning Incorporated, Corning, NY, USA) at 0.5 cells/well. We grew the cells only in the wells with a single colony. The first established subclone was named A431-1, and the subsequent subclones were named in the order in which they were established (A431-1 to A431-20). Among these subclones, A431-6 subclone has high invasive potential, while A431-7 cells showed low invasive potential, and we found that upregulation of type-I interferon pathway in A431-6 subclone by analyzing gene expression using DNA microarray. Since the type-I interferon production is induced by viral infection [35] and herpes virus mediate skin cancer [36], we tested the herpes virus infection using PCR. The result was negative. In addition, a previous study reported that A431 cells were not infected with human papillomavirus, a pathogen of vulvar cancer [37]. Parental A431 and sub-clonal cells were tested for mycoplasma contamination using a mycoplasma detection kit (VenorGeM Mycoplasma Detection Kit, Sigma-Aldrich Co. LLC) according to the manufacturer’s instructions and did not show any contamination symptoms. Thus, we confirmed that the elevation of type-I interferon pathway in A431-6 subclone was not caused through infection by microorganisms.

2-2-3 Development of Transgenic Cells

To construct the emerald-histone H2B encoding vector, Histone H2B encoding DNA was amplified by PCR using pKanCMV- mClover3-10aa-H2B (Addgene, Cambridge, MA, USA) and KOD-Plus (TOYOBO, Osaka, Japan). The primers used for the PCR is as follows: 5’-AAAGGATCCGCCACCATGCCTGAACCGGCAAAATC-3’ (forward) and 5’-AAAGAATTCAACTTGGAGCTGGTGTACTTGGTGAC-3’ (reverse). The fusion protein of histone H2B and emerald, a green fluorescent protein, was inserted into MCS of pIRES-ZsGreen 1 Vector (Clontech Laboratories, lnc., Palo Alto, California, USA). Puromycin-resistant genes

linked to emerald-histone H2B by IRES linker were inserted in exchange with ZsGreen. Xfect transfection reagent (Takara Bio Inc., Shiga, Japan) was used for transfection to cells. Selective cultures were performed using a culture media containing 2 mg/mL puromycin after transfection.

2-2-4. Collagen Gel Overlay Condition

Type-I collagen (1.6 mg/mL, Cell matrix IeP, Nitta Gelatin, Osaka, Japan) was used for collagen gel overlay conditions (Fig. 2.1). A 24-well cell culture plate was filled with 200 μL of collagen solution and incubated at 37°C for 30 min to induce gelation. Then, 8×10^4 cells were seeded on the collagen gel. The collagen solution was poured onto the cells 24 hours after cell seeding and was incubated for 30 min at 37°C. After gelation of the collagen gel, 500 μL of culture medium was added. Contact following in a cancer cell population was assessed using this culture system.

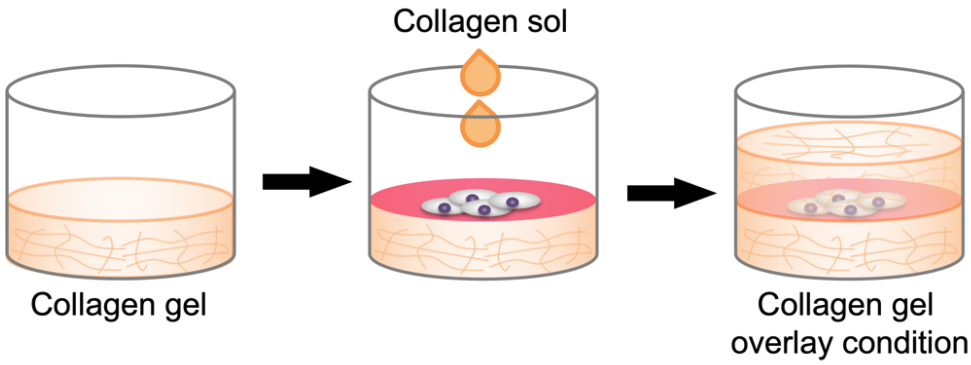

Fig. 2.1 Schematic illustration of collagen gel overlay condition

2-2-5. Single Cell-derived Spheroid Invasion Assay

The cells were embedded into type-I collagen gels (1.6 mg/mL, Cell matrix I-P; Nitta Gelatin) to assess their invasiveness (Fig. 2.2). Cell suspensions were prepared at a concentration of 1×10^5 cells/mL in a collagen solution. This solution containing cells (600 μL) was added to a hand-made 16 mm inner diameter glass dish and incubated for 30 min at 37°C to induce gelation. A431 cells formed spheroids in this culture system and eventually invaded as a collective cell strand. The sphericity of cell clusters was evaluated using this culture system.

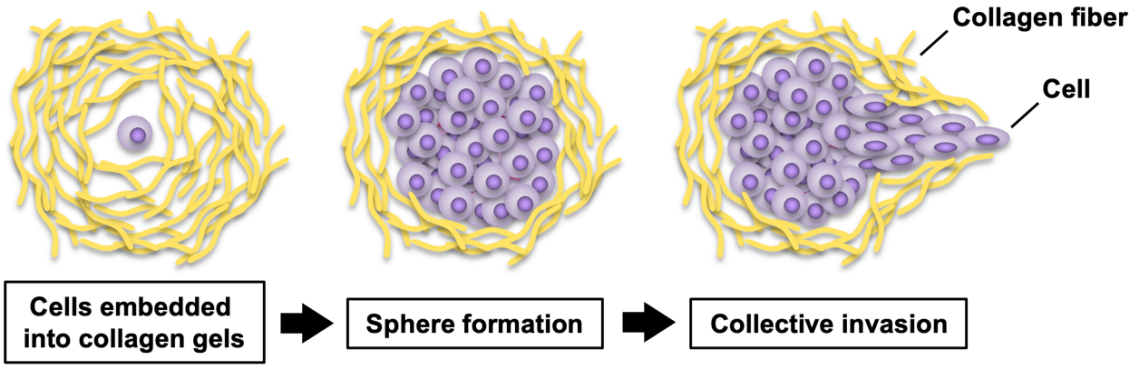

Fig. 2.2 Schematic illustration of single cell-derived spheroid invasion assay

2-2-6. Invasion Assay of Spheroid prepared using Hanging Drop Method

Multi-clonal spheroids were prepared using the hanging drop method. Each droplet (10 μL) was seeded to contain 500 cells. The spheroids were collected 2 days after seeding and embedded into 1.6 mg/mL collagen gels (Nitta Gelatin) and were cultured until they exhibited invasion.

2-3. Quantification of Collective Invasion Potential

2-3-1. Evaluation of Contact Following using Cosine Function

Nucleus of A431 cells expressing emerald-histone H2B were automatically tracked using the TrackMate plug-in of Fiji/Image J software (National Institutes of Health, Bethesda, MD, USA) to track cell movement [38]. Contact following was assessed using cosine function. Cosine values were calculated from the angle between the movement directions of neighboring cells (Fig. 2.3). Cells within 100 μm of a targeted cell were analyzed. The analysis was performed on all cells of the cell population.

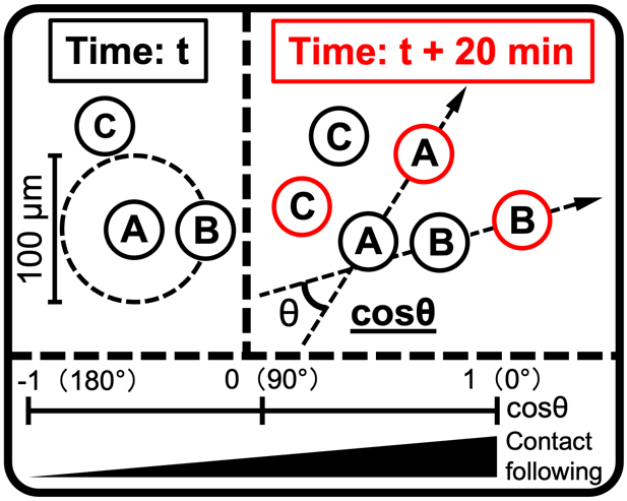

Fig. 2.3 The method to assess contact following of neighboring cells

2-3-2. Evaluation of Collective Invasion using Sphericity

3D images were constructed using Imaris software (Bitplane AG, Zürich, Switzerland). The sphericity ($36\pi V2/S3$) of cell clusters was calculated by the ratio of the circle's circumference (π), the surface area (S), and volume (V) of cell clusters, as calculated by Imaris.

2-4. Time-lapse Observation

Time-lapse observations of collagen gel overlay condition in the bright field were performed using a phase-contrast microscope (TE2000, Nikon, Tokyo, Japan) equipped with a 20 × objective lens. The Images in the bright field were captured every 5 min for 16 hours. Time-lapse imaging of collagen gel overlay condition in fluorescent field was carried out using confocal laser microscopy (A1R Confocal Imaging System; Nikon) equipped with a 20 × objective lens. The Images in the bright field were captured every 20 min for 16 hours.

Time-lapse observations for multi-clonal spheroids were performed using confocal laser microscopy (A1R) equipped with a 20 × objective lens. The Images were captured every 15 min for 48 hours. NIS-Elements Advanced Research software (Nikon) was used to capture images for above both time-lapse observations. A stage top incubator (STG-WSKMX-SET, Tokai Hit Co., Shizuoka, Japan) was used to maintain the samples at 37℃.

2-5. Immunofluorescent Staining

2-5-1. Collagen Gel Overlay Condition

Cells cultured in collagen gel overlay conditions were fixed with 4% paraformaldehyde (Nacalai tesque, Kyoto, Japan) for an hour at 4℃ and permeabilized with 0.1% saponin (Wako Pure Chemical Industries, Osaka, Japan) for 10 min at room temperature. Blocking was performed using 1% bovine serum albumin (BSA, Wako Pure Chemical Industries) in phosphate buffer saline (PBS) for an hour at 37℃. Cells were reacted with a primary antibody diluted in Can Get Signal immunostain (Immunoreaction Enhancer Solution B, TOYOBO, Osaka, Japan) overnight at 4℃. Next, the cells were reacted with a secondary antibody and Alexa Fluor-546 phalloidin in Can Get Signal Immunostain B for an hour at 25℃. Fluorescent images were captured by confocal laser microscopy (A1R).

2-5-2. Spheroids embedded in collagen

In fluorescent phalloidin staining, cell clusters in collagen gels were fixed with 4% paraformaldehyde in PBS for 2 hours at 4℃. Permeabilization and blocking were performed simultaneously using 1% BSA and 0.3% Triton X-100 (Sigma-Aldrich Co. LLC) in PBS for an hour at room temperature. Cells were incubated with Alexa Fluor-phalloidin 405 or 488 (Invitrogen, Carlsbad, CA, USA) diluted in Can Get Signal Immunostain B overnight at 4℃.

For fluorescent staining of interferon-β (IFNB), 0.1% collagenase (Wako Pure Chemical Industries) in PBS was added and incubated for 30 min at 37℃. The cells were then fixed with 4% paraformaldehyde in PBS for an hour at 4℃. Permeabilization and blocking were performed simultaneously using 1% BSA (Wako Pure Chemical Industries) and 0.1% Triton X-100 (Sigma-Aldrich Co. LLC) in PBS for an hour at room temperature. Cells were incubated with a primary antibody diluted in Can Get Signal Immunostain B overnight at 4℃. Next, the cells were incubated with a secondary antibody diluted with Can Get Signal Immunostain B and Alexa Fluor phalloidin 546 for an hour at room temperature.

For fluorescent staining of STAT1, the cells were pre-fixed with 4% paraformaldehyde in PBS for 30 min at 4℃. The cell-embedded gel was gently peeled off and transferred to a 1.5-mL tube, and post-fixation was performed using 4% paraformaldehyde in PBS for 30 min at 4℃. Permeabilization and blocking were performed simultaneously using 1% BSA and 0.3% Triton X-100 in PBS for an hour at room temperature. Cells were incubated with a primary antibody diluted in Can Get Signal Immunostain (Immunoreaction Enhancer Solution A, TOYOBO, Osaka, Japan) overnight at 4℃. Next, the cells were incubated with a secondary antibody diluted with Can Get Signal Immunostain A and Alexa Fluor phalloidin 647 for an hour at room temperature.

All fluorescent images were captured from the top to the bottom of the cell cluster at 1-μm intervals by confocal laser microscopy (A1R or C2+ Confocal Imaging System; Nikon) equipped with a 20× or 60× objective lens (Nikon).

2-6. Electron Microscopy

2-6-1. Transmission Electron Microscopy

The cells in collagen gels were treated with 0.1% collagenase in PBS for 30 min at 37°C and then fixed with 2.5% glutaraldehyde (Nacalai Tesque) in 0.1 M phosphate buffer (pH 7.4) overnight at 4°C. After postfixation with 1% OsO4 in ultrapure water for 90 min, the cells were embedded in a 2% agarose gel. The cells in agarose gels were dehydrated through a graded series of ethanol and embedded in Epon resin (Quetol 812) according to a conventional method. Ultra-thin sections stained with uranyl acetate and lead citrate were observed under a transmission electron microscope (JEM1400, JEOL Ltd, Tokyo, Japan). The distance between two cells in the cell clusters was manually measured using the pencil tool of Fiji/ImageJ.

2-6-2. Immunoelectron Microscopy

Cells were processed using the pre-embedding silver-intensified immunogold method as described in a previous study [39]. Anti-integrin-β1 antibody and anti-IFNB antibody were used as the primary antibody. Nanogold-anti rat IgG and nanogold-anti rabbit IgG was used as the secondary antibody. Gold signals were enhanced using HQ silver (Nanoprobes). Observations were carried out using a transmission electron microscope (H7100, Hitachi High-Technologies Corp., Tokyo, Japan) (JEM1400).

2-7. Immunohistochemistry

Immunohistochemistry for tissue microarray of invasive skin SCC (SK802b; US Biomax, Inc., Rockville, USA) and pre-invasive skin SCC, which is also known as SCC in situ or Bowen's disease, was performed as described in a previous study [39]. The data were independently assessed by two pathologists.

Human samples of Bowen's disease were obtained at the time of surgery from patients who provided written informed consent at the Nagoya University Hospital. This study was conducted in accordance with the principles of the Declaration of Helsinki for Human Research and approved by the Ethics Committee of Nagoya University Graduate School of Medicine (approval no. 2017-0127-3).

2-8. Gene Knockdown using siRNAs

Cells were seeded in 6-well plates at a density of 6×10^5 cells/well and transfected with the target siRNA or control siRNA with Lipofectamine RNAiMAX Reagent (Thermo Fisher Scientific). Transfection was performed with siRNA concentrations of 15 or 2.5 nM. Nucleotide blasts demonstrated that there was no homologous sequence of control siRNA.

2-9. RT-qPCR

RNA from the cells cultured in collagen gels was extracted with Tripure reagent (Roche Applied Science, Indianapolis, IN, USA) and purified using the FastGene RNA Basic Kit (NIPPON Genetics Co., Ltd, Tokyo, Japan). cDNA was synthesized using ReverTra Ace (TOYOBO). Quantitative PCR (qPCR) was performed using KAPA SYBR FAST qPCR Kits (KK4602; NIPPON Genetics Co., Ltd) and StepOnePlus (Thermo Fisher Scientific) according to the manufacturer's instructions. ACTB or GAPDH were used as an endogenous control.

2-10. Western Blotting

The protein samples were prepared from the cells in collagen gels. Cold 10% trichloroacetic acid (TCA, Sigma-Aldrich Co. LLC) in PBS was added to the cells and incubated for 10 min at 4℃. After rinsing three times with PBS to remove TCA, 0.1% collagenase (Wako Pure Chemical Industries) in PBS was added and incubated for 40 min at 37°C. After collagen gel digestion, collagenase was removed by centrifugation at 10,000 × *g* for 3 min. Proteins from the cells were extracted with sodium dodecyl sulfate (SDS) sample buffer (60 mM Tris HCl, 2.2% SDS, 10% glycerol, 100 mM dithiothreitol, pH 6.8) and boiled for 5 min. SDS-PAGEs were performed under constant voltage conditions of 200 V using 8 or 10% acrylamide gels, and separated proteins were transferred to PVDF membrane under constant current conditions of 86 mA for 60 min. The membrane was blocked by 2% BSA in TBS-T for an hour. The primary antibodies were diluted with Can Get Signal Solution 1 (TOYOBO). Horseradish peroxidase (HRP)-conjugated secondary antibodies were diluted with Can Get Signal Solution 2 (TOYOBO). Protein signals were detected using an Immobilon Western Chemiluminescent HRP substrate (EMD Millipore, Billerica, MA, USA). Chemiluminescence signals were captured using a ChemiDoc Touch (Bio-Rad Laboratories, Richmond, CA, USA).

2-11. Immunoprecipitation

Cell lysates were prepared with lysis buffer attached to Capturem IP & Co-IP Kit (Takara-Bio Inc., Shiga, Japan). The cell lysates were incubated with anti-COL17 (EPR18614, Abcam Plc.) or control rabbit IgG (Wako Pure Chemical Industries) for 24 hours at 4℃. Each antibody was used at 15 μg/mL. The immune complexes were obtained using Capturem IP & Co-IP Kit and analyzed by Western blotting.

2-12. Enzyme Liked Immuno-Sorbent Assay

Interferon-β concentration in the supernatant was measured by sandwich ELISA using the Human IFN-beta DuoSet (R&D Systems, Inc.). Ninety-six-well microplates were coated with capture antibody diluted in PBS. The antibody-coated wells were blocked with 1% BSA in PBS, and then each supernatant was added. After washing three times with PBS containing 0.05% Tween 20 (TPBS), biotin-conjugated detection antibody and HRP-conjugated streptavidin were added in order. After washing three times with TPBS, TMB solution (Wako Pure Chemical Industries) was used as the chromogenic substrate, and the coloring reaction was stopped by 1M sulfuric acid. The absorbance at 450 nm was measured using a microplate reader (Bio-Rad).

2-13. Statistical Analysis

2-13-1 For Chapter 3

Each experiment was independently repeated at least three times. All tests in this study were performed using the R software ver. 3.3.3 (R Development Core Team, Vienna, Austria). P-values less than 0.05 were considered statistically significant. Box-plot graphs showing cosine values were described using the R software ver. 3.3.3. Statistical analyses of contact following were performed using Wilcoxon rank sum test. For multiple comparison, p-values were corrected using Bonferroni correction. The signal intensity in western blotting was quantified using ImageJ/Fiji software and graphed using Microsoft Excel (Microsoft corp., Redmond, USA). Comparisons of this signal intensity were performed using Welch's t-test.

2-13-2 For Chapter 4

Statistical significance was set at $p < 0.05$. All data were graphed and tested using GraphPad Prism software (version 7.0; GraphPad Software Inc., San Diego, CA, USA). Statistical analysis was performed using Student’s t-test (ELISA and TEM), paired t-test (western blotting and qPCR in the two groups), and Dunnett’s multiple comparisons test (western blotting and qPCR with more than three groups). The sphericity of the cell clusters in the two groups was tested using the Mann-Whitney U test. For more than three groups, Dunn’s multiple comparison test was performed. All tests were two sided.

Chapter 3

The expression of integrins and ECM proteins in the intercellular site promotes contact following in a cancer cell population during collective invasion

3-1 Introduction

3-1-1 Integrins

Integrins are transmembrane proteins that function as an extracellular matrix (ECM) receptor by forming a heterodimer of α and β subunits (Fig. 3.1) [40]. Various combinations of α and β subunits provide a diversity of adhesion potential for various ECMs [41]. Integrin-β1, a receptor for collagen, laminin, and fibronectin, linked to actin filament (F-actin) via actin-binding proteins such as talin and vinculin [42, 43]. Thus, integrin-β1 plays a crucial role in cell motility and cell division by mediating the linkage of the ECM and F-actin [44-46].

In focal adhesion, integrin binding to the ECM promotes autophosphorylation at Tyr397 of focal adhesion kinase (FAK), thereby Src tyrosine kinase is recruited to focal adhesion for formation of an active FAK/Src kinase complex which phosphorylates distinct focal adhesion proteins including FAK, paxillin and p130cas, leading to the activation of signaling to cell migration and invasion [46-48]. Furthermore, integrin-β1 is also required for collective invasion in melanoma and cutaneous squamous cell carcinoma (SCC) [49, 50]. In this way, integrin-β1 contributes to cancer progression by enhancing cancer cell invasion. However, the molecular mechanisms behind this invasion, including how integrin-β1 promotes collective invasion, are not currently well known.

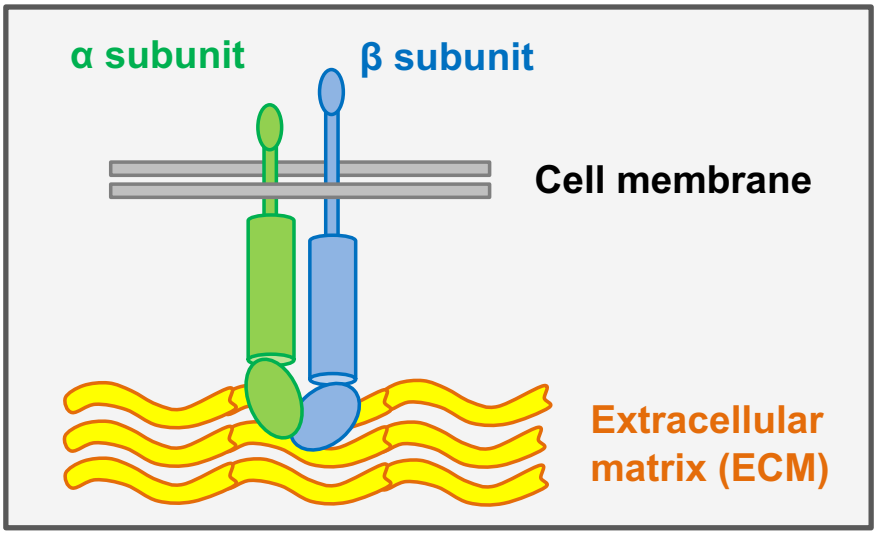

Fig. 3.1 Integrin binding extracellular matrix protein

Integrin complex, heterodimer of alpha and beta subunits, plays the role of ECM receptor.

3-1-2 Extracellular matrix (ECM)

Cancer cells are surrounded by ECMs such as connective tissues and basement membranes, which are composed of several proteins and polysaccharides, and ECMs contribute to cancer progression via the activation of survival, proliferation, and motility [51, 52]. In this study, collective invasion was reproduced *in vitro* using type I collagen gel, a major component of a connective tissue [53]. Type-I collagen proteins have a three-chain helical structure, in which three collagen polypeptide chains are intertwined each other [54]. This collagen proteins are further assembled to form collagen protofibers, which are further assembled to form thick collagen fibers [54].

In this study, we focused on collagen type XVII (COL17), a transmembrane collagen [55]. COL17 is mainly localized in hemidesmosomes at the basal epithelial cells and binds to laminin in the basement membrane, thereby anchoring cells to the basement membrane [56]. COL17 maintains epidermal homeostasis by regulating proliferation and polarity in epithelial cells [57, 58]. Its extracellular domain is cleaved by proteases on the plasma membrane and secreted out of the cells [58, 59]. The secreted form of COL17 is important for normal basement membrane formation, and its loss causes skin diseases such as blistering [60]. In addition, COL17 promotes migration of keratinocytes by participating in their adhesion to the ECM [61]. Further, depletion of COL17 expression in oral squamous carcinoma cells inhibited migration and invasion [62]. On the other hand, enhancement of COL17 expression in invasive breast cancer cells suppressed their migration and invasion [63]. Thus, although COL17 has been reported to be involved in migration and invasion in several cell types, its function differs among cells.

We also investigated on laminin, a component of basement membrane [51]. Laminin forms a heterotrimer composed of α, β, and γ chains. Laminin-332, a major component of basement membrane, contributes to the malignant transformation of many cancers [64, 65]. In particular, squamous cell carcinoma expresses high levels of laminin-332 and its contribution to proliferation and invasion is significant[65, 66]. Furthermore, laminin-332 has been shown to function not only as a basement membrane-like structural ECM, but also as a soluble factor that functions in an autocrine manner [67].

3-1-3 Contact Following

Collectiveness in a cancer cell population is required for collective invasion. This study focused on contact following, the phenomenon which is mediated by intercellular adhesion for the movement of neighboring cells in the same direction (Fig. 3.2), to investigate the mechanism in a cancer cell population which induces collectiveness. Contact following was proposed to account for the collective migration of Dictyostelium [68]. Also contact following is observed in the collective migration of MDCK epithelial cells [69]. As shown in a previous study, integrin-β1

is necessary for the collectiveness of MDCK cells [70]. Therefore, we hypothesize that integrin-β1 contributes to collective behaviors of a cancer cell population by promoting contact following.

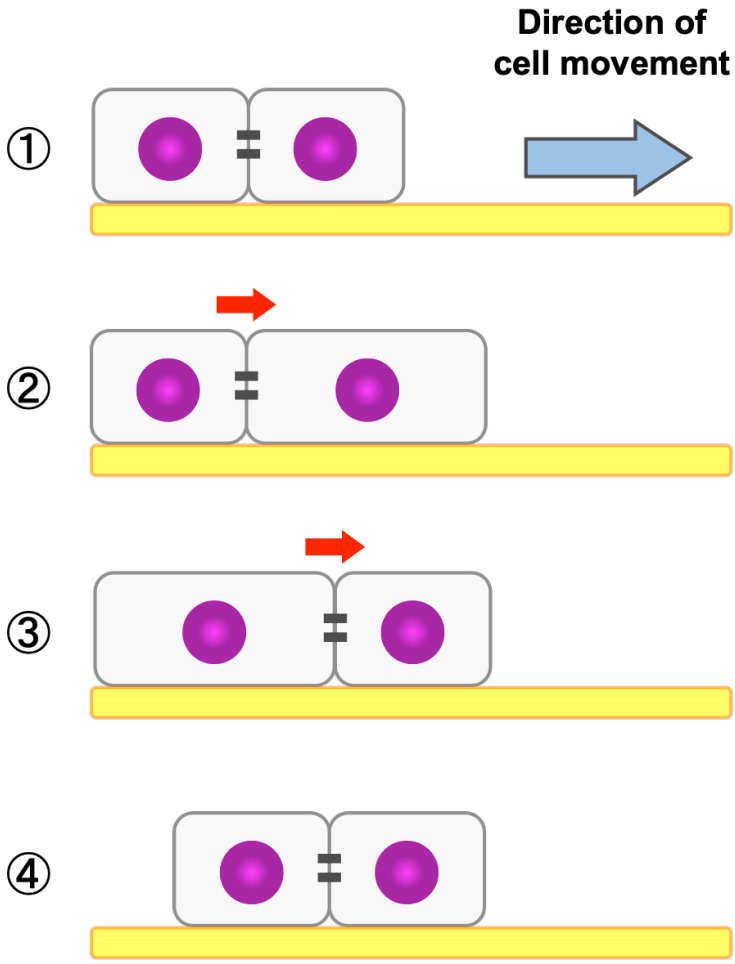

Fig. 3.2 Multicellular cell movement with contact following

Contact following mediates the movement of neighboring cells to the same direction.

3-2 Results

3-2-1 The collective invasion of A431 cells in a collagen gel overlay condition

Time-lapse imaging of collective invasion was performed to analyze the contact following of cancer cells. The existing experimental system for collective invasion can evaluate the movements of cancer cells in a three-dimensional direction [71]. However, to track cell movement in detail, it is desirable for cells to move in a two-dimensional direction. Therefore, we established a novel experimental system to observe the two-dimensional collective invasion. Collagen gel overlay conditions were used as an experimental system, and A431 skin squamous carcinoma cell line with collective invasive potential were cultured. The two-dimensional collective movement of A431 cells in collagen gel overlay conditions was observed using time-lapse imaging in the bright field (Fig. 3.3). In addition, A431 cells expressing the nuclear localized fluorescent protein (A431-emerald) was established to track cell movement. A431-emerald also showed two-dimensional collective movement (Fig. 3.4), and cell movement was successfully automatically tracked using Fiji/ImageJ software. Therefore, this experimental system was used to evaluate contact following in collective invasion.

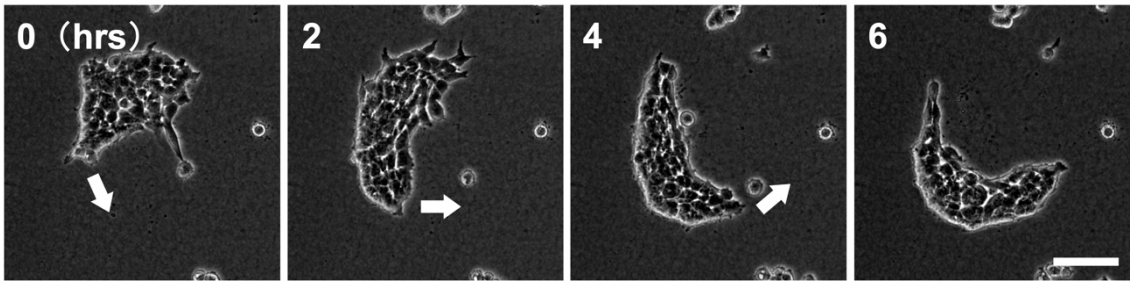

Fig. 3.3 A431 cells showed two-dimensional collective invasion in a collagen gel overlay condition.

Time-lapse imaging of A431 cells in the bright field. The arrow shows the direction of cell movement. The scale bar represents 100 μm.

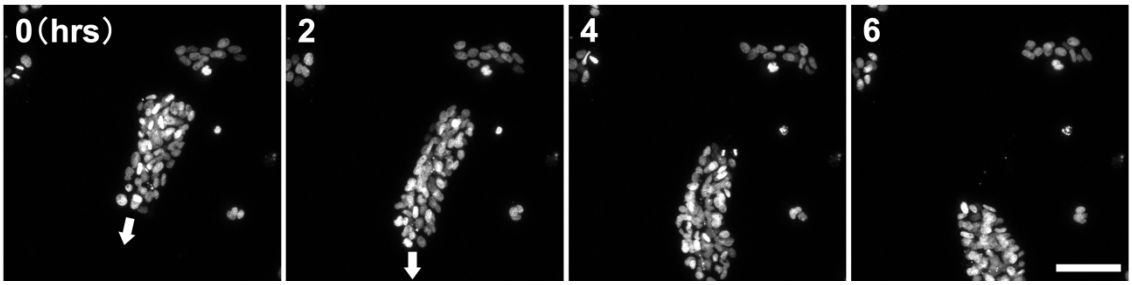

Fig. 3.4 A431-emerald cells also showed two-dimensional collective invasion.

Time-lapse imaging of A431-emerald cells in the fluorescent field. The arrow shows the direction of cell movement. The scale bar represents 100 μm.

3-2-2 Integrin-β1 is localized to the intercellular site and required for contact following

Previous studies found that the high expression of integrin-β1 in the leading cells contributes to the collective behaviors of MDCK cells and squamous carcinoma cells [50, 70]. Therefore, the localization of integrin-β1 in a collagen gel overlay condition using immunofluorescent staining was first investigated. It was found that integrin-β1 is expressed not only in cell-substrate but also in cell-cell sites (Fig. 3.5). In addition, immunofluorescent staining with an anti-active integrin-β1 antibody revealed that integrin-β1 in cell-substrate and cell-cell both are the active form (Fig. 3.6). Next, immunoelectron microscopy was performed to investigate the intercellular structure in A431 cells and localization of integrin-β1 in detail. As a result, it was found that A431 cells have an adherens junction, while integrin-β1 was localized to the cell surface in the intercellular site, but not adherens junction (Fig. 3.7).

Subsequently, to investigate the function of integrin-β1 in collective invasion, time-lapse imaging of A431 cells was performed in the presence of AIIB2, an inhibitory antibody of active integrin-β1. As a result, the inhibition of active integrin-β1 by AIIB2 suppressed the intercellular adhesion in A431 cells (Fig. 3.8). The data suggest that integrin-β1 plays essential role in the intercellular adhesion.

As integrin functions as a heterodimer of α and β subunits 21], the partner of integrin-β1 was investigated. It was found through immunofluorescent staining that integrin-α2, α3, α5, and α6 are expressed in the intercellular site in A431 cells (Fig. 3.9). In addition, the inhibition of integrin-α subunits by an inhibitory antibody revealed that the activity of integrin-α2 is required for intercellular adhesion (Fig. 3.10). These results suggest that the partner of integrin-β1 is integrin-α2, and integrin-α2β1 is necessary for intercellular adhesion in A431 cells.

We then examined the influence of AIIB2 on contact following using an evaluation system we established. The influence of AIIB2 on contact following with A431-emerald is shown in Fig. 3.11. As a result of the quantitative analysis, AIIB2 significantly suppressed contact following (Fig. 3.12). From this result, it was found that the activity of the intercellular integrin-β1 is required for contact following.

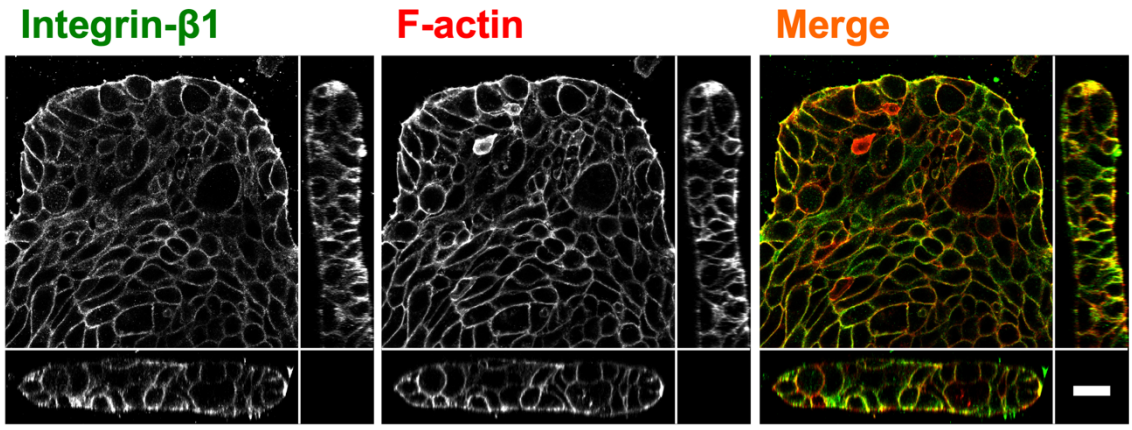

Fig. 3.5 Immunofluorescent staining of integrin-β1.

XY-, YZ-, and ZX-sectional views are shown. Green: integrin-β1. Red: actin filament (F-actin). The Scale bar represents 25 μm.

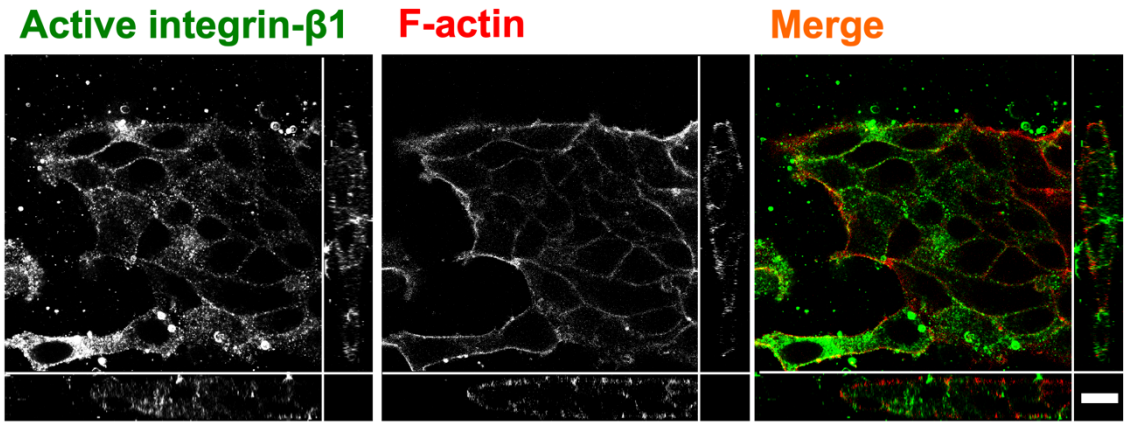

Fig. 3.6 Immunofluorescent staining of active integrin-β1.

XY-, YZ-, and ZX-sectional views are shown. Green: integrin-β1. Red: F-actin. The Scale bar represents 25 μm.

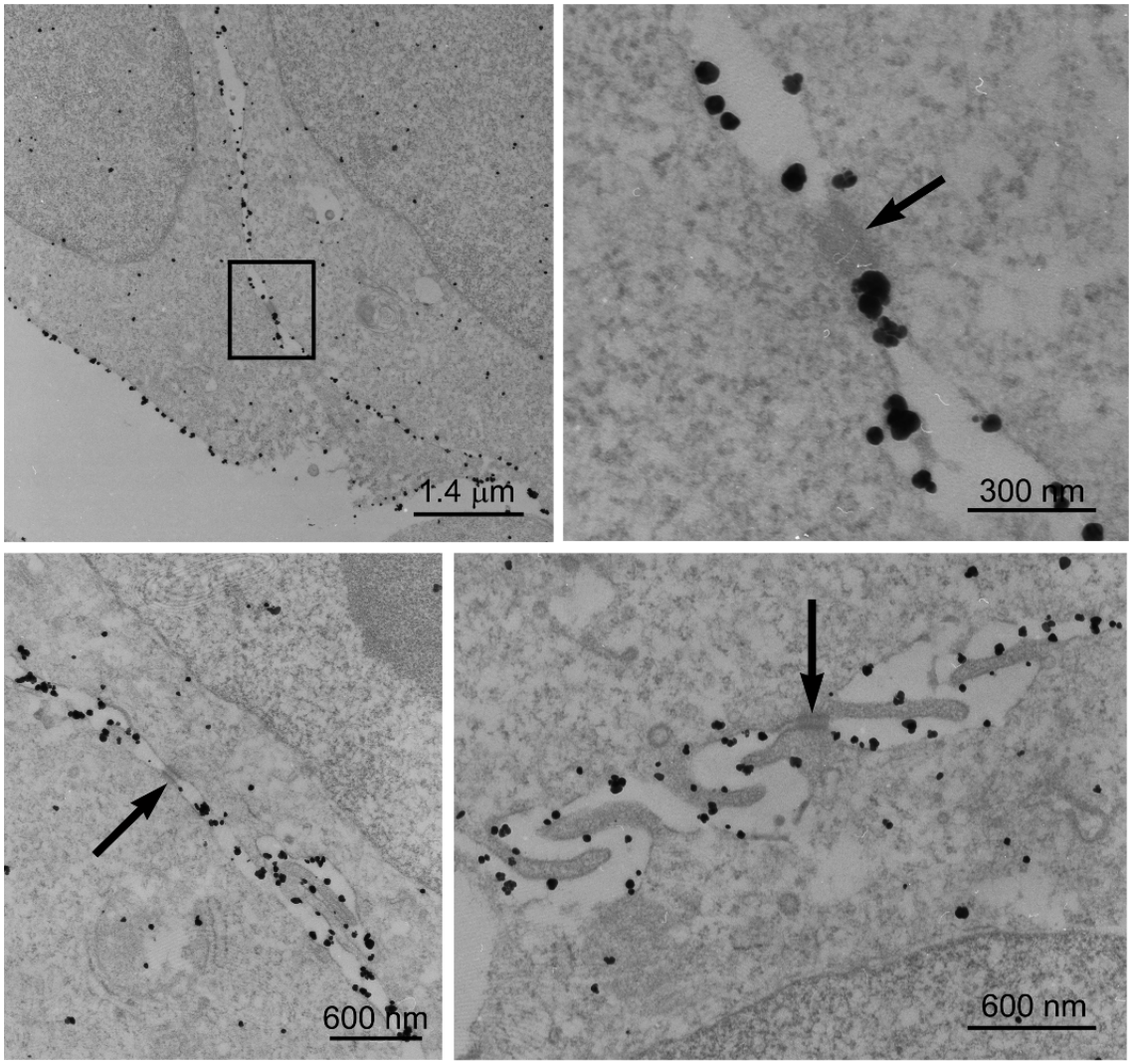

Fig. 3.7 Immunoelectron microscopy of integrin-β1.

Black particles show localization of integrin-β1. The square area is enlarged in the upper right panel. Arrows show the adherens junction.

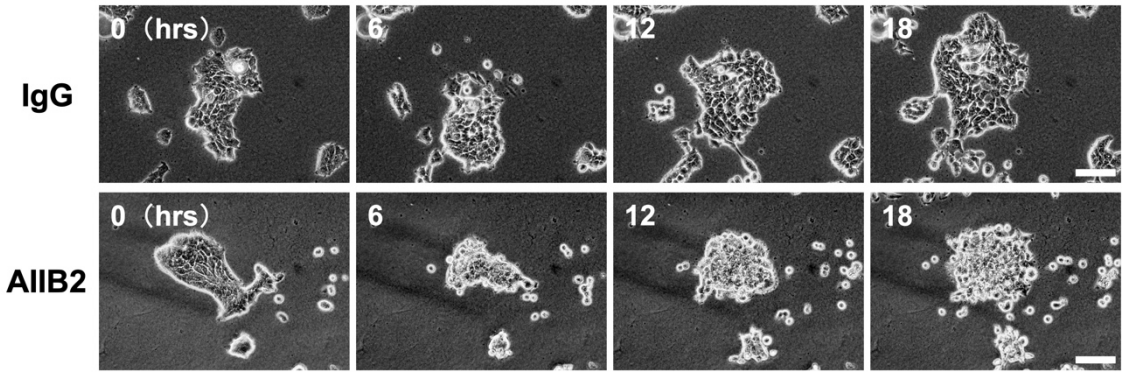

Fig. 3.8 Time-lapse observation in the presence of integrin-β1 inhibitory antibody.

The upper panels show treatment with negative control IgG. The lower panels show treatment with the integrin-β1 inhibitory antibody (AIIB2). Concentrations of each antibody are 2.0 mg/mL. Scale bars represent 100 μm.

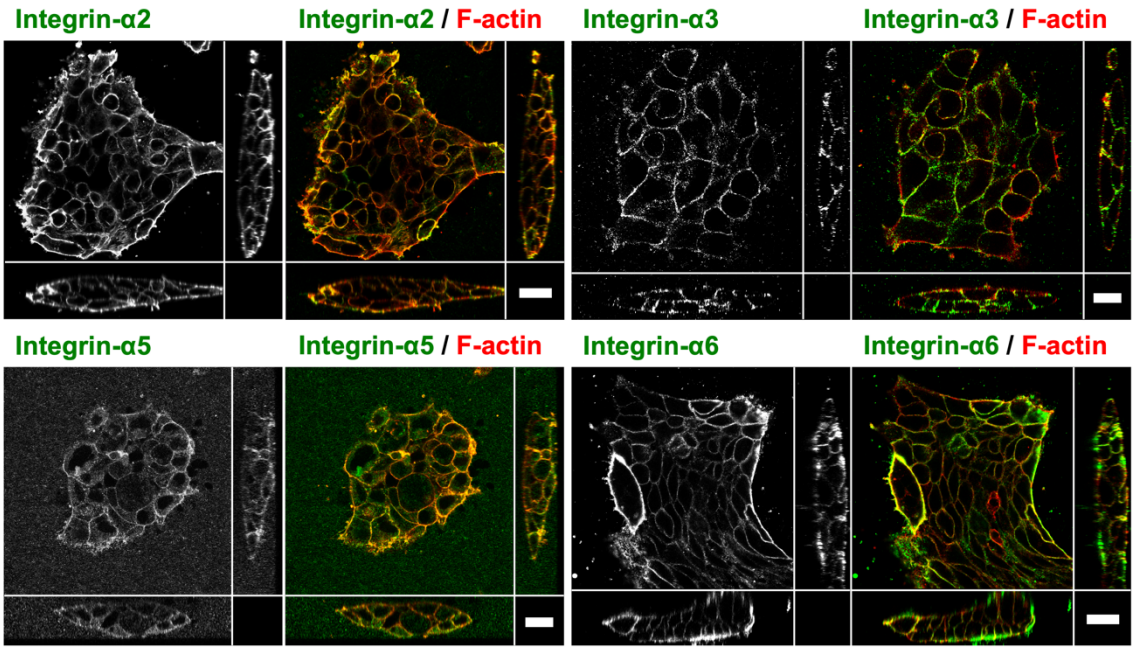

Fig. 3.9 Immunofluorescent staining of integrin-α subunits.

XY-, YZ-, and ZX-sectional views are shown. Green: integrin-α2, α3, α5, and α6. Red: F-actin. The Scale bars represent 25 μm.

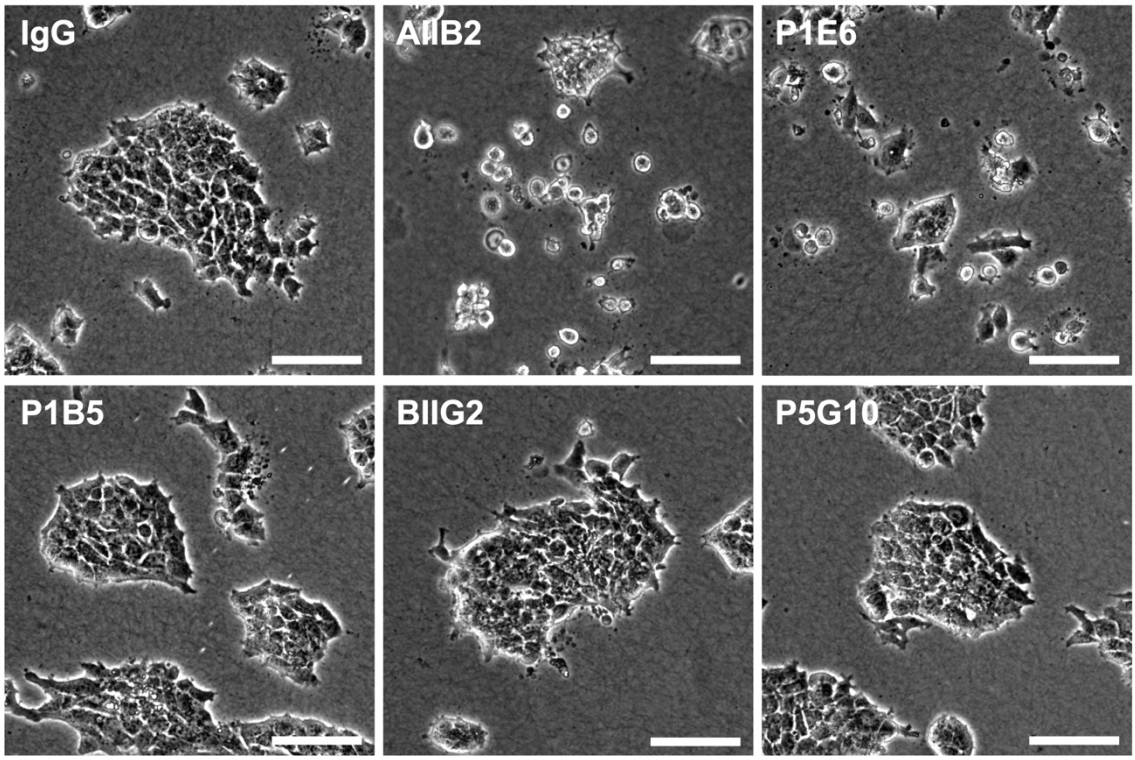

Fig. 3.10 Inhibition of integrin-α subunits using inhibitory antibodies.

The images show the A431 cell populations 24 hours after treatment with each inhibitory antibody. IgG: Negative control. AIIB2: anti-integrin-β1 P1E6: anti-integrin-α2. P1B5: anti-integrin-α3. BIIG2: anti-integrin-α5. P5G10: anti-integrin-α6. Concentrations of each antibody are 2.0 mg/mL. Scale bars represent 100 μm.

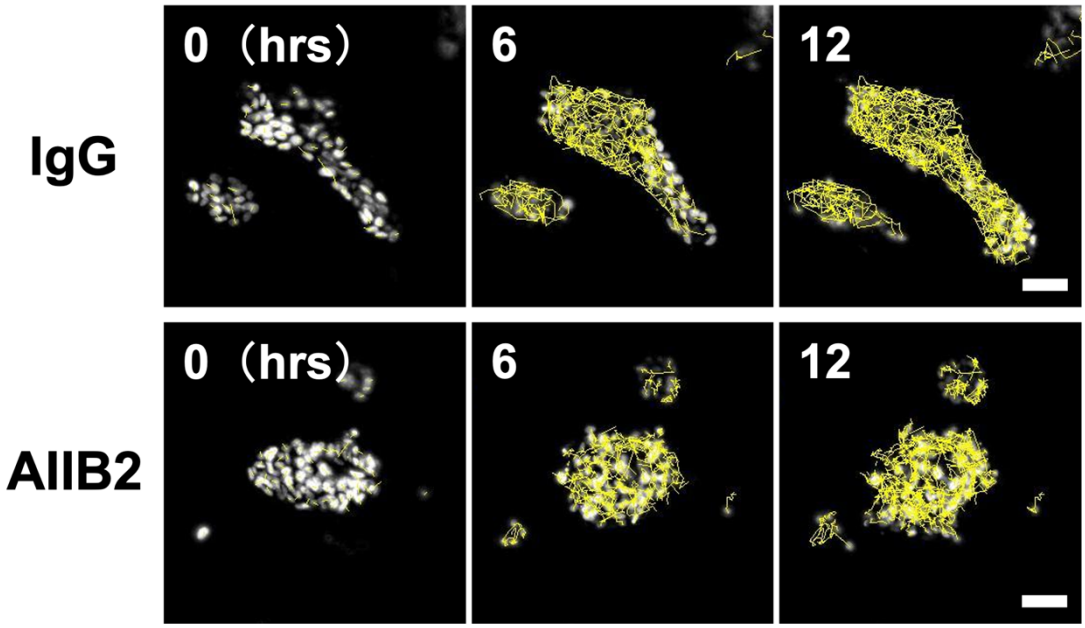

Fig. 3.11 Time-lapse observation of A431-emerald cells in the presence of integrin-β1 inhibitory antibody.

Time-lapse observation of A431-emerald cells in the presence of AIIB2, integrin-β1 inhibitory antibody. The upper panels show treatment with negative control IgG. The lower panels show treatment with AIIB2. Yellow lines are the trajectory of cell movement. Concentrations of each antibody are 2.0 mg/mL. Scale bars represent 50 μm.

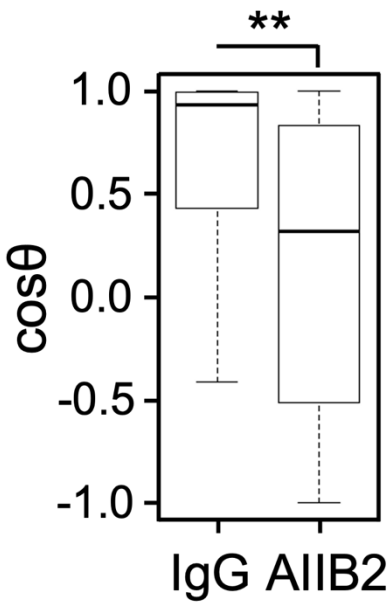

Fig. 3.12 Evaluation of contact following using cosine function.

Quantification of cosine values, cosθ. Boxplot shows median levels of cosθ under each condition. Boxes show interquartile range. Bars show maximum and minimum values within 1.5 IQR. **P < 0.01 by Wilcoxon rank sum test (n > 49).

3-2-3 ECM proteins are expressed in the intercellular site and are required for contact following

As previously described, integrin-β1 is an ECM receptor for collagen, laminin and fibronectin [41]. As the activity of intercellular integrin-β1 was required for intercellular adhesion and contact following, we hypothesized that ECM proteins exist in the intercellular site. By investigating the localization of several ECM proteins using immunofluorescent staining, it was found that type-XVII collagen (COL17) is expressed in the intercellular sites (Fig. 3.13). COL17 is a transmembrane collagen, but its extracellular domain is secreted into the surrounding ECM as its cleavage form [58, 59]. It was confirmed that the cleavage form of COL17 is secreted in A431 cells (Fig. 3.14). In addition, laminin-α3 and laminin-β3 constituting of laminin-332 were also expressed in the intercellular sites (Fig. 3.15). Type-I collagen, type-IV collagen, fibronectin, laminin-α1, and laminin-γ1 were not expressed in the intercellular sites (Fig. 3.16, 17).

Next, intercellular ECM proteins was depleted using small interference RNA (siRNA) to investigate the role of intercellular ECM proteins (Fig. 3.18). Depletion of ECM protein significantly suppressed contact following (Fig. 3.19, 20). The data indicate the expression of intercellular ECM proteins is also required for contact following. Furthermore, these results suggest that the interaction between integrin-β1 and ECM proteins in the intercellular sites promote contact following in collective invasion.

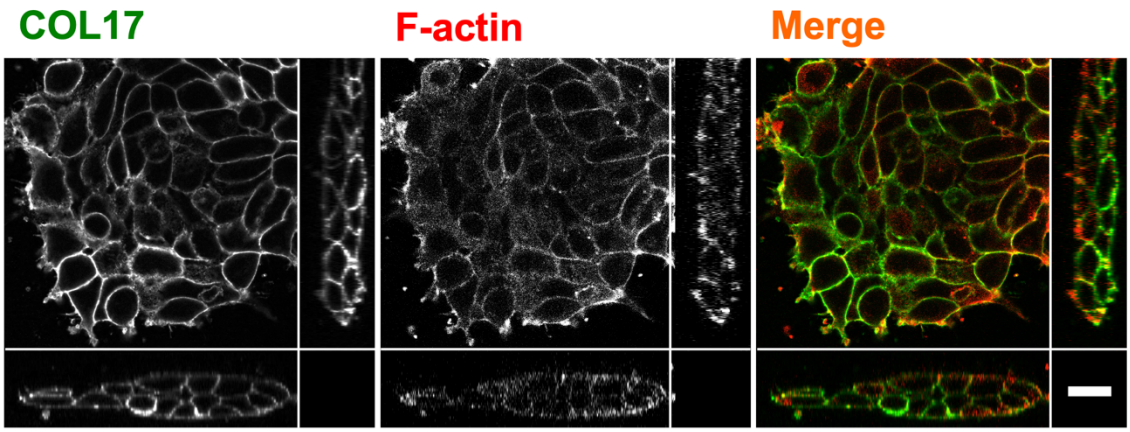

Fig. 3.13 Immunofluorescent staining of type-XVII collagen (COL17).

XY-, YZ-, and ZX-sectional views are shown. Green: COL17. Red: F-actin. The Scale bar represents 25 μm.

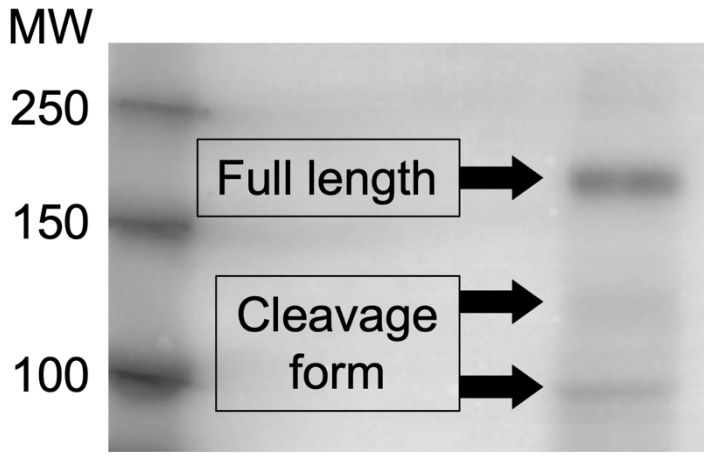

Fig. 3.14 Western blotting for COL17 with anti-extracellular domain of COL17 antibody.

The arrows show COL17 bands around 180, 120, and 97 kDa.

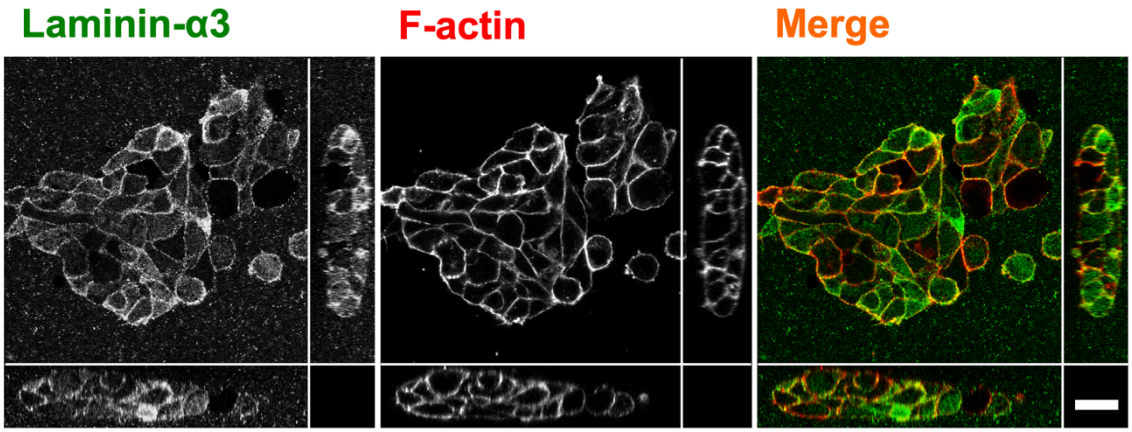

Fig. 3.15 Immunofluorescent staining of laminin-α3.

XY-, YZ-, and ZX-sectional views are shown. Green: laminin-α3. Red: F-actin. The Scale bar represents 25 μm.

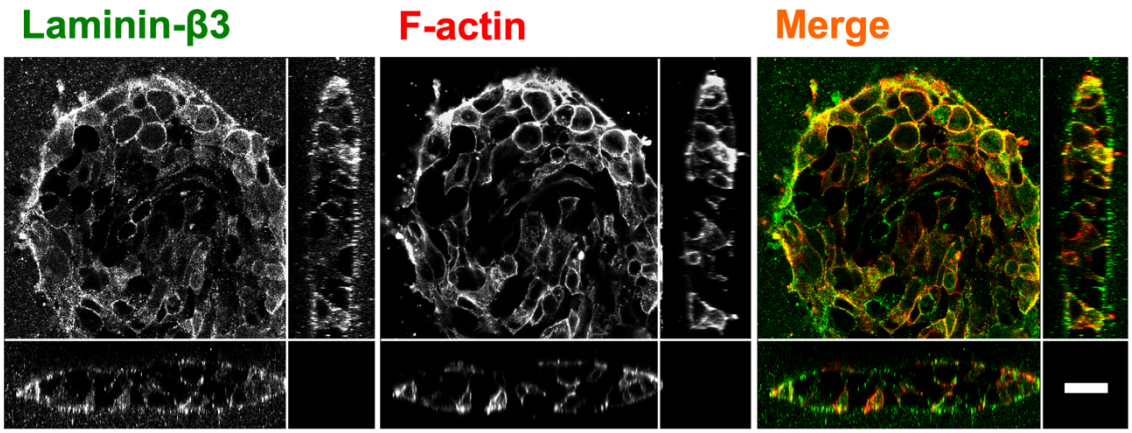

Fig. 3.16 Immunofluorescent staining of laminin-β3.

XY-, YZ-, and ZX-sectional views are shown. Green: laminin-β3. Red: F-actin. The Scale bar represents 25 μm.

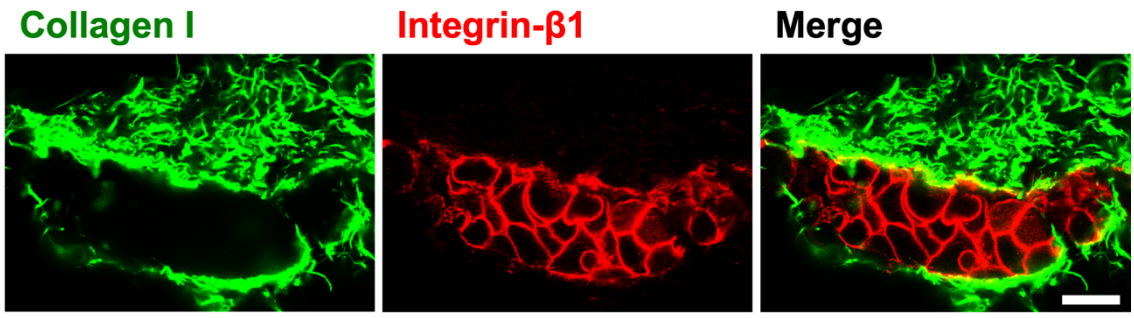

Fig. 3.17 Immunofluorescent staining of collagen I and integrin-β1.

Frozen sections of A431 cells cultured in a collagen gel overlay condition were used for immunostaining. Green: collagen I. Red: integrin-β1. The Scale bar represents --- μm.

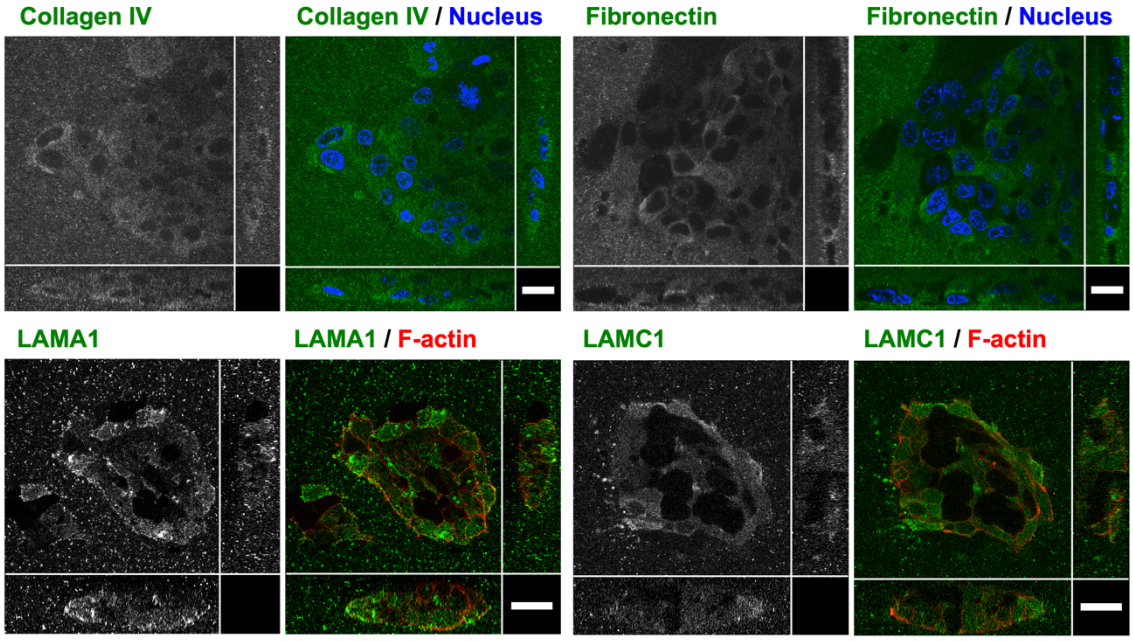

Fig. 3.18 Immunofluorescent staining of candidate ECM proteins.

XY-, YZ-, and ZX-sectional views are shown. Green:---. Red: F-actin. The Scale bar represents 25 μm.

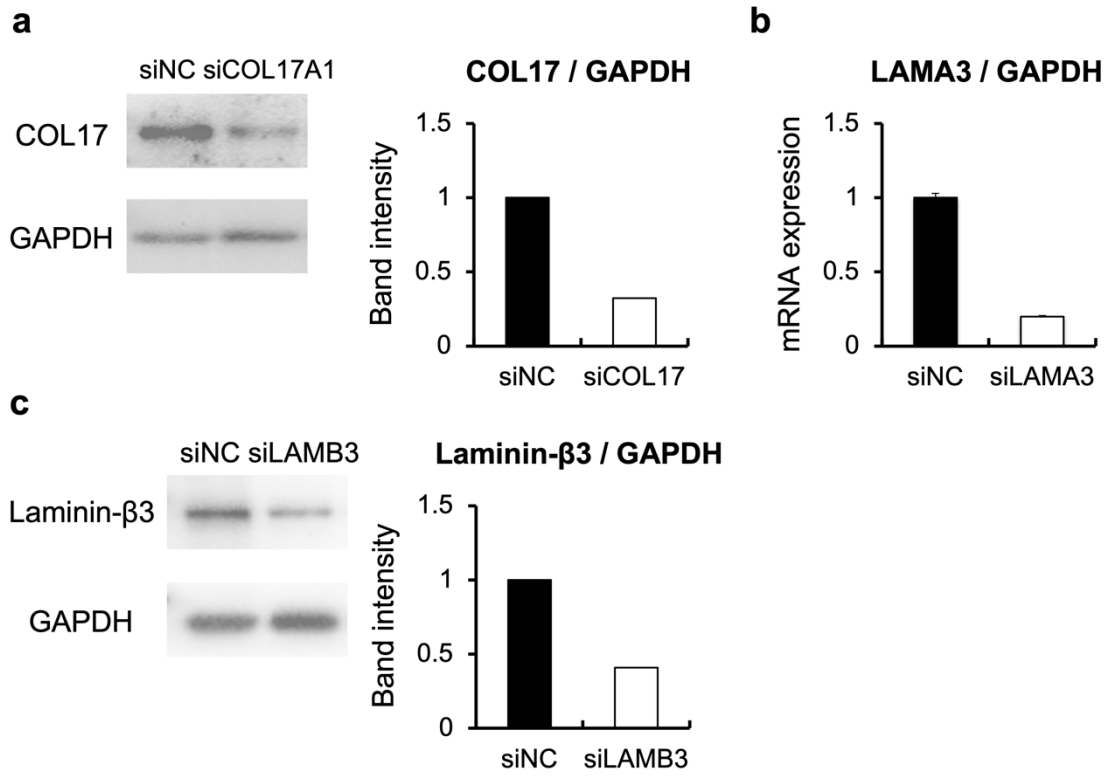

Fig. 3.19 Confirmation of knockdown efficiency with siRNA.

(a) Representative result of western blotting. siNC: negative control siRNA-treated cells. siCOL17A1: COL17 coding gene knockdowned cells. GAPDH was used for normalization as an endogenous control in quantification. (b) RT-qPCR result to check depletion of laminin-α3 mRNA. siLAMA3: laminin-α3 coding gene knockdowned cells. GAPDH was used for normalization as an endogenous control in quantification. (c) Representative result of western blotting. siLAMB3: laminin-β3 coding gene knockdowned cells. GAPDH was used for normalization as an endogenous control in quantification.

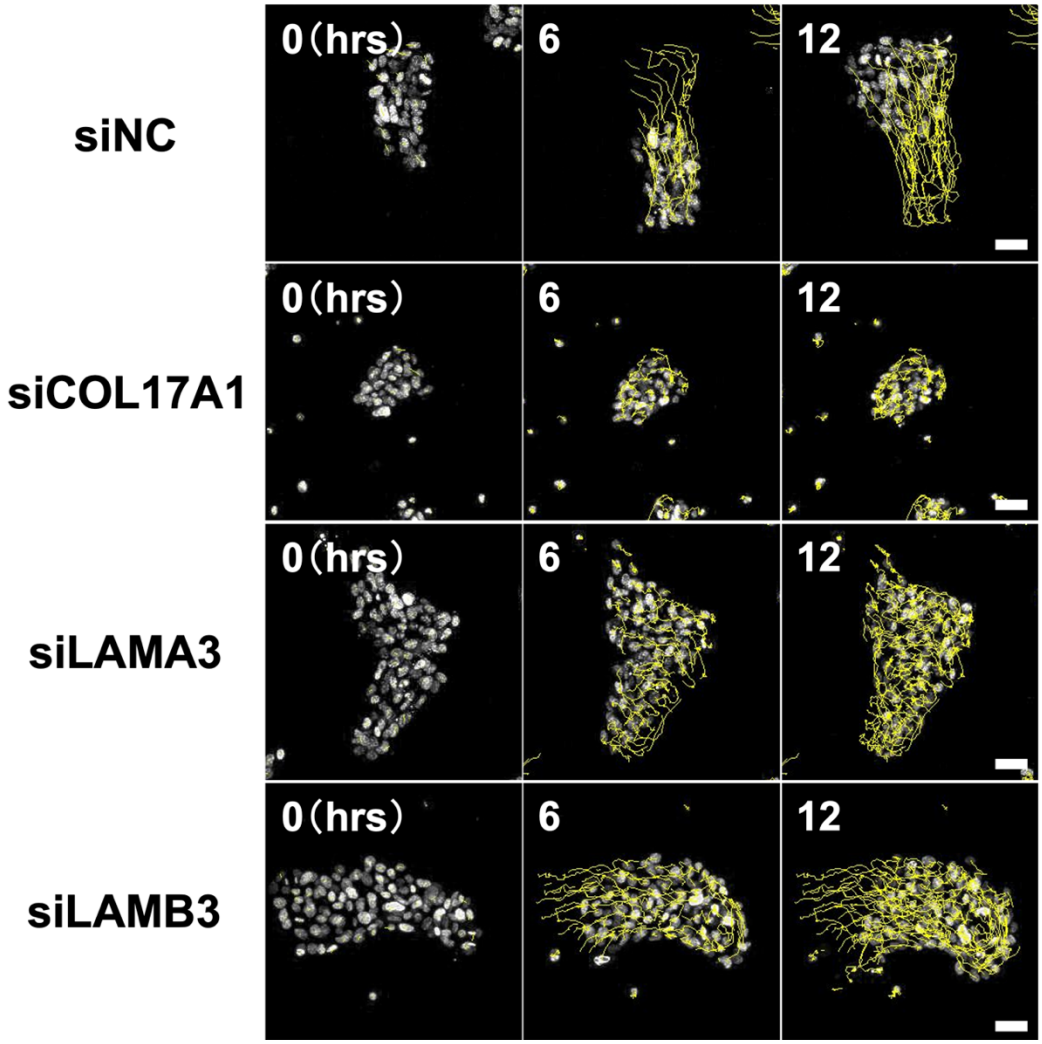

Fig. 3.20 Time-lapse observation of A431-emerald cells in ECM protein depleted conditions.
Time-lapse observation of A431-emerald cells in each knockdown condition. The top panels show the cells treated with negative control siRNA (siNC). Other panels show the cells treated with siRNA targeting COL17 (siCOL17A1; second), laminin-α3 (siLAMA3: third), laminin-β3 (siLAMB3; bottom). Yellow lines are the trajectory of cell movement. Scale bars represent 50 μm.

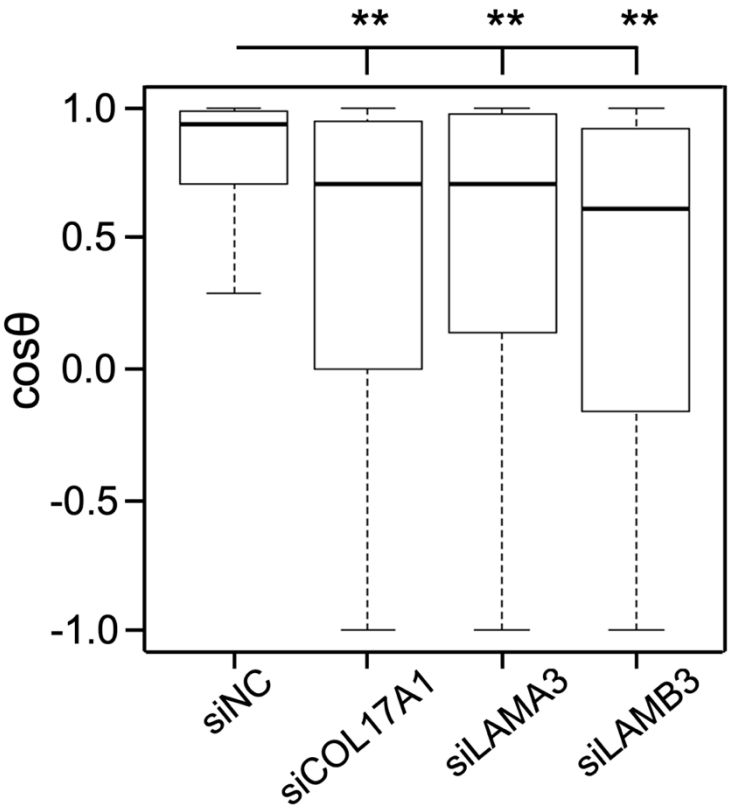

Fig. 3.21 Evaluation of contact following using cosine function in ECM protein depleted A431 cells.

Quantification of cosine values, cosθ. Boxplot shows median levels of cosθ in each knockdown condition. Boxes show interquartile range. Bars show maximum and minimum values within 1.5 IQR. **P < 0.01 by Wilcoxon rank sum test (n > 40).

3-2-4 The interaction between integrin-β1 and ECM proteins

The capacity of complex formation between integrin-β1 and ECM proteins was then investigated. Previous studies suggest that integrin-β1 interact with COL17 in HEK293 cells [72]. Therefore, whether integrin-β1 and COL17 form a complex by immunoprecipitation (IP) using anti-COL17 was investigated. As a result of the IP experiment, integrin-β1 was not detected in the obtained IP fraction of COL17 (Fig. 3.22). Thus, we could not prove a complex formation of integrin-β1 and COL17. Next, the complex formation between COL17 and laminin-332 was investigated. IP experiment showed that laminin-β3 was detected in the obtained IP fraction of COL17 (Fig. 3.22). As laminin-332 is the major ligand of integrin-β1, it was hypothesized that COL17 affects the interaction between integrin-β1 and laminin-332. Therefore, the influence of COL17 depletion on laminin-332 expression was investigated. As a result of quantification, COL17 depletion significantly suppressed laminin-β3 levels (Fig. 3.23). Therefore, it is suggested that the COL17 level modulates the interaction between integrin-β1 and laminin-332 by controlling laminin-332 levels.

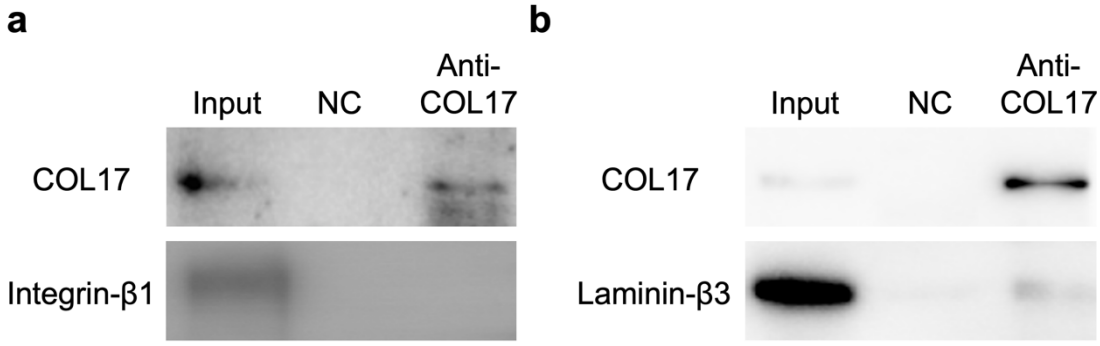

Fig. 3.22 COL17 formed a complex with laminin-β3.

Input obtained from A431 cells were immunoprecipitated with anti- COL17 antibody followed by western blotting with indicated antibodies. (a) integrin-β1 (b) laminin-β3

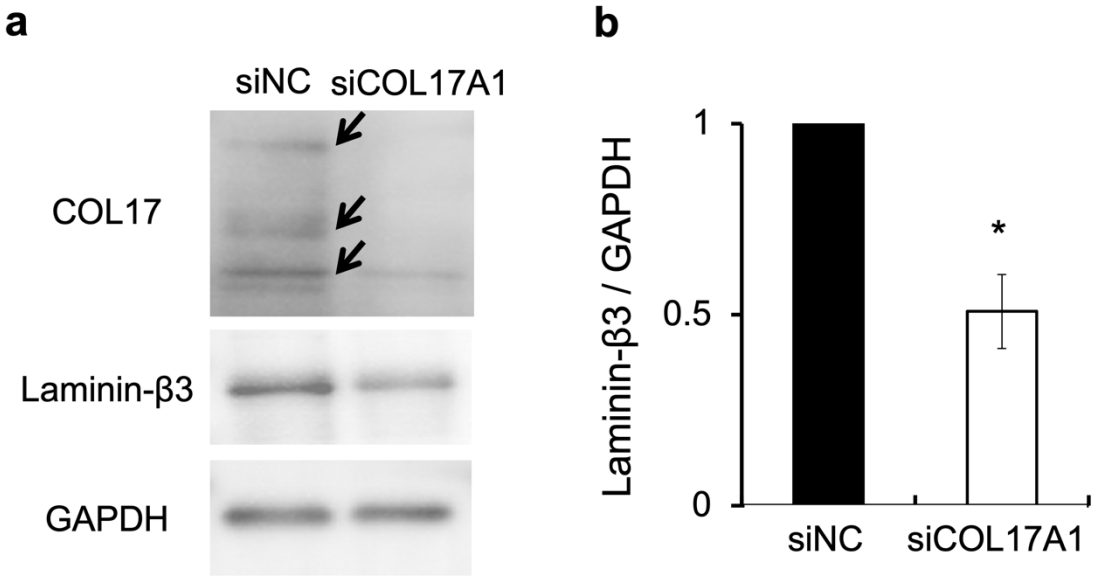

Fig. 3.23 COL17 depletion decreased laminin-β3 protein level.

(a) Representative western blotting. The arrows show COL17 bands around 180, 120, and 97 kDa. (b) Quantification of (a). The bars represent mean ± SEM. in 3 independent experiments. *P < 0.05 by Welch's t-test.

3-2-5 The high expression of integrin-β1 and ECM proteins positively correlates with the poor prognosis of various patients with SCC

The relationship between gene expression and the overall survival of patients with SCC was examined based on the data of cervical, head-neck, and lung squamous cell carcinoma present in the Kaplan Meier-plotter [73]. Significant positive correlation between high gene expression and poor prognosis of the patients with SCC was found in cervical and lung SCC in ITGB1 (Fig. 3.24a), lung SCC in COL17A1 (Fig. 3.24b), cervical SCC in LAMA3 (Fig. 3.24c), and each SCC in LAMB3 (Fig. 3.24d). No significant negative correlation with the poor prognosis of SCC patients was found in the high expression of each gene. Therefore, the genes regulating contact following may contribute to SCC progression.

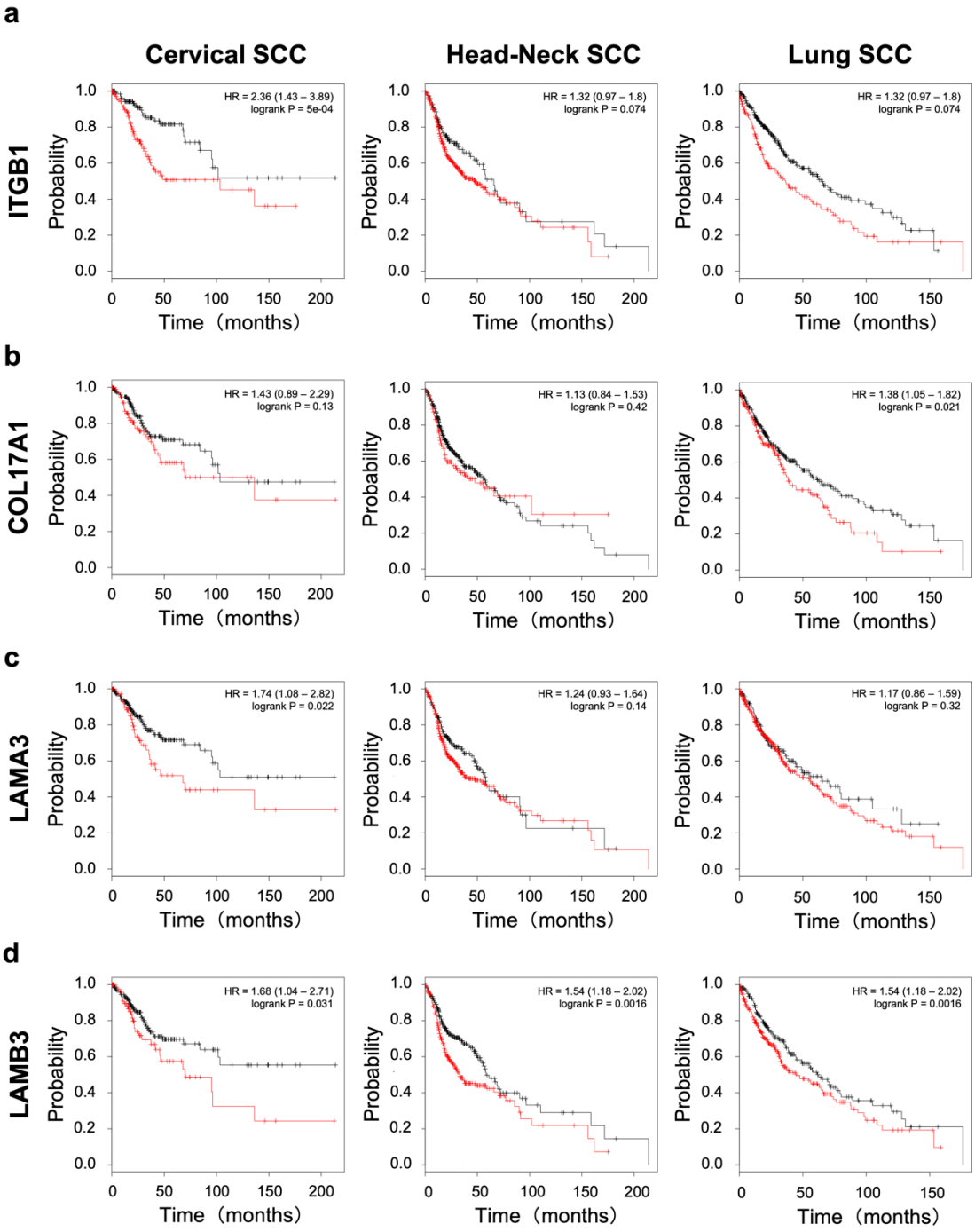

Fig. 3.24 The high expression of integrin-β1 and ECM proteins positively correlates with the poor prognosis in various patients with SCC.

The high expression of ITGB1 (a), COL17A1 (b), LAMA3 (c), and LAMB3 (d) is correlated with a poor prognosis for some types of SCC. Kaplan–Meier survival curves show the probability of overall survival. Red lines indicate patients with high expression of the gene and black lines indicate patients with low expression of the gene.

3-3 Discussion

In this study, we established a novel evaluation system for contact following in collective invasion. A431 cells showed two-dimensional collective movement in collagen gel overlay conditions. In addition, this system enabled the automatic tracking of cell movement, whereby contact following in collective invasion could be investigated. In the existing experimental system, cancer cells needed several days to invade collectively [71]. On the other hand, A431 cells invaded on a short time scale of a few hours in our experimental system. As a result, experimental tools acting immediately such as molecular inhibitors and siRNA are applicable. Furthermore, a new method was also developed to analyze contact following using the cosine function. When movement direction is measured using an angle, the measurement becomes a circular variable that ranges from 0 to 360°. Therefore, in contact following analysis, x and (360-x) degrees refer to the same direction. However, cosine functions determine the association of directions uniquely i.e., cos(x) = cos(360-x). Thus, cosine transformation does not require the circular statistics method to analyze contact following.

The activity of integrin-β1 in the intercellular site was found to regulate contact following in the collective invasion of A431 cells. Moreover, this study shows that laminin-332, a ligand of integrin-β1, is expressed in the intercellular site and is required for contact following. Furthermore, COL17 levels modulate contact following via the regulation of laminin-332 levels. A previous study shows that integrin-β1 contributes to not only cell-matrix adhesion but also intercellular adhesion [74]. In addition, structural ECM such as fibronectin mediates intercellular adhesion by integrin-β1 in glioblastoma [75]. In A431 cells, laminin-332 exists in the intercellular site and is required for collectiveness. As laminin-332 is a major component of the basement membrane, it was considered that the basement membrane-like structural ECM consisting of laminin-332 exists in the intercellular site. However, it was not possible to observe a structural ECM in the intercellular site through electron microscopy. Intriguingly, laminin-332 promotes cancer progression as not only structural ECM but also autocrine soluble factor via binding to cell surface integrins [67]. Therefore laminin-332 is expected to act as a soluble factor in the intercellular site of A431 cells.

COL17 is cleaved by proteases on the cell surface, whereby the extracellular domain is secreted into the surrounding ECM [76]. The extracellular cleavage of COL17 is required for correct cutaneous basement membrane formation by contributing to the stabilization of laminin-332 [58]. Here we showed that the cleavage form of COL17 is secreted in A431 cells and COL17 levels control laminin-β3 levels, which is a constituent of laminin-332. The data suggested that COL17 modulates the interaction between integrin-β1 and laminin-332 by regulating laminin-β3, whereby COL17 contributes to contact following (Fig. 3.25).

Taken together, here we suggest that the interaction of integrin-β1 and laminin-332 is a key regulator of contact following in the collective invasion of A431 cells. Therefore, it is possible that inhibition of this interaction may be an effective way to suppress collective invasion in cancer cells.

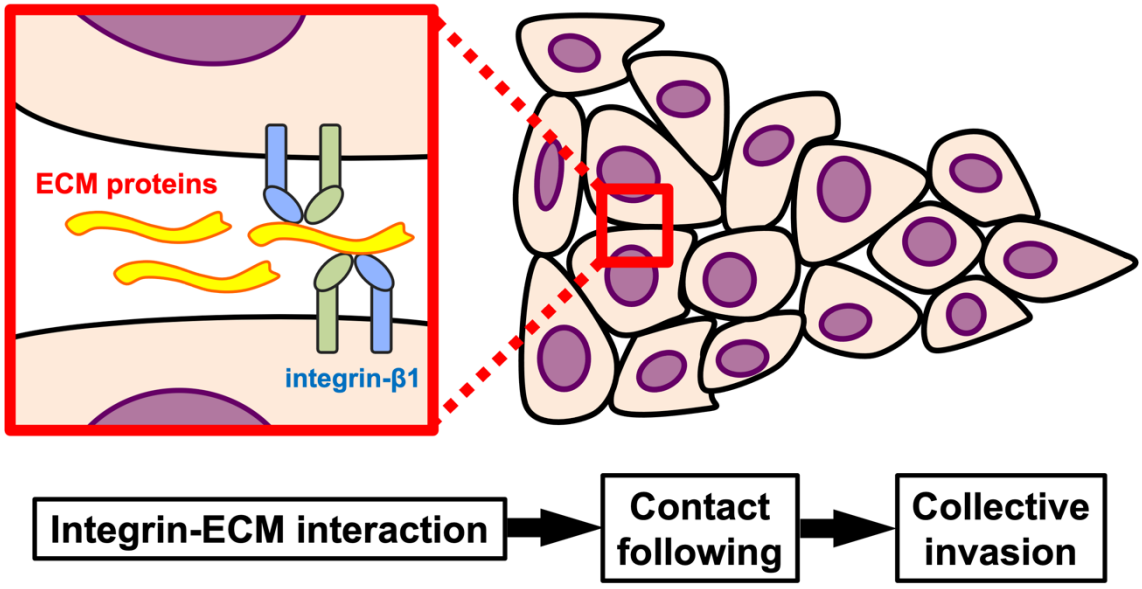

Fig. 3.25 A model of contact following in cancer collective invasion

Integrin-β1, COL17, and laminin-332 are localized to the intercellular site of the cancer cell population with collective invasive potential. COL17 forms a complex with laminin-332 and contributes to laminin-332 stabilization. Laminin-332 activates integrin-β1, and active integrin-β1 promotes contact following in the collective invasion of a cancer cell population.

Chapter 4

Interferon-β in sealed intercellular spaces drives the collective invasion of skin squamous cell carcinoma via STAT1 activation

4-1 Introduction

4-1-1 Interferons and STAT1

Interferons are expressed in response to viral infection and classified as either Type-I or Type-II [77, 78]. Virus-infected cells undergo programmed cell death, represented by apoptosis, to prevent viral replication and dissemination. Interferons induce apoptosis via activation of caspases by cytochrome c released from mitochondria [79, 80]. Type-I interferons are subdivided into alpha, beta, delta, epsilon, kappa, tau, and omega [77, 78, 81]. These have considerable structural homology, and all binds a common cell-surface receptor, which is known as type-I interferon receptor (IFNAR) [35]. By contrast, interferon-gamma is only one Type-II interferon and binds a different cell-surface receptor, which is known as type-II interferon receptor [82]. Interferon-gamma is a basically different protein than the type-I interferons, but it was classified as an interferon family because it functions similarly to type-I interferons [78].

As described above, interferons are widely known to contribute to viral response by causing cell death of virus-infected cells. However, interferons also affect many other cellular functions, such as cell growth and resistance to cell deaths, in cancer [83, 84]. In addition, these functions of interferons are mainly mediated by signal transducer and activator of transcription 1 (STAT1) (Fig.4.1) [35, 85]. STAT1 is a transcription factor that responds to interferons and is universally expressed in a variety of cell types, including cancer cells [86]. Phosphorylated STAT1 is the active form to translocate to nucleus, and interferons promote phosphorylation of STAT1 via dimerization of its receptors and activation of Janus kinase (JAK), an IFNAR-coupled kinase. STAT1 activation enhanced proliferation, invasiveness, and resistance to apoptosis in various cancer in vivo and in vitro [87, 88]. Furthermore, increased expression of STAT1 has been shown to be involved in resistance to radiotherapy in clinical practice [89]. The contribution of STAT1 to cancer malignancy has been reported in previous studies; however, its role in collective invasion and collective metastasis remains unclear.

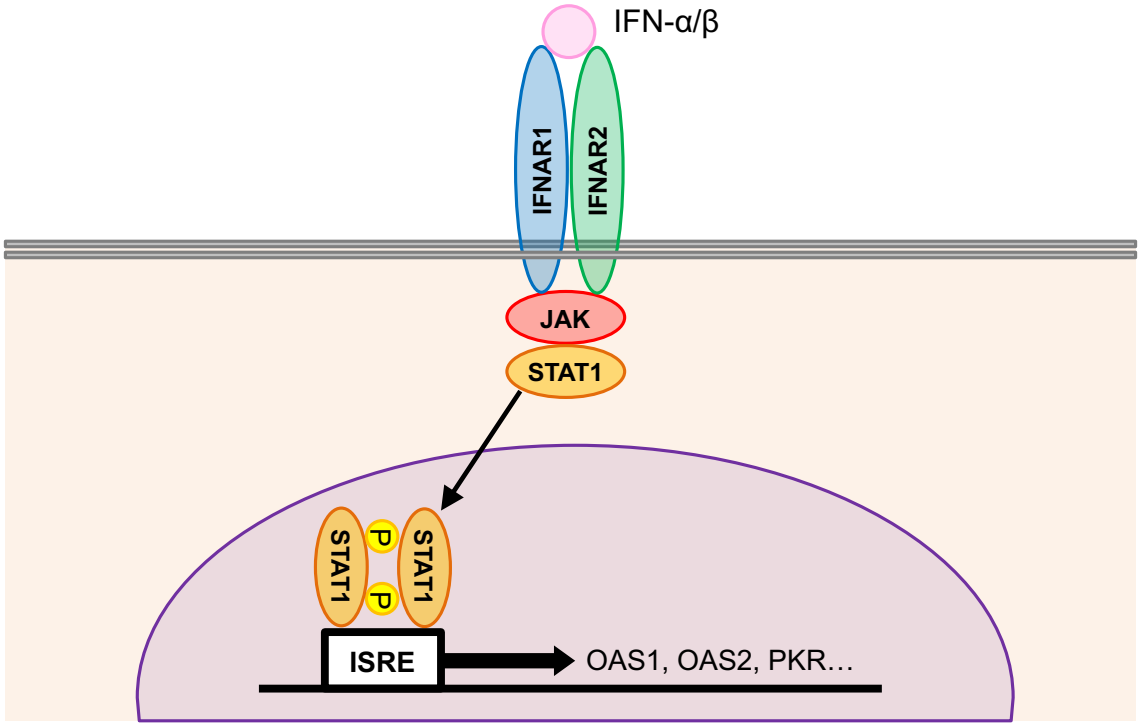

Fig. 4.1 General type-I interferon pathway through STAT1 activation.

Type-I interferons (IFN-α/β) induce dimerization of IFNAR1 and IFNAR2, resulting autophosphorylation of JAK. JAK can activate STAT1, which binds to ISRE promoter region.

4-1-2 Cancer heterogeneity

Recently, it has been reported that collective invasion occurs in a cancer cell cluster consisting of polyclonal cancer cells [26, 90, 91]. This leads to metastatic foci consisting of polyclonal cancer cells, causing heterogeneity of metastases (Fig.4.2) [26, 32, 90-92]. In targeted therapy, minority cancer cells that are not targeted by drugs can survive [93]. In addition, minority cancer cells support drug resistance and growth in dominant cancer cells [94]. Thus, the heterogeneity of cancer cells is associated with difficulties in targeted cancer therapy. Since collective invasion generates heterogeneity of metastases, inhibition of collective invasion is considered to improve cancer treatment. Attacking the cells that drive collective invasion in polyclonal cancer cells could achieve this inhibition; however, such cells are not well understood. Thus, we carried out subcloning of a cancer cell population to identify the cells responsible for collective invasion, and upregulated signaling pathways in these cells were investigated.

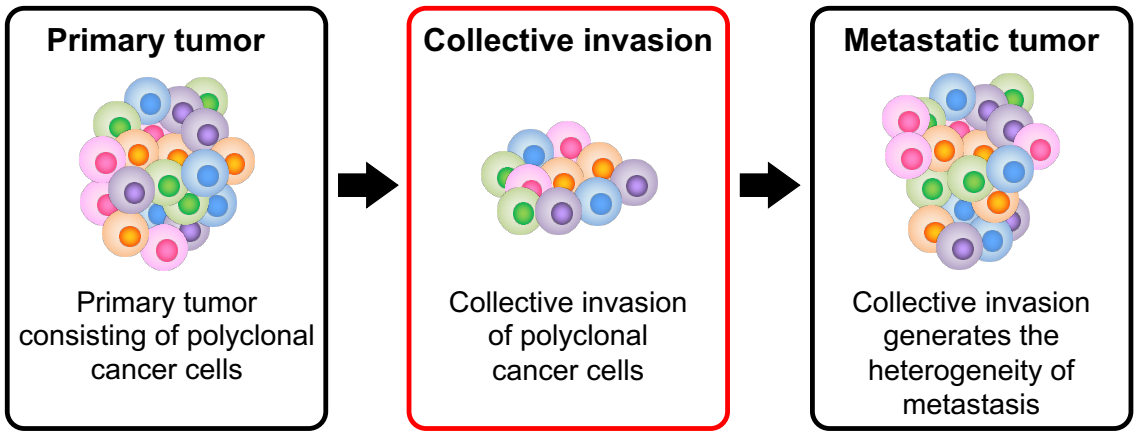

Fig. 4.2 Heterogeneity of metastasis caused by collective invasion from primary tumor.
Collective invasion leads to metastatic foci consisting polyclonal and heterogenous cancer cell population because primary tumor is also polyclonal and heterogenous. Therefore, appropriate target cells to inhibit collective invasion is unclear.

4-2 Results

4-2-1 Establishment of A431 subclones with various invasiveness from A431 wild type cells consisted of heterogeneous cells.

Collective cancer cell invasion was evaluated using single cell-derived spheroid invasion assay in a collagen gel. To assess the invasive potential of each cell in a cancer cell line, cells were embedded in collagen gels at a low cell density (6 × 104 cells in 600 μL of collagen gel). In this experimental system, single cell-derived spheroids were formed by seeding cells at a low density, and the spheroids invaded the surrounding collagen gel. This invasive property of cells was used to assess the invasiveness of cancer cells. First, we examined the invasiveness of A431-wild type (WT) cells by culturing in this experimental system and found that A431-WT cells consisted of invasive and non-invasive cells (Fig. 4.3); invasive cell clusters formed invasive protrusions into the surrounding matrix, whereas non-invasive cell clusters showed a round-shaped morphology without invasive protrusion, suggesting that A431-WT cells are a mixture of cells with various invasive potential. In addition, the invasive protrusion consisted of multiple cells, indicating that collective invasion occurred (Fig. 4.4). The Imaris software was used for three-dimensional image construction in order to calculate the sphericity of cell clusters based on their surface area and volume to quantify collective invasion (Fig. 4.4). When a cell cluster exhibits a round morphology without invasion, its sphericity value approaches 1 (Fig. 4.5). Conversely, when a cell cluster invades the surrounding matrix, the surface area of the cell cluster increases because of the bumpy surface; therefore, its sphericity approaches zero (Fig. 4.5). Thus, because sphericity and invasiveness are inversely correlated, we defined sphericity as an index of collective invasion. Since A431-WT cells are a mixture of heterogeneous cells, subcloning of A431-WT cells was performed to establish subclones with different invasive potentials using limited dilution method. We established a total of 20 subclones (A431-1 to A431-20) and assessed their sphericity as an indicator for invasiveness (Fig. 4.6). A431-3, 8, 12, 18, and 19 cells were omitted because they did not form a cell cluster (e.g., cell deaths or no cell-cell junction) that could be evaluated. From the data, we selected A431-6 as a high-invasive subclone and A431-7 as a low-invasive subclone, which exhibited bumpy-shaped morphology with invasion and round-shaped morphology without invasion, respectively (Fig. 4.7 and 4.8). We confirmed that the sphericity of A431-6 cell clusters was observed to be significantly lower than that of A431-7 cell clusters (Fig. 4.9). Furthermore, the volume of A431-6 cell clusters was significantly larger than that of A431-7 cell clusters, indicating that the proliferative capacity of A431-6 subclone was higher than that of A431-7 (Fig. 4.10). In addition, A431-6 and A431-7 subclones retained their differences in invasiveness, even after undergoing 13 passages each (Fig. 4.11). Taken together,

we succeeded in establishing subclones with different invasiveness and a novel and unique system for evaluating collective invasion by analyzing the sphericity of cell clusters.

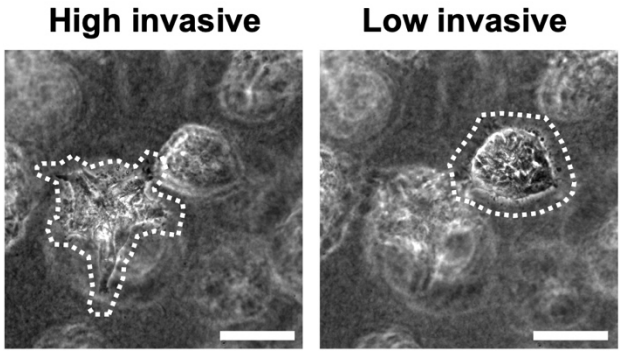

Fig. 4.3 There are various invasive cell clusters in A431-WT cells

Representative phase-contrast images of the invasive cell cluster (left) and low-invasive cell cluster (right) in A431-WT cells cultured in a three-dimensional collagen gel culture system; both were captured in the same field. The dotted lines show the contours of the cell clusters. Scale bars represent 100 μm.

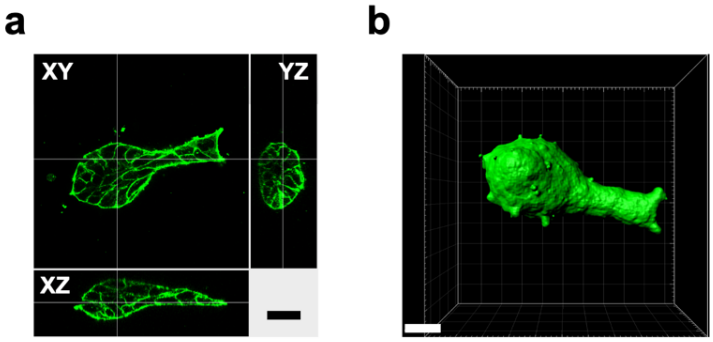

Fig. 4.4 Three-dimensional image construction of an invasive cell cluster.

(a) F-actin staining of the invasive cell cluster in A431-WT cells cultured in three-dimensional collagen gel culture with XY, YZ, and XZ sectional views. Scale bar represents 25 μm. (b) Three-dimensional constructed image of (a) using the Imaris software. Scale bar represents 30 μm.

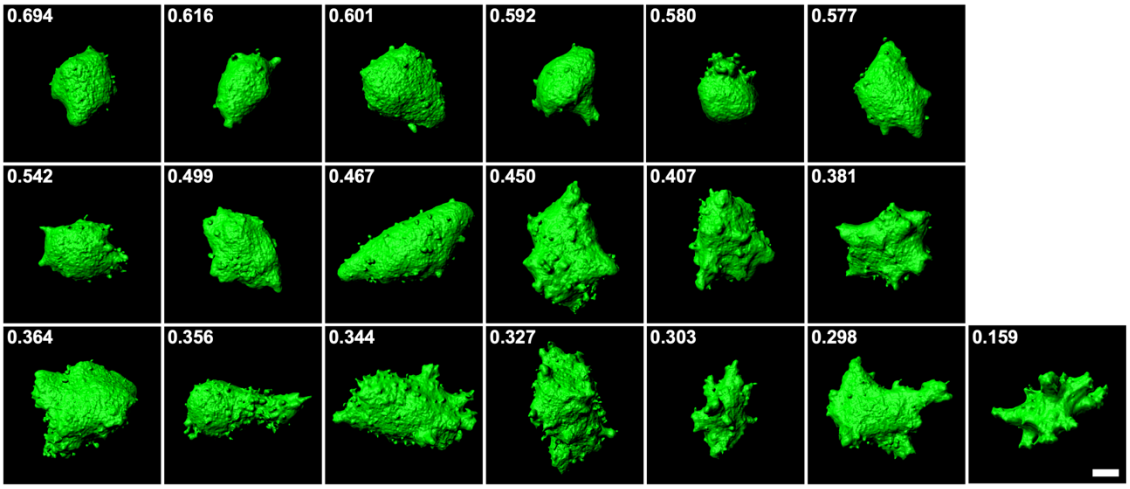

Fig. 4.5 Sphericity of A431-WT cell clusters.

Three-dimensional constructed images of A431-WT cell clusters cultured in a three-dimensional collagen gel culture system. The values show the sphericity of each cell cluster. Scale bars represent 30 μm.

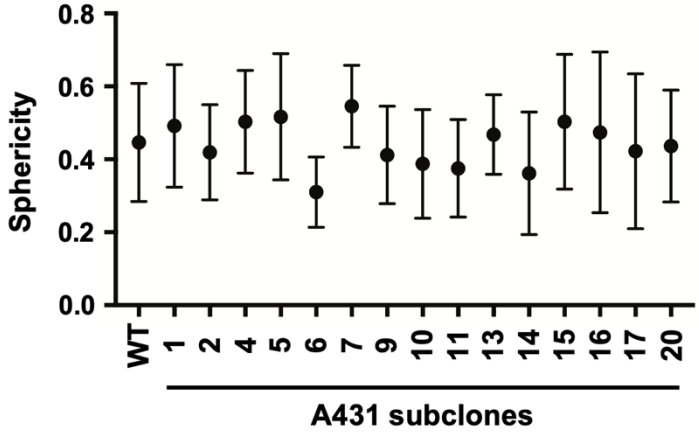

Fig. 4.6 Sphericity of established A431 subclones.

Sphericity of the cell clusters in each subclone. The dots show the mean with standard deviation (SD) for 10 clusters.

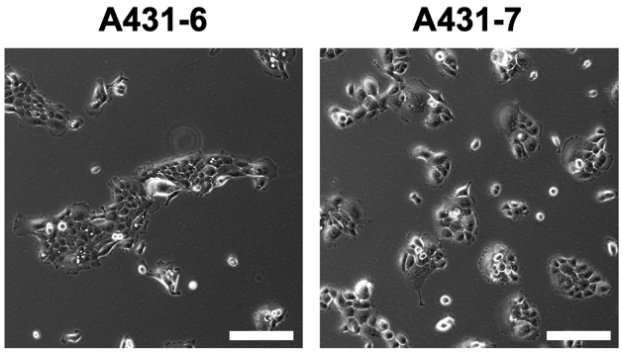

Fig. 4.7 Phase contrast images of A431 subclones

Phase contrast images of the high-invasive A431-6 and low-invasive A431-7 subclones. Scale bars represent 200 μm.

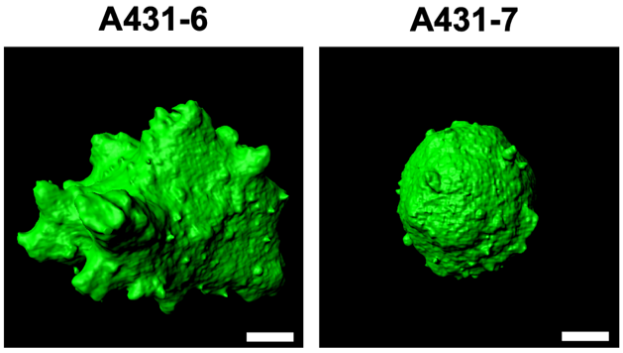

Fig. 4.8 The 3D image of A431-6 and A431-7 cell cluster.

Representative three-dimensional constructed images of A431-6 and A431-7 cell clusters cultured in a three-dimensional collagen gel culture system. The sphericity of A431-6: 0.221 and A431-7: 0.715. Scale bars represent 30 μm.

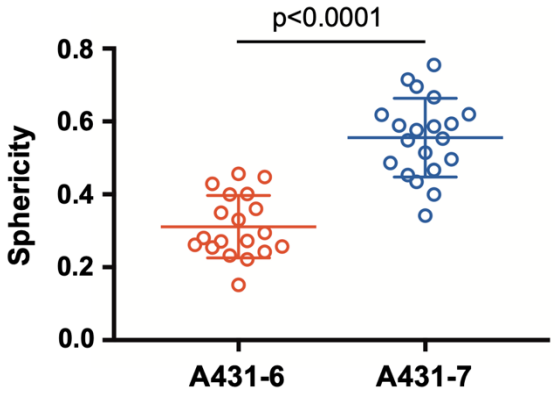

Fig. 4.9 Quantification of sphericity in A431-6 and A431-7 cell clusters.

Lines show the mean with standard deviation (SD) for n = 19 (A431-6) and n = 19 (A431-7) clusters by two independent experiments.

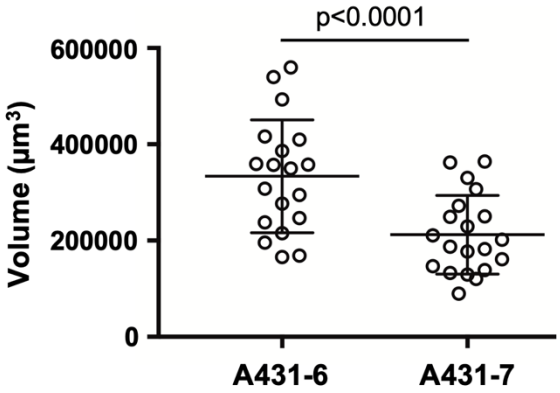

Fig. 4.10 Comparing the volume of sub-clonal cell clusters.

Quantification of the cell cluster volume is shown. 1f. Lines show the mean with standard deviation (SD) for n=19 (A431-6) and n=20 (A431-7) clusters in two independent experiments.

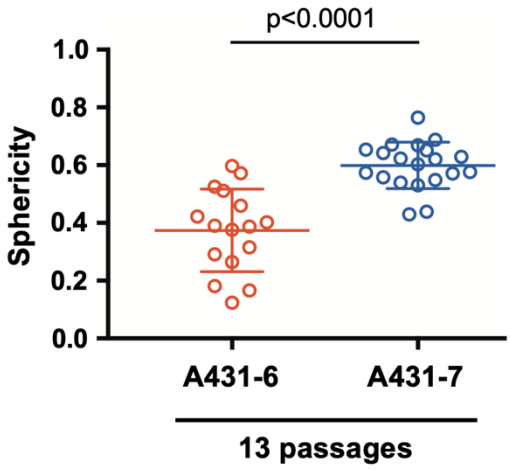

Fig. 4.11 Sphericity of 13 passaged sub-clonal cell clusters.

Sphericity of cell clusters in the A431-6 and A431-7 subclones after 13 passages. Lines show the mean with standard deviation (SD) for n=16 (A431-6) and n=20 clusters in two independent experiments.

4-2-2 STAT1 is necessary for collective invasion of high-invasive A431-6 cells.

Although A431-6 and A431-7 cells were established from the same parental cell line, their invasiveness were significantly different. Thus, we hypothesized that comparing the gene expression profiles of A431-6 and A431-7 cells would be effective for revealing the molecular mechanisms underlying the collective invasion of the cells. We then performed DNA microarray of GeneChip to identify the genes that are differentially expressed in A431-6 and A431-7 cells. DNA microarray analysis revealed that several genes induced by type I interferon, such as interferon-induced protein 44 like (IFI44L) and 2'-5'-oligoadenylate synthetase 2 (OAS2), were notably upregulated in A431-6 cells compared to those in A431-7 cells (Fig.4.12). In addition, we confirmed the reproducibility of the microarray results using quantitative PCR (qPCR) (Fig. 4.13). Gene set enrichment analysis (GSEA) revealed the enrichment of response to type-I interferon in A431-6 cells (Fig. 4.14). The data strongly suggest that the enhancement of the type-I interferon pathway directs collective invasion.

Type-I interferon activates the Janus kinase (JAK)-STAT1 pathway by inducing dimerization of the type-I interferon receptor (IFNAR). STAT1 is phosphorylated by JAK and translocated to the nucleus, where it acts as a transcription factor 31, 32]. Since many genes regulated by STAT1 were highly expressed in A431-6 cells [95], we carried out western blotting to investigate the protein levels of total and phosphorylated STAT1 in each subclone. In A431-7 cells, both STAT1 and phosphorylated STAT1 were detected at negligible levels, whereas A431-6 cells had notable high expression levels (Fig. 4.15), suggesting that the differential activity of STAT1 generates differential gene expression between A431-6 and A431-7 cells. Next, we depleted STAT1 using siRNAs to investigate the role of STAT1 in collective invasion (Fig. 4.16). STAT1 depletion increased the sphericity of A431 cell clusters (Fig.4.17 and 4.18), which suppressed collective invasion. In addition, STAT1 depletion did not affect the volume of the cell clusters, indicating that STAT1 controls collective invasion without affecting cell proliferation (Fig. 4.19). Therefore, factors other than STAT1 might have caused a difference in the proliferative capacity between A431-6 and A431-7 cells. We also confirmed that STAT1 depletion suppressed the collective invasion of the parental A431-WT cells (Fig. 4.20). These findings indicate that STAT1 plays a crucial role in the collective invasion of high-invasive A431-6 and A431-WT cells.

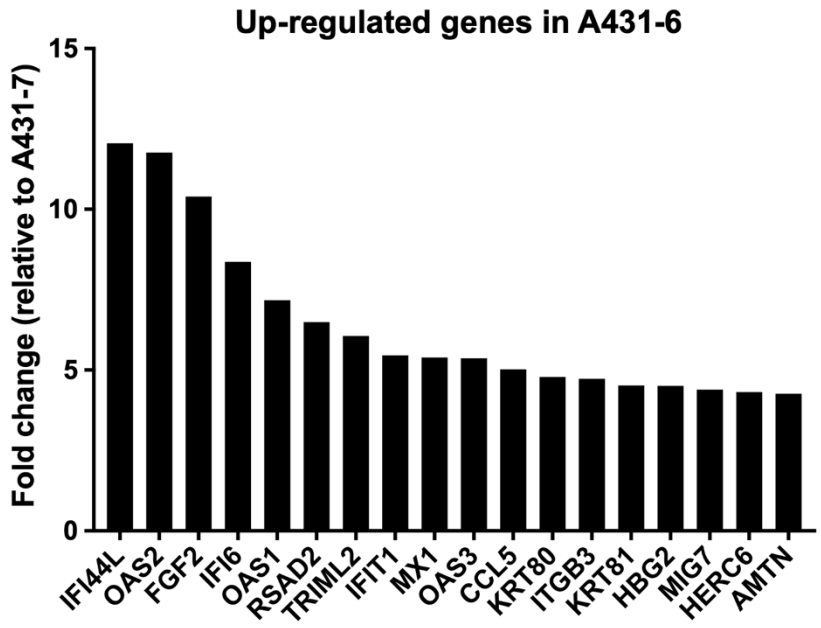

Fig. 4.12 Up-regulated genes in A431-6 subclone comparing to A431-7 subclone.

The DNA microarray result comparing the A431-6 and A431-7 subclones. Genes with more than a 4-fold increase in A431-6 are shown.

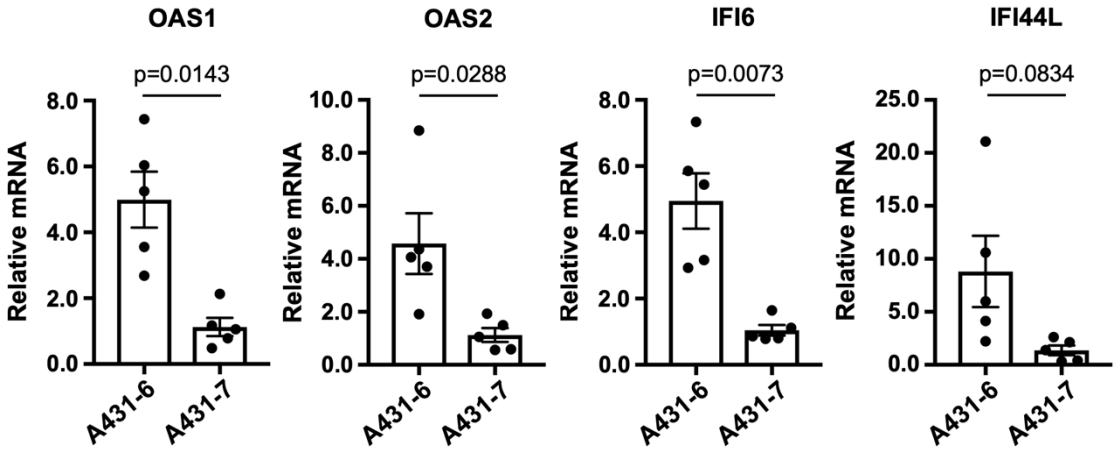

Fig. 4.13 Confirming reproducibility of DNA microarray using RT-qPCR.

RT-qPCR results of the type-I interferon pathway-related genes (OAS; 2'-5'-oligoadenylate synthetase, IFI6; interferon alpha inducible protein 6, IFI44L; interferon-induced protein 44 like) in the A431-6 and A431-7 subclones. Bars represent the mean ± SEM. in five independent experiments.

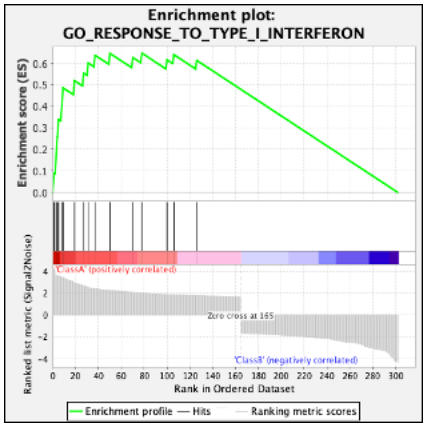

Fig. 4.14 GSEA using the results of DNA microarray.

GSEA showing increased response to type-I interferon in A431-6 cells.

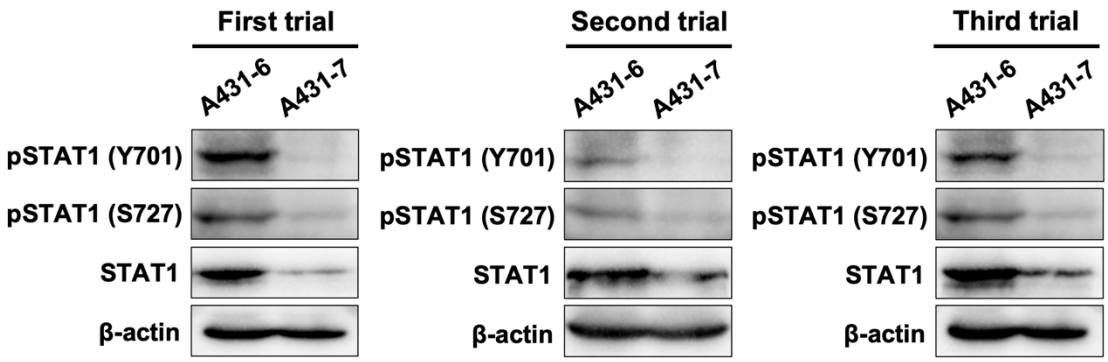

Fig. 4.15 Western blotting for pSTAT1 and STAT1 in A431 subclones.

Western blotting images for pSTAT1 (Y701), pSTAT1 (S727), STAT1, and β-actin in A431-6 and A431-7 cells.

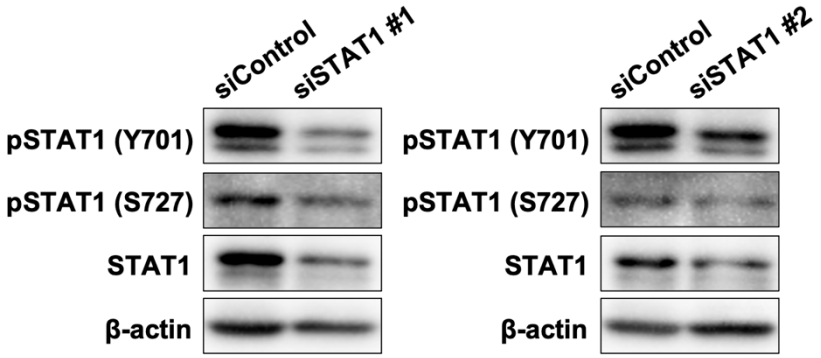

Fig. 4.16 Western blotting for pSTAT1 and STAT1 to confirm STAT1 knockdown.

Western blotting results to validate the knockdown efficiency in siSTAT1#1 or siSTAT1#2-treated A431-6 cells.

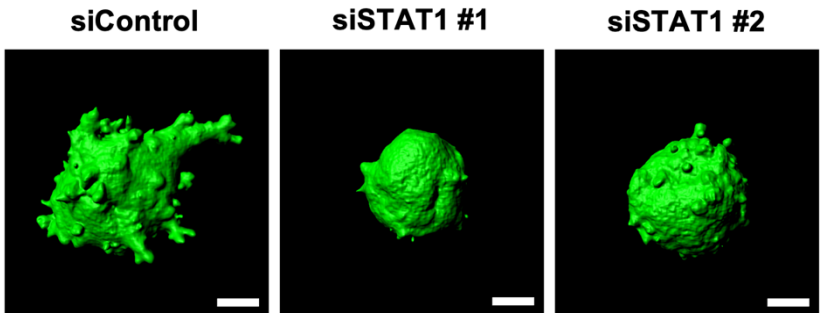

Fig. 4.17 STAT1 depletion suppressed collective invasion of A431-6 cell cluster.

Representative three-dimensional constructed images of siControl-, siSTAT1 #1- or STAT1 #2-treated A431-6 cell clusters cultured in a three-dimensional collagen gel culture system. The sphericity of siControl: 0.263, siSTAT1#1: 0.638, and siSTAT1#2: 0.633. Scale bars represent 30 μm.

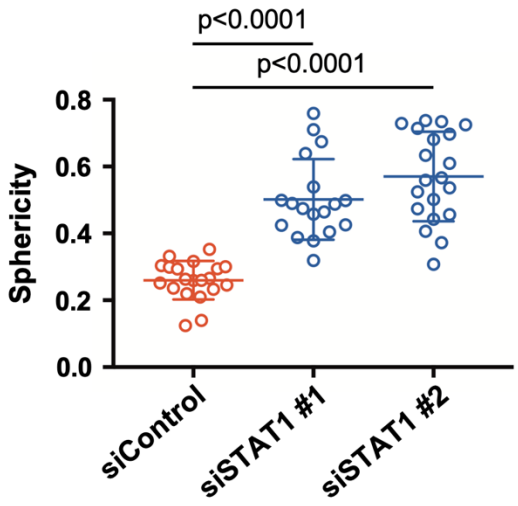

Fig. 4.18 Sphericity of siSTAT1-transfected A431-6 cell cluster.

Quantification of sphericity in Fig. 4.17. Lines show the mean with SD for n = 20 (siControl), n = 18 (siSTAT1#1), and n = 20 (siSTAT1#2) clusters by two independent experiments.

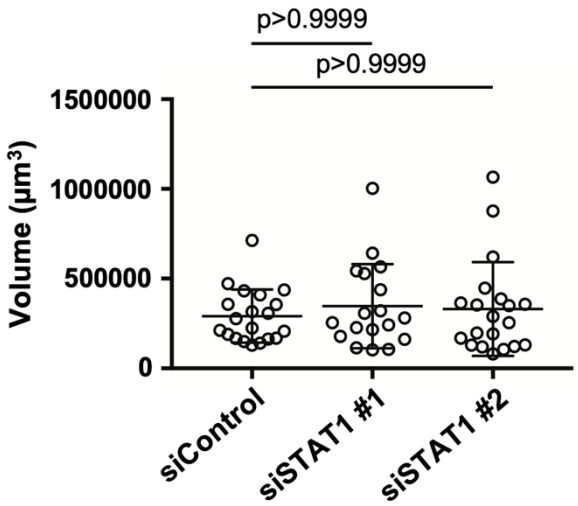

Fig. 4.19 STAT1 depletion was not involved in the volume of cell clusters.

Quantification of the cell cluster volume is shown in Fig. 4.17. Lines show the mean with standard deviation (SD) for n=20 (siControl), n=18 (siSTAT1#1), and n=20 (siSTAT1#2) clusters in two independent experiments.

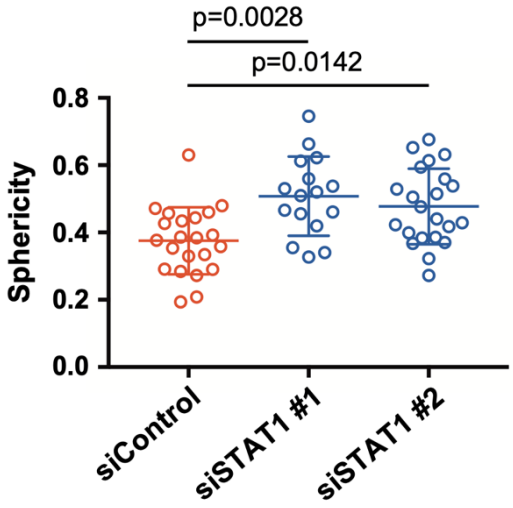

Fig. 4.20 Sphericity of siSTAT1-transfected A431-WT cell cluster.

The sphericity of siControl-, siSTAT1 #1-, or STAT1 #2-treated A431-WT cell clusters were cultured in a three-dimensional collagen gel culture system. Lines show the mean with SD for n=22 (siControl), n=16 (siSTAT1#1), and n=22 (siSTAT1#2) clusters in two independent experiments.

4-2-3 JAK and IFNAR are upstream molecules responsible for STAT1 activity, contributing to collective invasion.

In the type-I interferon pathway, JAK1 is a representative kinase that phosphorylates STAT1 [85]. Because there are notable differences in the phosphorylation of STAT1 between A431-6 and A431-7 cells, western blotting of phosphorylated JAK1 was performed in each subclone. As expected, phosphorylated JAK1 in A431-6 cells was significantly higher than that in A431-7 cells (Fig. 4.21). A431-6 cells were treated with JAK inhibitor I, an inhibitor of all JAKs (JAK1, JAK2, JAK3, and TYK2, at IC50 (15 nM)) to investigate the contribution of JAKs to phosphorylation of STAT1. Since JAK inhibitor I significantly depleted phosphorylated STAT1 in A431-6 cells (Fig. 4.22), it is conceivable that STAT1 is phosphorylated in a JAK-dependent manner. Subsequently, we examined the influence of JAK inhibition on the collective invasion of the A431-6 cell clusters. JAK inhibitor I treatment in A431-6 cells significantly increased sphericity, that is, decreased the collective invasion potential (Fig. 4.23 and 4.24). These data demonstrate that JAK plays an important role in the collective invasion of A431-6 cell clusters by modulating STAT1 activity.

IFNAR, a representative type-I interferon receptor, is a heterodimer consisting of IFNAR1 and IFNAR2 32]. JAK is coupled to IFNARs and transmits signals from the ligand of IFNAR to STAT1 31, 32]. Next, we examined whether IFNAR depletion suppressed the phosphorylation of STAT1 and collective invasion in A431-6 cells (Fig. 4.25). The depletion of IFNAR1 and IFNAR2 by siRNA significantly decreased the amount of phosphorylated STAT1 (Fig. 4.26). Moreover, the sphericity of A431-6 cell clusters was notably increased by siRNA treatment (Fig.4.27 and 4.28). These findings demonstrate that the expression of IFNAR1 and IFNAR2 is required for the phosphorylation of STAT1 and collective invasion in A431-6 cell clusters. These data suggest that type-I interferon modulates STAT1 activity through both JAK and IFNAR.

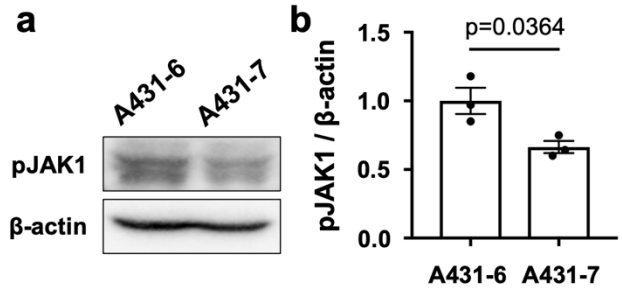

Fig. 4.21 Western blotting for pJAK1 in A431 subclones.

(a) Representative western blotting images for pJAK1 and β-actin in A431-6 and A431-7 cells. (b) Quantification of (a). Bars represent the mean ± standard error of the mean (SEM) of three independent experiments.

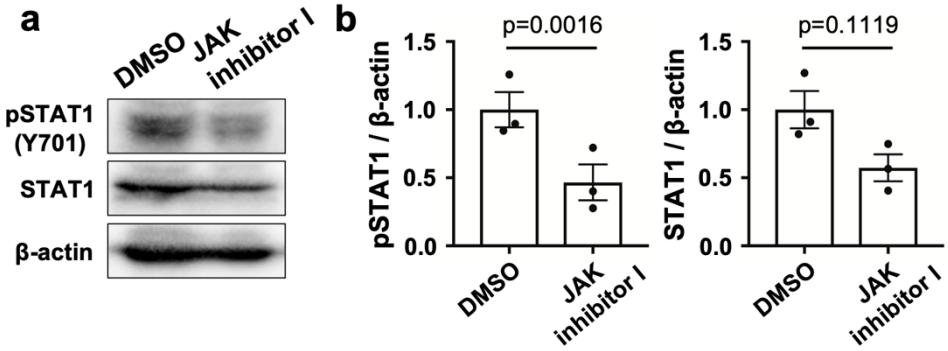

Fig. 4.22 Western blotting to assess the influence of JAK inhibition on pSTAT1.

(a) Representative western blotting images for pSTAT1 (Y701), STAT1, and β-actin in DMSO or JAK inhibitor I (15 nM)-treated A431-6 cells. (b) Quantification of (a). Bars represent the mean ± standard error of the mean (SEM) of three independent experiments.

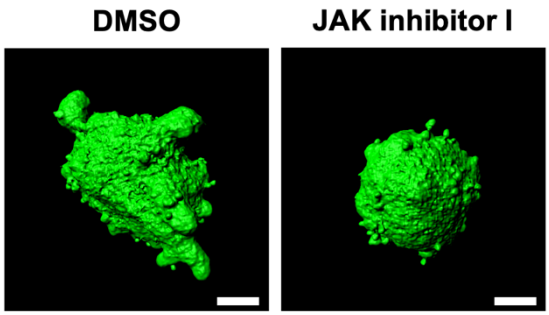

Fig. 4.23 JAK inhibition suppressed collective invasion of A431-6 cell cluster.

Representative three-dimensional constructed images of DMSO or JAK inhibitor I (15 nM)-treated A431-6 cell clusters cultured in a three-dimensional collagen gel culture system. The sphericity of DMSO: 0.247, JAK inhibitor I: 0.671. Scale bars represent 30 μm.

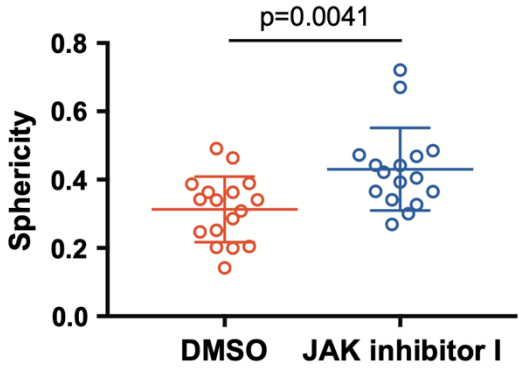

Fig. 4.24 Sphericity of JAK-inhibited A431-6 cell cluster.

Quantification of sphericity in Fig. 4.23. Lines show the mean with SD for n = 17 (DMSO) and n = 16 (JAK inhibitor I) clusters by two independent experiments.

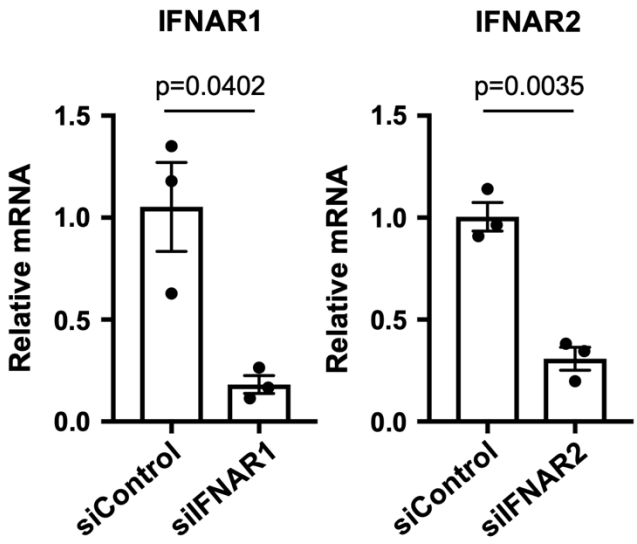

Fig. 4.25 RT-qPCR to confirm knockdown efficiency.

PCR results to validate the knockdown efficiency in siIFNAR1- or siIFNAR2-treated A431-6 cells. Bars represent mean ± SEM. in three independent experiments.

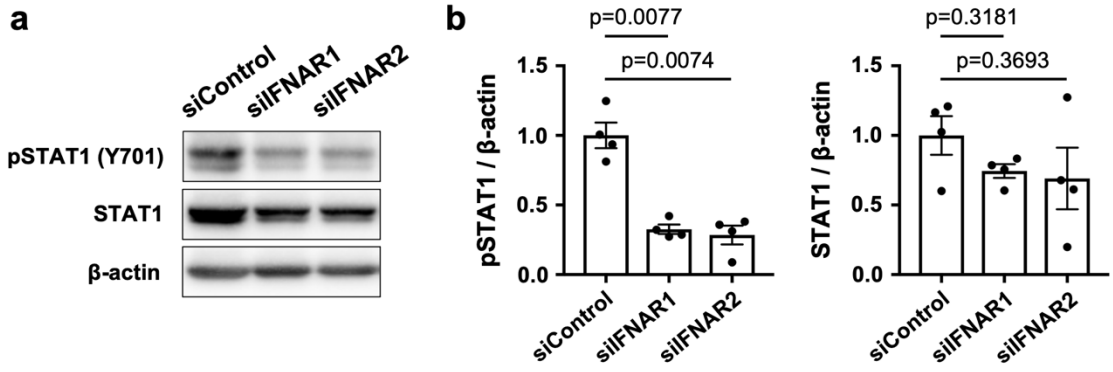

Fig. 4.26 IFNAR depletion suppressed phosphorylation of STAT1.

Representative western blotting images for pSTAT1 (Y701), STAT1, and β-actin in siControl-, siIFNAR1-, or siIFNAR2- treated A431-6 cells. h Quantification of protein bands in (f). Bars represent the mean ± SEM of four independent experiments

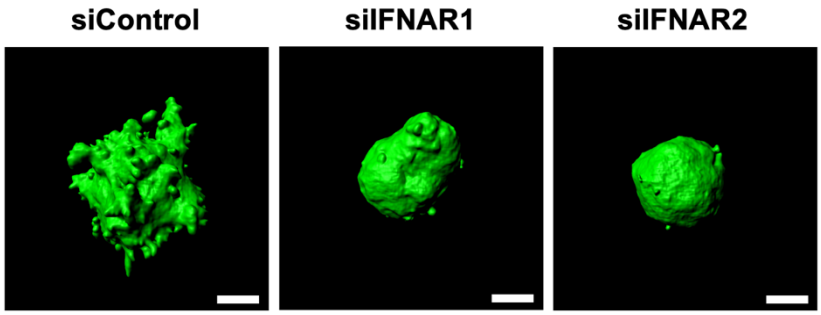

Fig. 4.27 IFNAR depletion suppressed collective invasion of A431-6 cell cluster.

Representative three-dimensional constructed images of siControl, siIFNAR1, or siIFNAR2-treated A431-6 cell clusters cultured a in three-dimensional collagen gel culture system. The sphericity of siControl: 0.176, siIFNAR1: 0.688, and siIFNAR2: 0.712. Scale bars represent 30 μm.

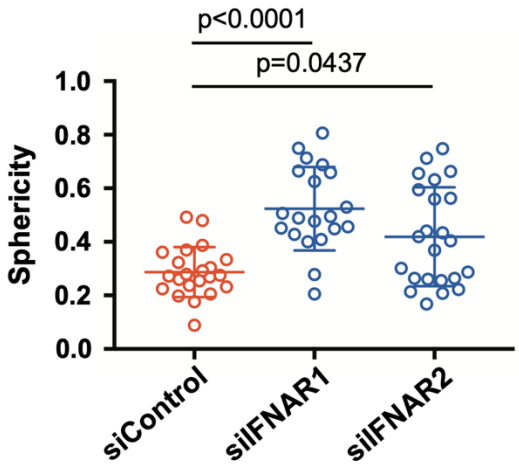

Fig. 4.28 Sphericity of siIFNAR transfected A431-6 cell cluster.

Quantification of sphericity in Fig. 4.27. Lines show the mean with SD for n = 22 (siControl), n = 20 (siIFNAR1), and n = 23 (siIFNAR2) clusters by two independent experiments.

4-2-4 Interferon-b contributes to the collective invasion of cancer cells with sealed intercellular spaces

Type-I interferons include interferon-a (IFNA) and interferon-b (IFNB), and both can interact with IFNAR [35]. To investigate the function of IFNA in A431-6 cells, IFN alpha-IFNAR-IN-1, a low-molecular-weight inhibitor of the IFNA and IFNAR interaction, was added to A431-6 cells. IFN alpha-IFNAR-IN-1 treatment did not affect the phosphorylation of STAT1 in A431-6 cells (Fig. 4.29). Subsequently, IFNB expression was depleted by siRNA in A431-6 cells to investigate the role of IFNB in phosphorylation of STAT1 (Fig. 4.30). Phosphorylated STAT1 was significantly decreased (Fig. 4.31) and the sphericity was increased; that is, collective invasion was suppressed by IFNB depletion (Fig. 4.32 and 4.33). These data indicate that IFNB, but not IFNA, promotes collective invasion through the activation of STAT1 in A431-6 cell clusters.

To assess how IFNB contributes to phosphorylated STAT1 and collective invasion, we performed immunofluorescence staining for IFNB. IFNB immunoreactivity was localized to the intercellular sites in A431-6 cell clusters, whereas there were no obvious immunoreactivities in the intercellular sites in A431-7 cell clusters (Fig. 4.34). There was no significant difference between A431-6 and A431-7 cells in the intensity of IFNB immunoreactivity on the surface of cell clusters. The mRNA levels of IFNB and its receptors were higher in A431-7 cells than in A431-6 cells (Fig. 4.35). Enzyme-linked immunosorbent assay (ELISA) results also showed that the culture supernatant of A431-7 cells had a higher IFNB concentration than that of A431-6 cells (Fig. 4.36). Furthermore, treatment with recombinant human IFNB to A431-7 cell clusters did not affect the sphericity and collective invasion (Fig. 4.37). When IFNB neutralizing antibody was added to inhibit the activity of extracellular IFNB, there was no change in the invasive ability of A431-6 cell clusters (Fig. 4.38). In addition, we confirmed that its receptor, IFNAR2, is expressed in the intercellular site of the A431-6 cell cluster (Fig. 4.39). These data suggest that intercellular IFNB, but not extracellular IFNB, is required for collective invasion.

Recent research has shown that the sealed intercellular structure enhances the accumulation of soluble factors such as epidermal growth factor receptor (EGFR) ligands at intercellular sites, whereby triple-negative breast cancer becomes malignant [96]. Transmission electron microscopy (TEM) was carried out to investigate the ultrastructural difference, especially intercellular structures, between A431-6 and A431-7 cell clusters. We found that the edges of A431-6 cell clusters were sealed, whereas those of the A431-7 cell clusters were not sealed (Fig. 4.40), although intercellular junctions were well-developed in A431-7 cell clusters but not in A431-6 cell clusters. Furthermore, the intercellular spaces of the A431-7 cell clusters were notably wider than those of the A431-6 cell clusters (Fig. 4.41). Next, immunoelectron microscopy was carried out to investigate the localization of IFNB in detail. As a result,

immunolabeling of IFNBs adhering to the cell bodies in the intercellular spaces of A431-6 cells was performed (Fig. 4.42). The cells were then treated with ethylene glycol tetraacetic acid (EGTA), a calcium-selective chelator, to open the sealed intercellular structure. 5mM of EGTA disrupted intercellular adhesion, whereas 1 mM loosened intercellular adhesion. In both cases, intercellular IFNB was not detected by immunofluorescent staining (Fig. 4.43). Since cells retained a cell cluster morphology in 1 mM EGTA, sphericity was measured and was significantly higher than that of non-treated cells (Fig. 4.44). It is possible that the sealed edge of the intercellular spaces prevents secreted INFB from leaking out of A431-6 cell clusters. Collectively, these data suggest that the sealed and narrow intercellular spaces in A431-6 cell clusters contribute to the IFNB-induced increase in phosphorylation of STAT1 and elevated collective invasiveness.

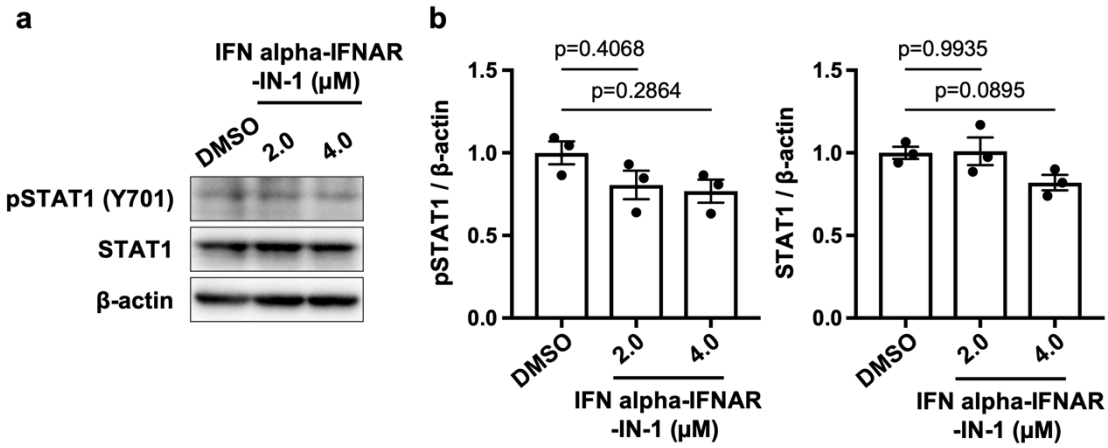

Fig. 4.29 Western blotting to assess the influence of IFN-α inhibition on pSTAT1

Representative western blotting images for pSTAT1 (Y701), STAT1, and β-actin in DMSO, 2 μM- or 4 μM-IFN alpha-IFNAR-IN-1-treated A431-6 cells. Bars represent mean ± SEM. in three independent experiments.

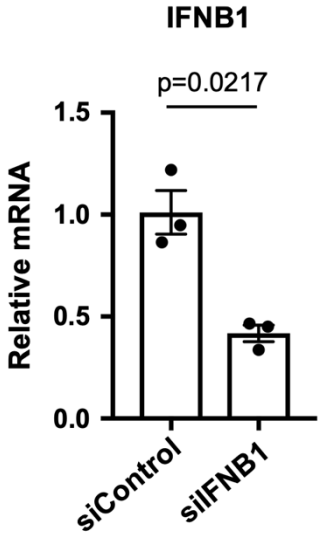

Fig. 4.30 RT-qPCR to confirm knockdown efficiency.

PCR results to validate the knockdown efficiency in siIFNB1-treated A431-6 cells. Bars represent mean ± SEM. in three independent experiments.

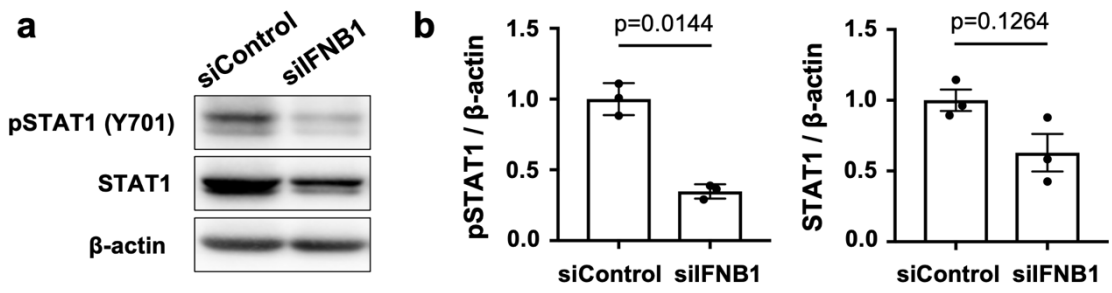

Fig. 4.31 IFNAR depletion suppressed phosphorylation of STAT1.

(a) Representative western blotting images for pSTAT1 (Y701), STAT1, and β-actin in siControl- or siIFNB1 -treated A431-6 cells. (b) Quantification of protein bands in (a). Bars represent the mean±SEM of three independent experiments.

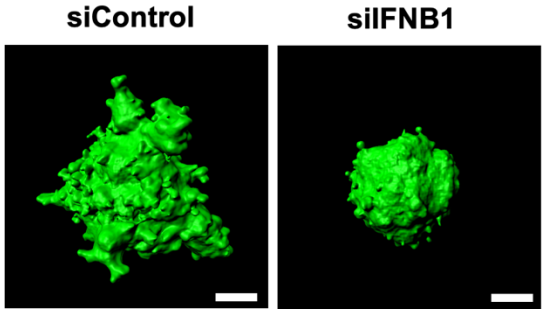

Fig. 4.32 IFNB1 depletion suppressed collective invasion of A431-6 cell cluster.

Representative three-dimensional constructed images of siControl- or siIFNB1-treated A431-6 cell clusters cultured in a three-dimensional collagen gel culture system. The sphericity of siControl: 0.147 and siIFNB1: 0.558. Scale bars represent 30 μm.

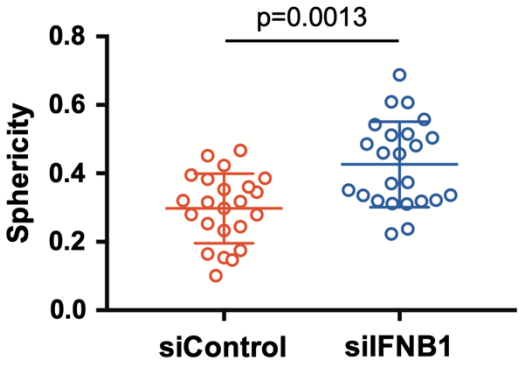

Fig. 4.33 Sphericity of siIFNB1 transfected A431-6 cell cluster.

Quantification of sphericity in Fig. 4.32. Lines show the mean with SD for n = 23 (siControl) and n = 24 (siIFNB1) clusters by two independent experiments.

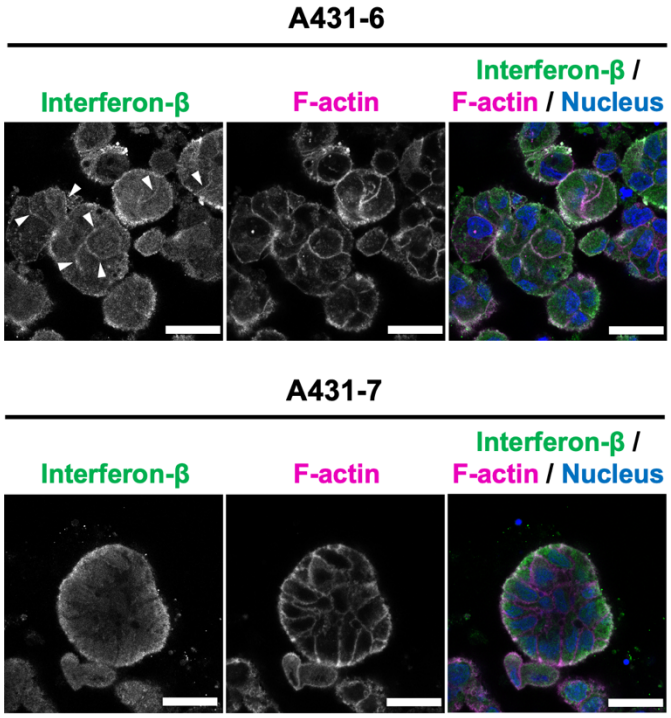

Fig. 4.34 IFNB was localized to intercellular sites in A431-6 cell cluters.

Immunofluorescence images for interferon-β (INFB; green) with F-actin (magenta) and nucleus (blue) in A431-6 and A431-7 cell clusters in a three-dimensional collagen gel culture system. Arrowheads show immunoreactivity for IFNB in the intercellular spaces. Scale bars represent 25 μm.

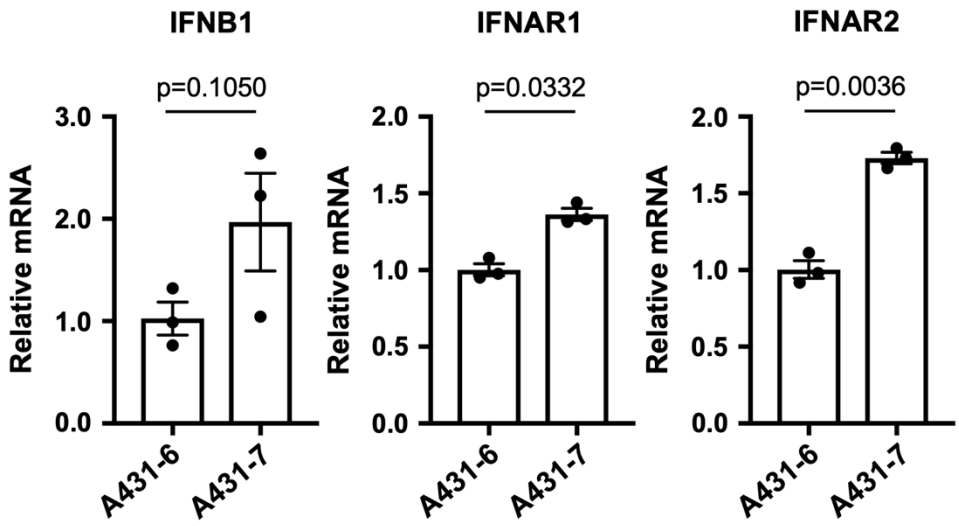

Fig. 4.35 Comparing IFNB1 and its receptors expression in subclones using RT-qPCR.
RT-qPCR results of IFNB1, IFNAR1, and IFNAR2 in A431-6 and A431-7 subclones. Bars represent mean ± SEM. in three independent experiments.

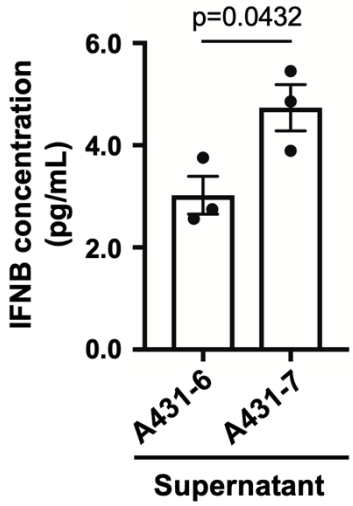

Fig. 4.36 IFNB in supernatant of A431-7 was enriched more than that of A431-6.
Measurement of IFNB concentration in culture supernatants of A431-6 and A431-7 cells by ELISA. Bars represent the mean ± SEM in three independent experiments.

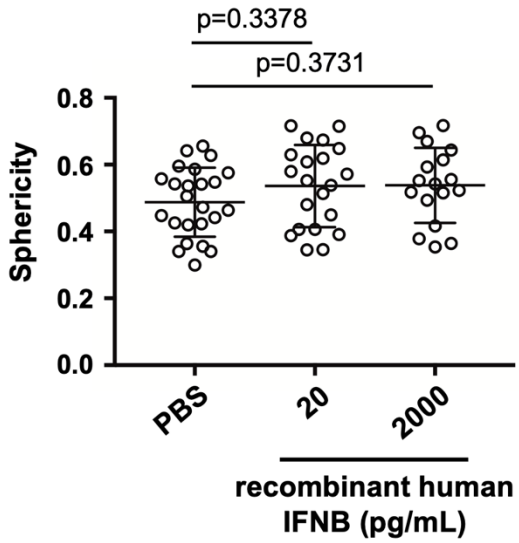

Fig. 4.37 Additional extracellular IFNB did not affect sphericity.

The sphericity of 20 or 2000 pg/mL IFNB-treated A431-7 cell clusters was evaluated in a three-dimensional collagen gel culture system. Lines show the mean with SD for n=24 (PBS), n=21 (20 pg/mL), and n=17 (2000 pg/mL) clusters in two independent experiments.

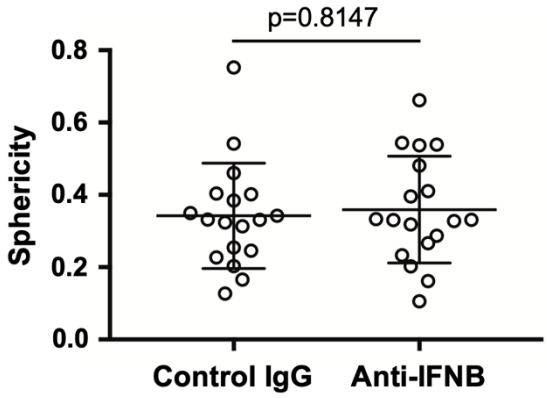

Fig. 4.38 Neutralization of extracellular IFNB did not change sphericity.

The sphericity of 10 ng/mL IFNB neutralization antibody-treated A431-6 cell clusters cultured in a three-dimensional collagen gel culture system. Lines show the mean with SD in n=18 (control IgG) and n=18 (anti-IFNB) clusters from two independent experiments.

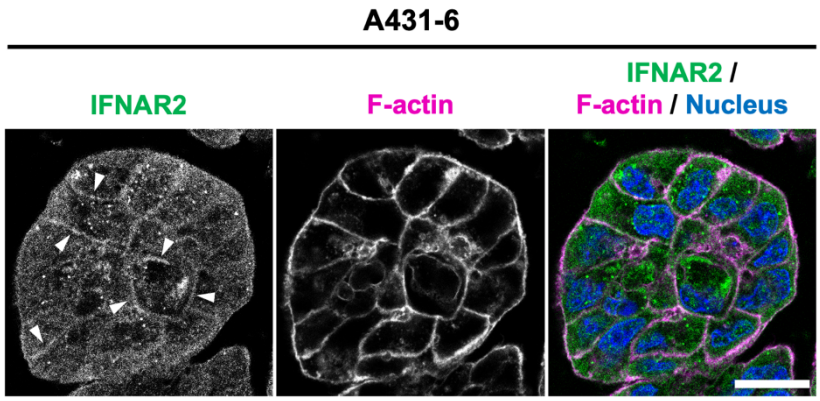

Fig. 4.39 IFNAR2 was localized to intercellular sites.

Immunofluorescence images of interferon receptor (IFNAR2; green) with F-actin (magenta) and nucleus (blue) in A431-6 cell clusters in a three-dimensional collagen gel culture system. Arrowheads show immunoreactivity for IFNB in intercellular spaces. Scale bars represent 20 μm.

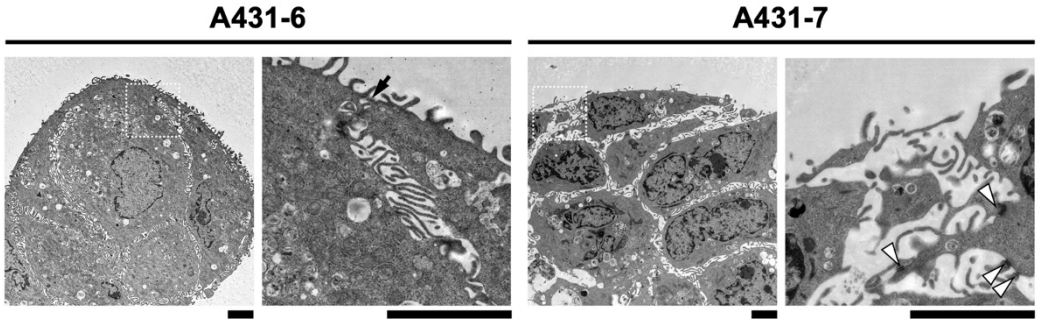

Fig. 4.40 Transmission electron microscopy of A431-6 and A431-7 cell clusters

The regions surrounded by the white dotted squares are magnified on the right. The arrow shows the sealed edge of the intercellular space. Arrowheads show intercellular junctions. Scale bars represent 3 μm.

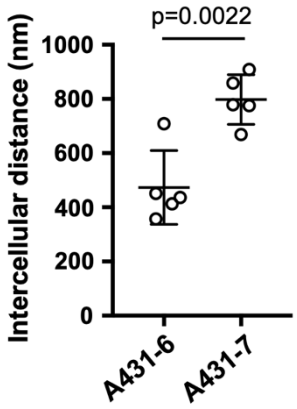

Fig. 4.41 A431-7 cell clusters had wider intercellular distance.

Quantification of intercellular distances in Fig. 4.40. Lines show the mean with SD in five clusters.

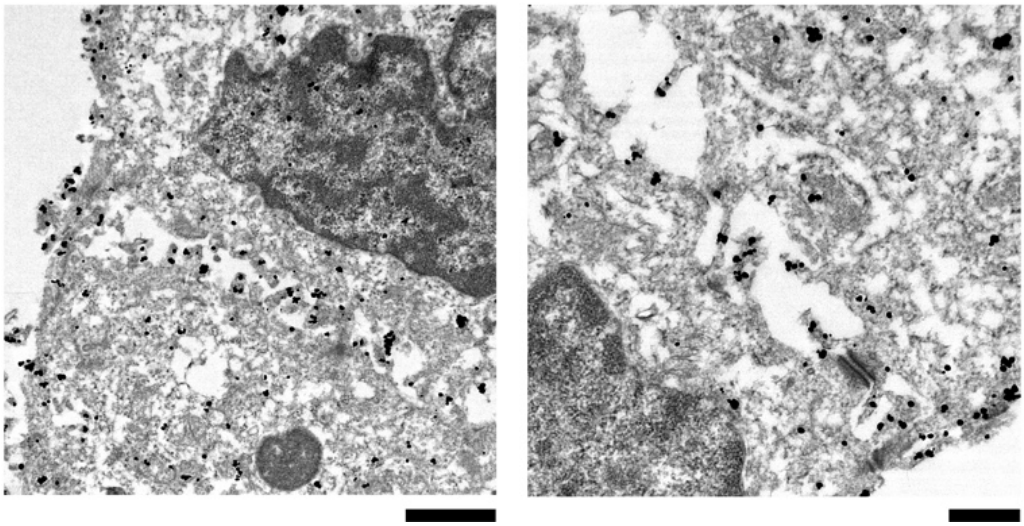

Fig. 4.42 IFNB was localized to sealed intercellular spaces in A431-6 cell clusters.

Immunoelectron microscopy of IFNB. Black particles show localization of IFNB. Scale bars 500 nm.

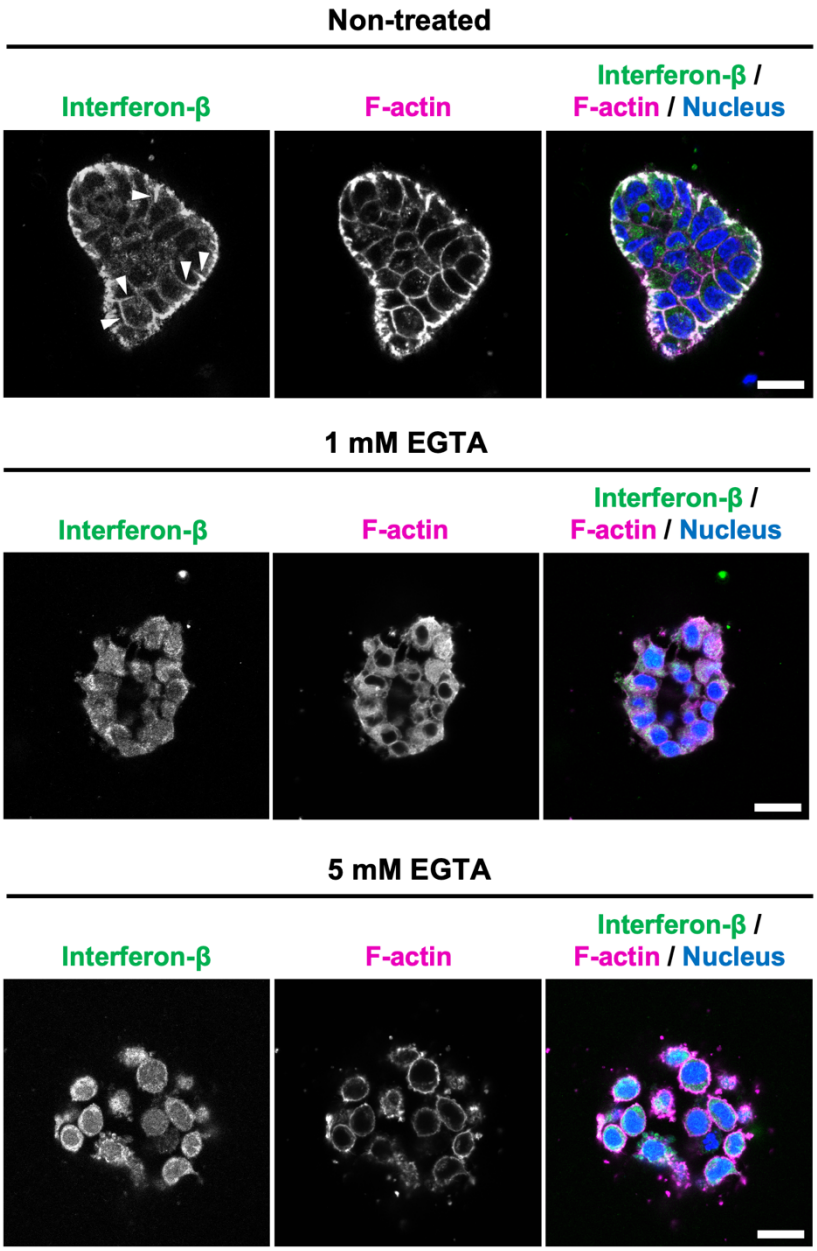

Fig. 4.43 EGTA suppressed intercellular adhesion and localization of IFNB in intercellular sites.

Immunofluorescence images of IFNB (green) with F-actin (magenta) and nucleus (blue) in 1 or 5 mM EGTA-treated A431-6 cell clusters in a three-dimensional collagen gel culture system. Arrowheads show immunoreactivity for IFNB in intercellular spaces. Scale bars represent 25 μm.

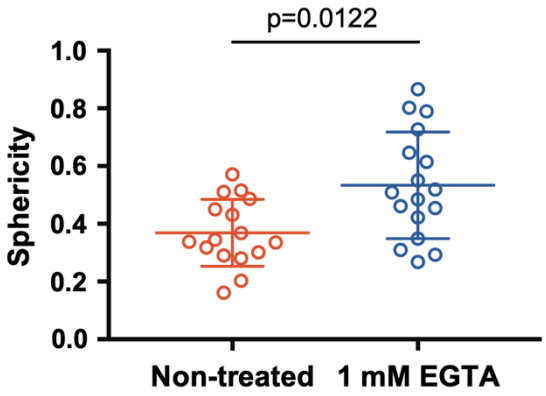

Fig. 4.44 EGTA increased sphericity of A431-6 cell clusters.

The sphericity of 1 mM EGTA-treated A431-6 cell clusters cultured in a three-dimensional collagen gel culture system. Lines show the mean with SD for n=16 (Non-treated) and n=17 (1 mM EGTA) clusters by two independent experiments.

4-2-5 Depletion of keratin (KRT) leads the formation of sealed and narrow intercellular structure and STAT1 activation.

Next, we focused on the upregulated genes in A431-7 cells compared to those in A431-6 cells, which may be related to their low-invasive potential. Microarray results showed that keratin genes, such as KRT1, KRT10, and KRT14 were notably upregulated in A431-7 cells (Fig. 4.45). GSEA also showed the enrichment of keratinization in A431-7 cells (Fig. 4.46). We confirmed the reproducibility of the microarray results using qPCR (Fig. 4.47). Keratin filament, a typical cytoskeletal component in squamous epithelial cells, is involved in the formation of intercellular adhesions such as desmosomes [97]. We assumed that upregulated keratin genes in A431-7 cells influenced the morphology of the intercellular structure; thus, depletion of keratin genes using siRNAs were performed (Fig. 4.48). Interestingly, KRT1-depleted A431-7 cell clusters possessed narrow intercellular spaces, and the edges of the cell cluster were sealed like those of A431-6 cell clusters (Fig. 4.49). Furthermore, the quantitative analysis on cell-cell distance demonstrated that the intercellular spaces of KRT1-depleted A431-7 cell clusters were significantly narrower than those of control A431-7 cell clusters (Fig. 4.50). In addition, the phosphorylation of STAT1 and the total amount of STAT1 proteins were significantly increased by the depletion of keratin genes, especially KRT1 and KRT10 (Fig. 4.51). In summary, we revealed that keratin genes are involved in the formation of wider and open intercellular spaces of A431-7 cell clusters, and the depletion of keratin genes promotes sealed intercellular structure generation and subsequent STAT1 phosphorylation.

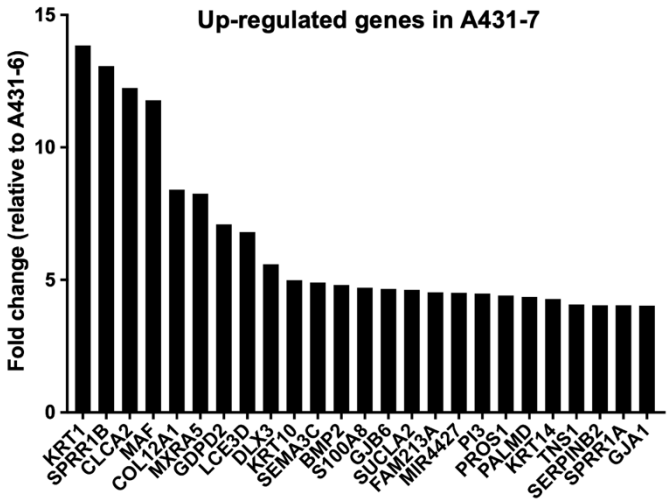

Fig. 4.45 Up-regulated genes in A431-7 subclone comparing to A431-6 subclone.

The DNA microarray result comparing the A431-6 and A431-7 subclones. Genes with more than a 4-fold increase in A431-7 are shown.

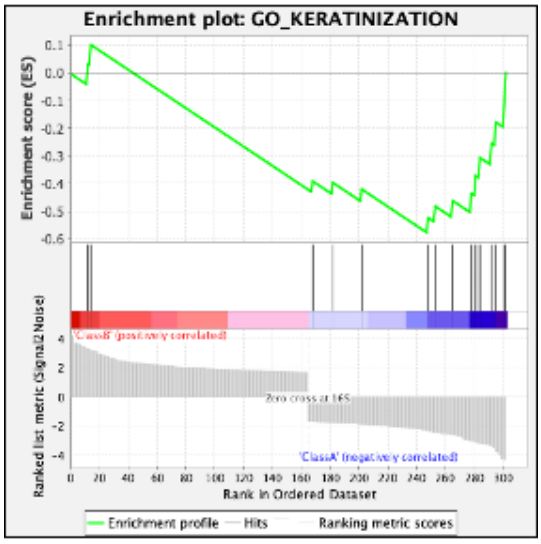

Fig. 4.46 GSEA using the results of DNA microarray.

GSEA showing keratinization in A431-7 cells.

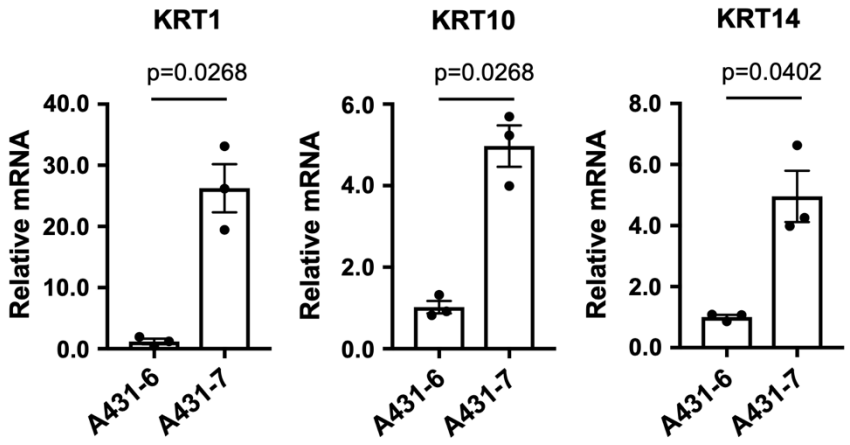

Fig. 4.47 Confirming reproducibility of DNA microarray using RT-qPCR.

RT-qPCR results of KRT1, KRT10 and KRT14 in A431-6 and A431-7 subclones. Bars represent mean ± SEM. in three independent experiments.

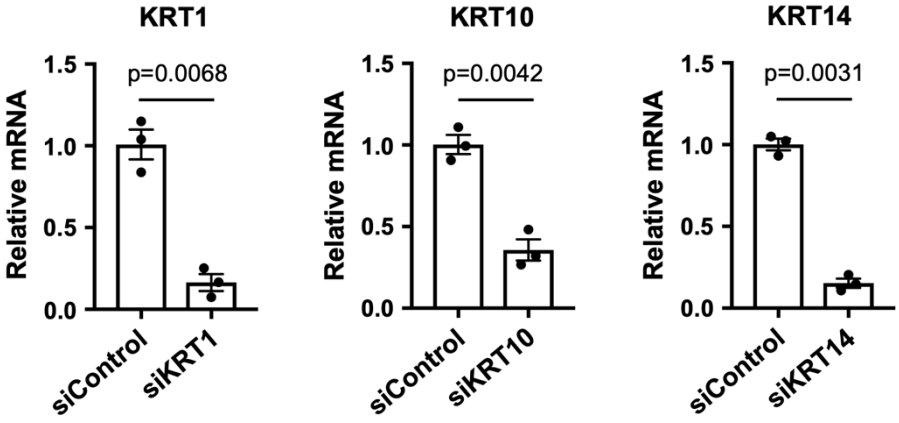

Fig. 4.48 RT-qPCR to confirm the efficiency of siRNAs.

RT-qPCR results to validate the knockdown efficiency in siKRT1-, siKRT10-, or siKRT14-treated A431-7 cells. Bars represent mean ± SEM. in three independent experiments.

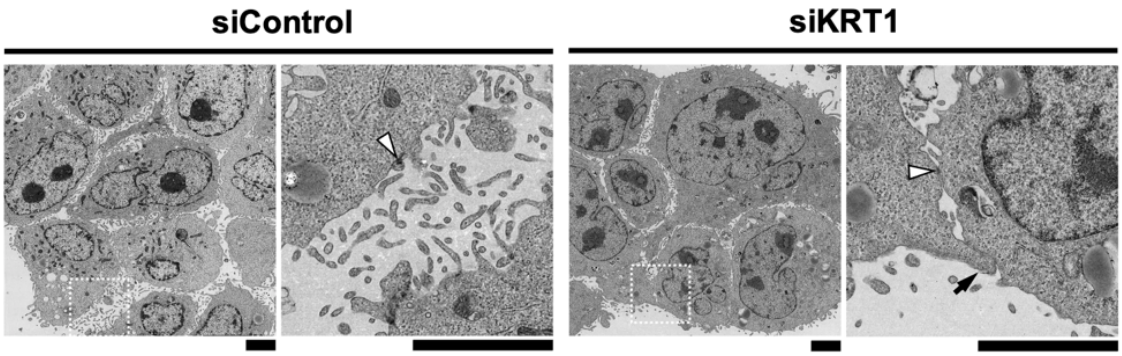

Fig. 4.49 KRT1 depletion induced formation of the sealed intercellular structure.
Representative transmission electron microscopic images of siControl- or siKRT1-treated A431-7 cell clusters cultured in a three-dimensional collagen gel culture system. The regions surrounded by white dotted squares are magnified on the right. The arrow indicates the sealed edge of the intercellular space. Arrowheads show intercellular junctions. Scale bars represent 3 μm.

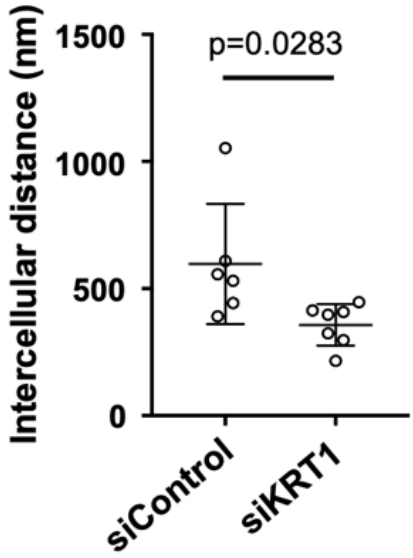

Fig. 4.50 KRT1 depletion made intercellular distance narrower.
Quantification of intercellular distances in Fig.4.49. Lines show the mean with SD in >5 clusters by two independent experiments.

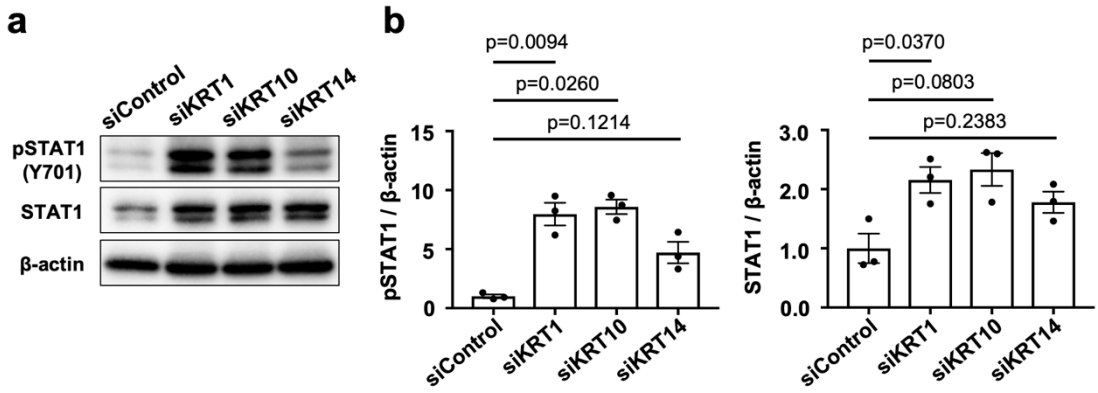

Fig. 4.51 Up-regulated genes in A431-7 subclone comparing to A431-6 subclone.

(a) Representative western blotting images for pSTAT1 (Y701), STAT1, and β-actin in siControl-, siKRT1-, siKRT10-, or siKRT14-treated A431-7 cells. (b) Quantification of protein bands in (a). Bars represent mean ± SEM. in three independent experiments.

4-2-6 Direct contact with high-invasive subclone drives invasion of low-invasive subclone.

Several studies have shown that high-invasive cancer cells drive the invasion of low-invasive cancer cells through both direct and non-direct interactions [92, 98, 99]. Because an investigation on the interaction between phenotypically different cells is important for understanding collective invasion by polyclonal cancer cells, co-culture experiments with high-invasive A431-6 and low-invasive A431-7 sub-clonal cells were performed. First, we developed A431-6-scarlet-histone H2B (6-scarlet) and A431-7-emerald-histone-H2B (7-emerald) cells to distinguish the subclones in the co-culture environment. There was no significant change in invasive potential by histone modification: 6-scarlet cell clusters with low sphericity scores invaded the surrounding matrix, while 7-emerald cell clusters with high sphericity scores did not (Fig. 4.52). Subsequently, we examined whether non-direct or direct interaction of subclones influences their collective invasion potential. To investigate the effect of non-direct interaction, both 6-scarlet and 7-emerald cells were seeded together in a collagen gel, where each subclone formed independent cell clusters (Fig. 4.52). There was no significant influence of the non-direct contact co-cultures (Fig. 4.52 and 4.53): 6-scarlet cell clusters showed high invasive potential, whereas the invasiveness of 7-emerald cell clusters did not change. Next, we performed co-culture with direct contact to investigate the effects of cell-cell contact between the subclones with different invasiveness (Fig. 4.54). To achieve this, mixed spheroids of 6-scarlet and 7-emerald cells were prepared using the hanging drop method and cultured in a collagen gel until collective invasion was observed. Intriguingly, 7-emerald cells were included in the collective invasion chain mainly consisting of 6-scarlet cells, and polyclonal collective invasion was observed (Fig. 4.54). In addition, time-lapse imaging demonstrated that 6-scarlet cells were located at the invasive front of the collective invasion, and 7-emerald cells appeared to follow it (Fig. 4.55). Furthermore, immunofluorescent staining clarified that the nuclear localization of STAT1 was notably enhanced in the cells, leading to collective invasion of 6-scarlet and 7-emerald (Fig. 4.56). We then prepared mixed spheroids of IFNB-knockdown and non-treated A431-6 cells to investigate whether the collective invasion chain contained IFNB-knockdown cells. To distinguish knockdown cells from non-treated cells, 6-scarlet cells were transfected with IFNB siRNA and mixed with A431-6 cells without the fluorescent tag. As a result, the collective invasion chain contained INFB knockdown cells surrounded by non-treated cells (Fig. 4.57). These data suggest that direct interaction of the low-invasive sub-clonal cells and high-invasive sub-clonal cells drives polyclonal collective invasion, where high-invasive sub-clonal cells lead to low-invasive sub-clonal cells.

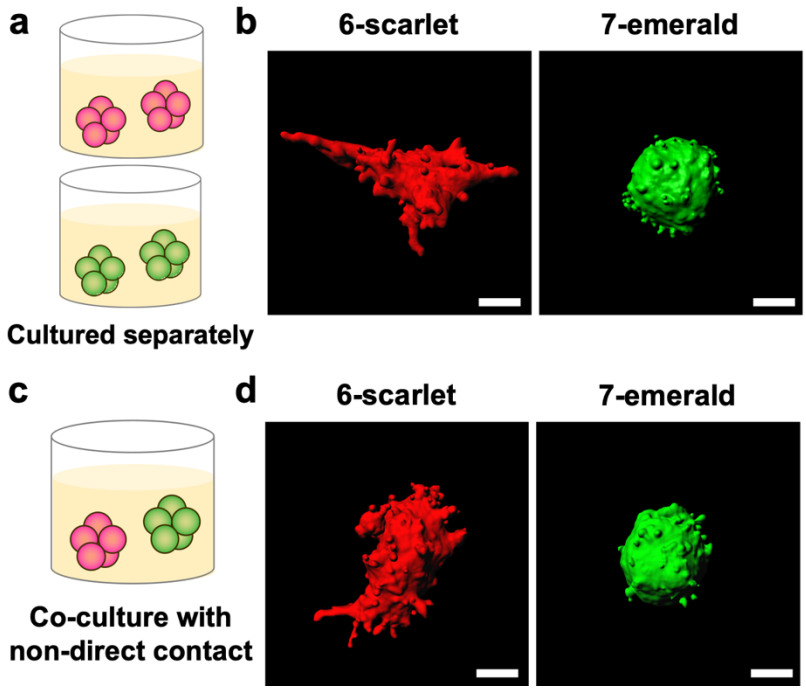

Fig. 4.52 Co-culture of 6-scarlet and 7-emerald with indirect contact.

(a) Schematic illustration of the culture of A431-6 cells expressing scarlet-histone H2B (6-scarlet, red) and A431-7 cells expressing emerald-histone H2B (7-emerald, green) cell clusters. (b) Representative three-dimensional constructed images of (a). 6-scarlet and 7-emerald cell clusters were cultured in a three-dimensional collagen gel culture system. The sphericity of 6-scarlet: 0.099 and 7-emerald: 0.596. Scale bars represent 30 μm. (c) Schematic illustration of the experiment culturing 6-scarlet and 7-emerald cell clusters with non-direct contact. (d) Representative three-dimensional constructed images of (c). 6-scarlet and 7-emerald cell clusters were cultured in a three-dimensional collagen gel culture system. The sphericity of 6-scarlet: 0.137 and 7-emerald: 0.604. Scale bars represent 30 μm.

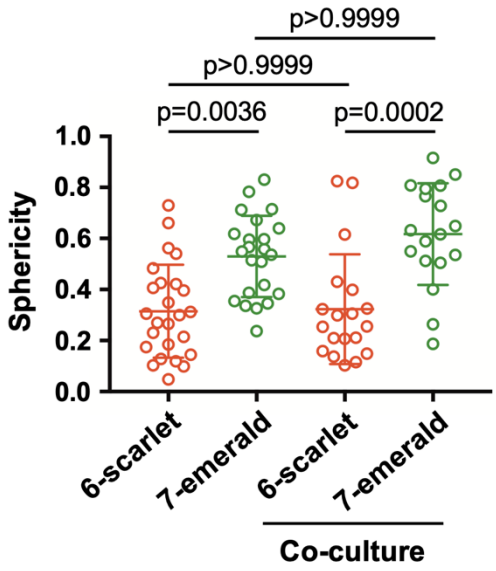

Fig. 4.53 Indirect contact did not affect invasiveness.

Quantification of sphericity in (Fig. 4.52). Lines show the mean with SD in >16 clusters by two independent experiments.

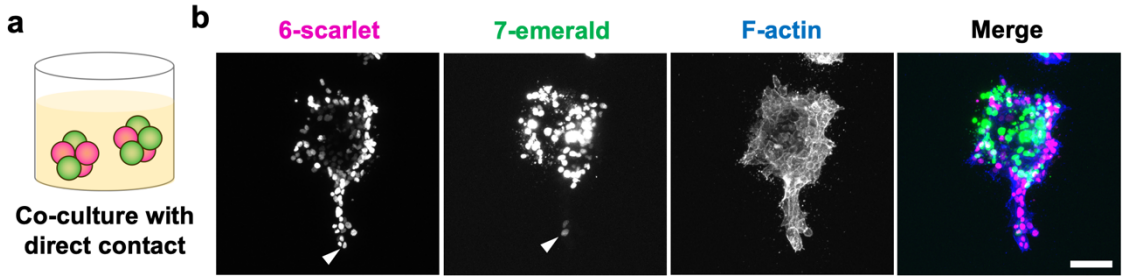

Fig. 4.54 Direct contact drives the invasion of A431-7 cells.

(a) Schematic illustration of the experiment with mixed spheroids of 6-scarlet and 7-emerald cells in direct contact. (b) Representative images of a mixed spheroid consisting of 6-scarlet (magenta) and 7-emerald (green) cells cultured in a collagen gel. Arrowheads show invading sub-clonal cells. The merged image is shown by F-actin (blue). Scale bars represent 30 μm.

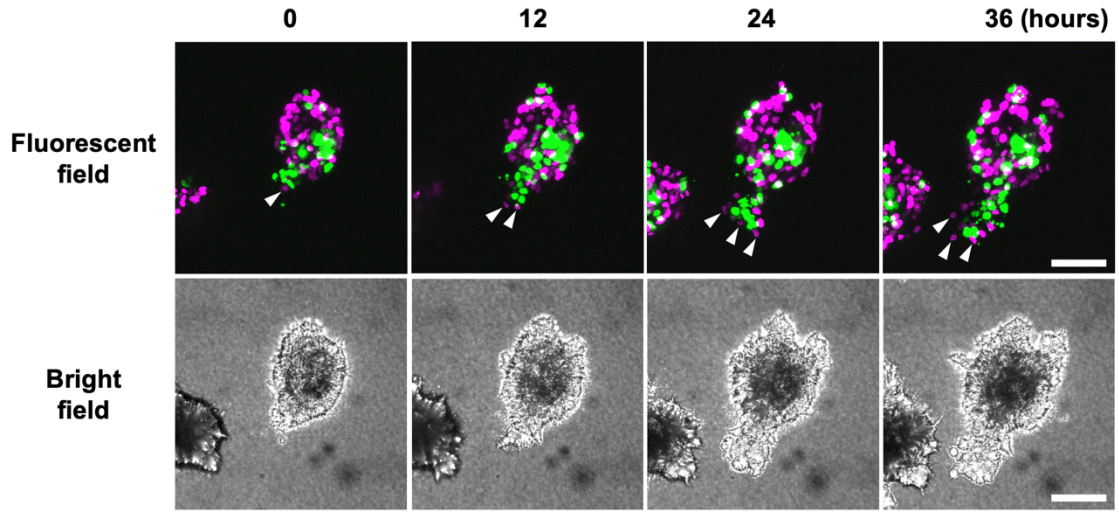

Fig. 4.55 6-scarlet cells were located at the invasive front and lead the invasion of 7-emerald.
Time-lapse imaging of a mixed spheroid consisting of 6-scarlet (magenta) and 7-emerald (green) cells cultured in a collagen gel. Arrowheads show 6-scarlet cells leading to polyclonal collective invasion. Scale bars represent 100 μm.

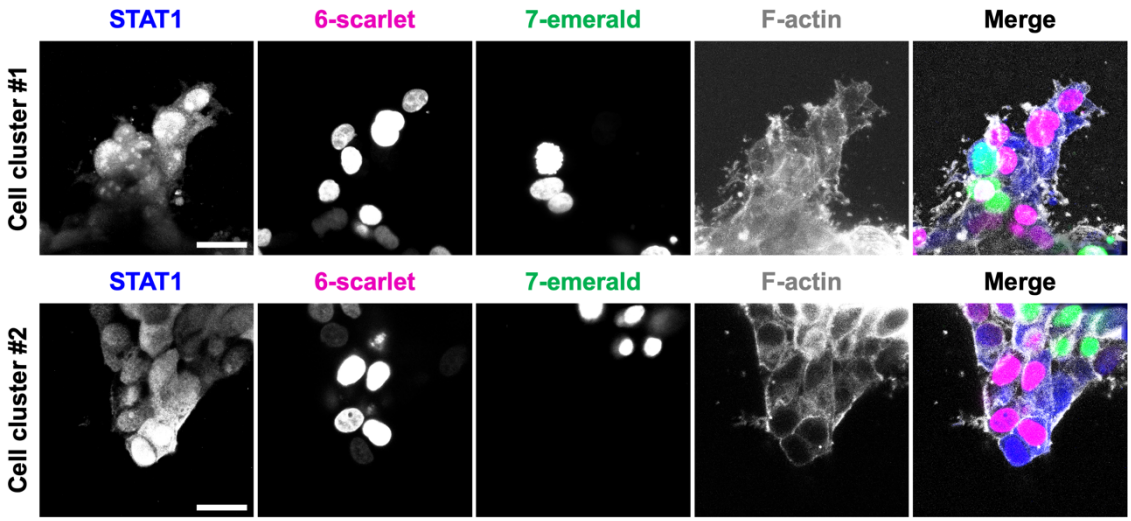

Fig. 4.56 STAT1 was highly expressed at the invasive front in direct contact culture.
Immunofluorescence images for STAT1 (blue) with F-actin (gray) in a mixed spheroid consisting of 6-scarlet (magenta) and 7-emerald (green) cells cultured in a collagen gel. Scale bars represent 25 μm.

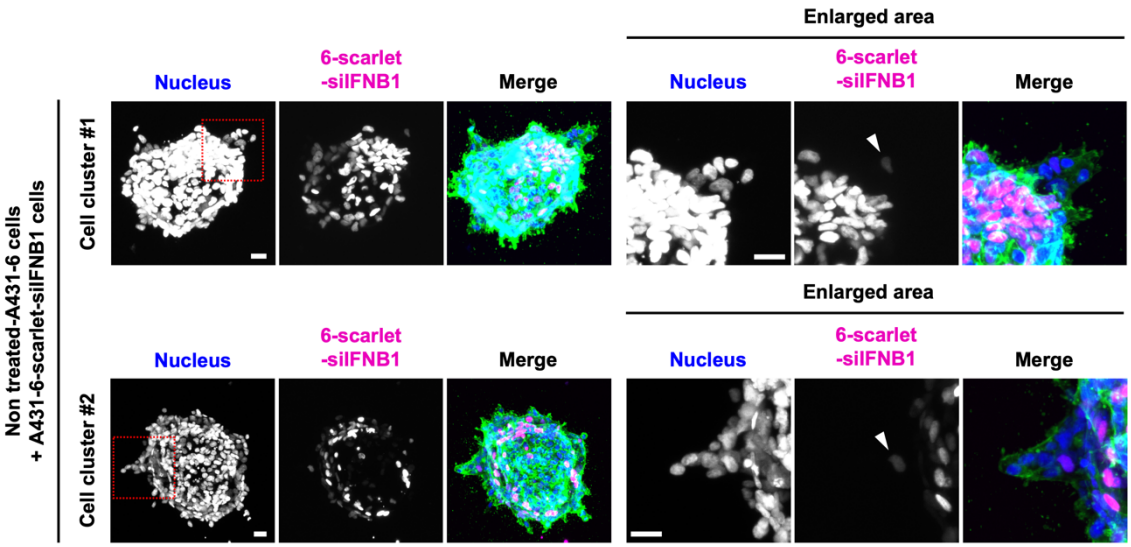

Fig. 4.57 IFNB knockdown cells were included in invasive protrusion.

The images showing the collective invasion of A431-6 cell cluster containing IFNB1-knockdown cells (6-scarlet-siIFNB, magenta). The region surrounded by red squares was enlarged in the right. Arrowheads show IFNB-knockdown cell in invasive protrusion. Blue: nucleus, Green: F-actin. Scale bar represents 30 μm.

4-2-7 STAT1 is highly expressed at the invasive front of human skin SCCs.

Finally, immunohistochemistry for STAT1 was performed on 76 samples of skin SCC patients and four samples of normal skin tissue in the human tissue microarray of skin SCCs. The results were independently assessed by two pathologists. Immunohistochemistry showed that 53 of 76 SCCs (69.7%) were STAT1-positive (Fig. 4.58). Furthermore, the enrichment of STAT1 at the invasive front was observed in 29 of 76 SCCs (38.2%) (Fig. 4.58). As mentioned in Fig. 4.58, STAT1 was highly expressed and significantly localized to the nucleus in SCC cells adjacent to the stroma, specifically, cells at the invasive front (Fig. 4.59). At this time, STAT1 staining was negative in all normal tissues (Fig. 4.59). Furthermore, enrichment of STAT1 expression in the nuclei of cancer cells located at the edges of cancer cell nests was also observed in some cases of human SCC in situ (Bowen's disease), supporting the notion that STAT1 expression may be a prerequisite for initiating or promoting the collective invasion of cancer cells (Fig. 4.60). Taken together, these data suggest that STAT1-high expressing cells drive polyclonal collective invasion by leading STAT1-low expressing cells in SCC patients.

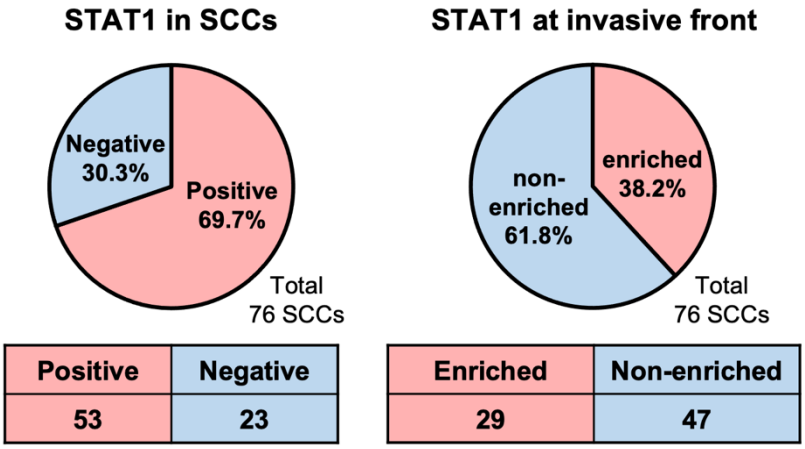

Fig. 4.58 Histological analysis on STAT1 using tissue microarray of skin SCC.

The pie charts and tables show the percentage and number of STAT1 positive skin squamous cell carcinoma (SCC) in human tissue microarray (left) and those of SCC with enriched STAT1 at the invasive front (right), respectively. The results were independently assessed by two pathologists.

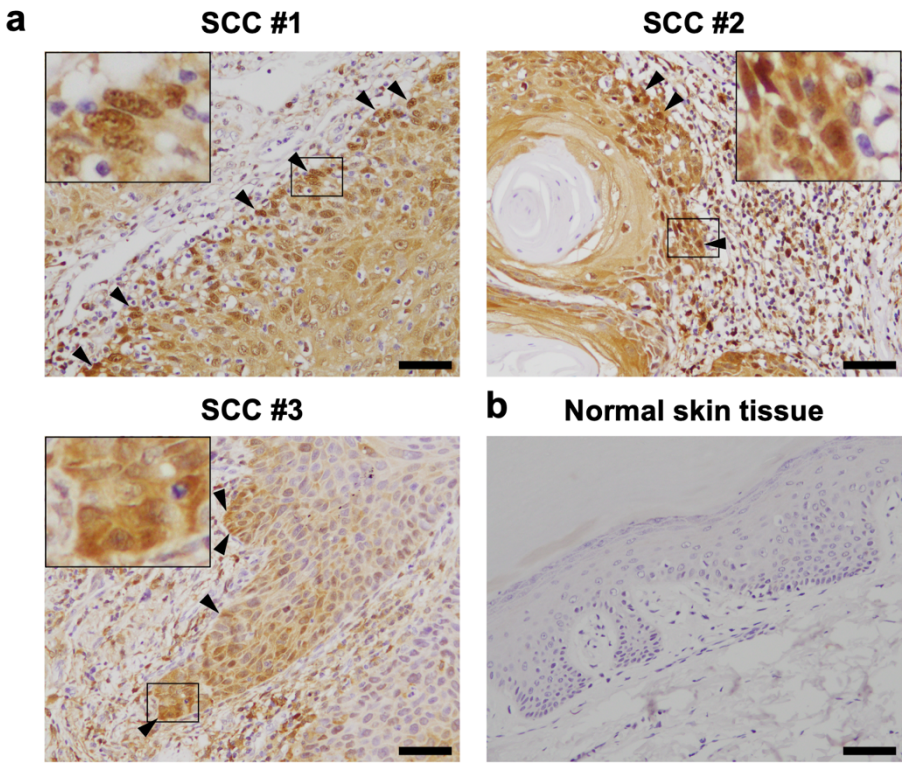

Fig. 4.59 STAT1 was enriched at invasive fronts of skin SCCs.

Representative images showing enrichment of STAT1 in the invasive front of SCC. Arrowheads indicate high STAT1 expression in leading cancer cells at the invasive fronts of SCC cancer cell groups. The regions surrounded by squares were magnified. The scale bars represent 50 μm.

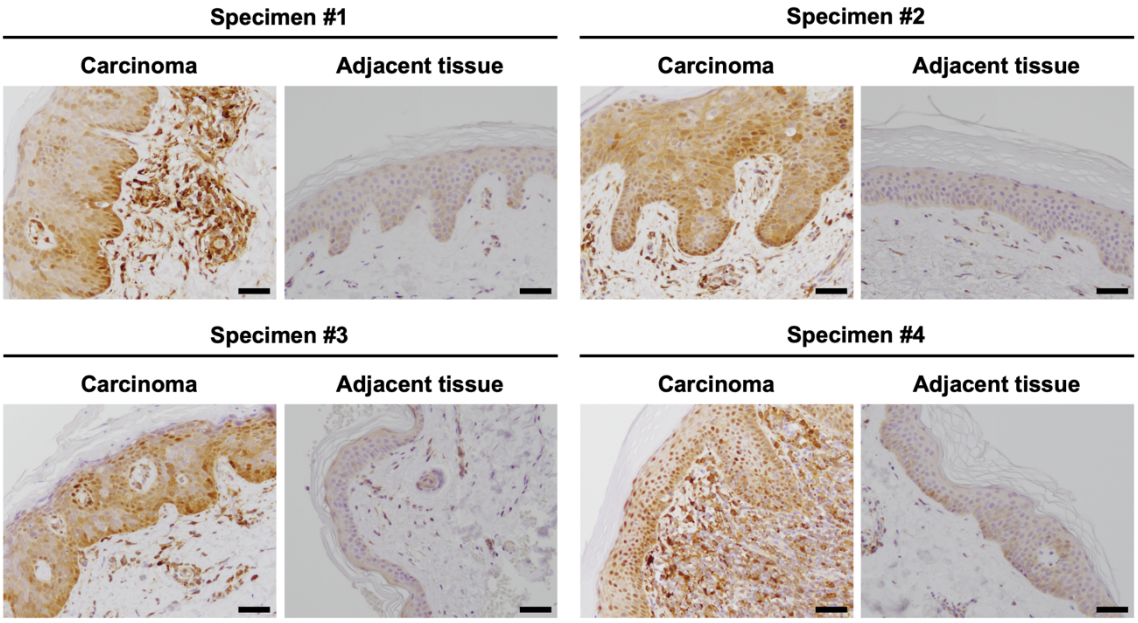

Fig. 4.60 STAT1 staining for Bowen's disease.

Representative images of immunohistochemistry for STAT1 in human SCC in situ (Bowen's disease). Carcinoma and adjacent tissue are a pair of the same specimens. The scale bars represent 50 μm.

4-3 Discussion

This study demonstrates that the interferon-b/STAT1 axis drives the collective invasion of cancer cells with sealed intercellular spaces (Fig. 4.61), and that STAT1-activated cells drive polyclonal collective invasion by leading STAT1 deficient cells (Fig. 4.62). A schematic illustration of the results of the present study is shown in Fig. 4.61 and 4.62. We found that the high-invasive cell cluster has a hermitically sealed and narrow intercellular space, while low-invasive cell cluster has a non-sealed and wide intercellular space. INFB is expressed in the sealed intercellular spaces of high-invasive cell clusters and promotes phosphorylation of STAT1 and collective invasion through the IFNAR and JAK pathways. Co-culture experiments with a mixed spheroid of subclones, where high-invasive cells and low-invasive cells directly contact each other, showed that high-invasive sub-clonal cells drive polyclonal collective invasion by leading low-invasive sub-clonal cells. Furthermore, immunohistochemical analysis of tissue microarray revealed the enrichment of STAT1 at the invasive front of human skin SCCs.

We succeeded in establishing subclones with high- or low- invasive potentials from A431 SCC cell line consisting of polyclonal cells with heterogeneous invasiveness and developed a novel unique evaluation system based on the morphology of whole cell clusters. In conventional experimental systems, it is difficult to visualize whole cell clusters by embedding artificially prepared spheroids into the extracellular matrix because of the size of the spheroid. In contrast, our experimental system can assess the behavior of <100 cell clusters; therefore, we were able to evaluate the morphology of the whole cell cluster. By analyzing the sphericity of the cell cluster, we could evaluate the invasive potential of each cell cluster. However, there is a problem with this experimental system: the sphericity varies even without invasion. For instance, even if the surface of the cell cluster is bumpy without invasion, the sphericity will decrease. Therefore, since sphericity acts only as an index, it is necessary to determine whether invasion actually occurs from the original data.

By comparing gene expression profiles between high- and low invasive subclones through DNA microarray, we determined that the activity of STAT1 drives collective invasion. Previous studies have reported that STAT1 contributes to migration and invasion in a variety of cancer cells [87, 88, 100, 101]. One study showed that STAT1 modulates the binding of cells to fibronectin by forming a complex with focal adhesion kinase (FAK) in focal adhesion; moreover, it enhances cell migration [101]. Previously, we reported that integrin-β1, a major regulator of FAK, plays a crucial role in the two-dimensional collective invasion of parental A431 cells [102]. These findings suggest that STAT1 contributes to collective invasion by modulating the functions of integrin-β1 and FAK.

We found that cell clusters of high-invasive sub-clonal cells have sealed and narrow intercellular spaces where INFB is expressed. A recent study reported that the accumulation of

soluble factors, such as EGFR ligand, in the sealed intercellular spaces defined as “nanolumina” contributes to metastasis of triple-negative breast cancer [96]. The clusters of high-invasive subclone have hermetically sealed intercellular structures that resemble “nanolumina”, and localized INFB elevates collective invasion via STAT1 phosphorylation. Furthermore, this study identified KRT1 as one of the factors that negatively regulates “nanolumina”-like structure. Intriguingly, well-developed intercellular junctions were found in the low-invasive subclone with non-sealed and wider intercellular spaces, rather than in the high-invasive subclone. DNA microarray results also showed that the expression of genes involved in intercellular junctions (e.g., DSG1, desmoglein 1, GJA1, gap junction protein alpha 1) was higher in A431-7 than in A431-6. These data suggest that the sealed intercellular structures and the width of intercellular spaces in cell clusters are independent of intercellular junctions. In normal keratinized squamous epithelial tissue of the skin, there are wide spaces between the cells, which are connected by intercellular bridges [103]. Even in well-differentiated squamous cell carcinomas with high keratin expression, intercellular bridges and wide intercellular spaces exist between cells [104]. The A431-7 subclone, with wide and unsealed intercellular spaces, had higher keratin expression than the A431-6 subclone, with narrow and sealed intercellular spaces. It is possible that a decrease in keratin expression, that is, the transition from a highly differentiated to a poorly differentiated form, results in narrower and sealed intercellular spaces.

An intercellular structure similar to “nanolumina” has been observed not only in the collective cancer invasion but also in collective migration during epithelial morphogenesis [105]. Thus, “nanolumina”-like structures are considered a universal phenomenon in diverse cell types; however, its biological significance has yet to be fully evaluated. This study demonstrated the significance of the sealed intercellular structure like “nanolumina” in collective invasion of cancer cells and is expected to accelerate future research about sealed intercellular structures.

We determined that the high-invasive subclone with high STAT1 activity was located at the invasive front of the invasive protrusion, resulting in collective invasion with the low-invasive subclone. Leader cells are located at the invasive front of the cell population and promote polyclonal collective invasion by leading low-invasive cells called follower cells [50, 99, 106, 107]. Our data indicate that cancer cells with high STAT1 activity act as leader cells during polyclonal collective invasion. In addition, previous studies have shown that enhanced fibronectin production in leader cells modulates the capacity to lead follower cells in polyclonal collective invasion [106, 107]. In the present study, DNA microarray analysis revealed that the amount of fibronectin-coding mRNA was increased approximately 3-fold in the A431-6 cells compared to that in the A431-7 cells. This supports the hypothesis that A431-6 cells with high STAT1 activity play the role of leader cells. Furthermore, the analysis on the tissue microarray of skin SCC specimens revealed that STAT1 is notably expressed in the invasive front of SCCs, suggesting

that STAT1 also works in leader cells in vivo to drive polyclonal collective invasion. However, the percentage of STAT1 enrichment cells at the invasive front of skin SCC was 38.2% (29/76), and there were STAT1-negative SCCs and STAT1-positive SCCs without enrichment of STAT1 at the invasive front. Integrin-b1, previously mentioned in relation to STAT1, has also been reported to be enriched at the invasive front in skin SCC, and the percentage of integrin-b1 enrichment at the invasive front was 65% (8/13) [50]. Namely, it has been suggested that the enrichment of STAT1 at the invasive front is not remarkably higher than that of representative molecules such as integrin-b1. Thus, further investigations are needed to clarify whether STAT1 could be a therapeutic target for skin SCC. The findings of this study demonstrate that the INFB/STAT1 axis promotes the collective invasion of cancer cells with sealed intercellular spaces. Furthermore, it has been suggested that cancer cells with STAT1 activation act as leader cells to drive the polyclonal collective invasion of skin SCC.

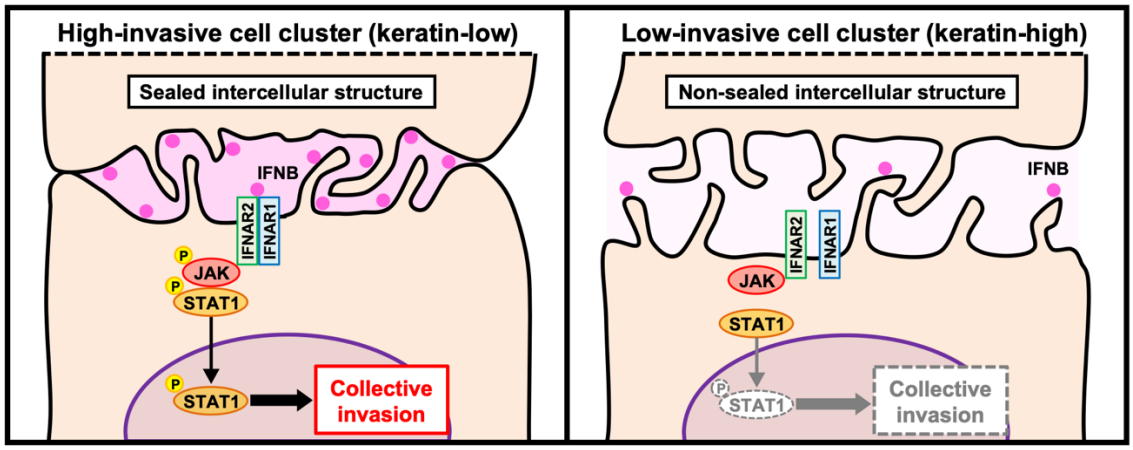

Fig. 4.61 A sealed intercellular structure promotes collective invasion by localizing IFNB to intercellular spaces.

Interferon-β (IFNB) is localized to a sealed intercellular structure and promotes collective invasion via activation of the type-I interferon receptor (IFNAR), Janus kinase (JAK), and signal transducer and activator of transcription 1 (STAT1) in the high-invasive cell clusters (left), whereas low-invasive cell clusters with high keratin expression possess non-sealed wider intercellular spaces, showing low STAT1 activity (right).

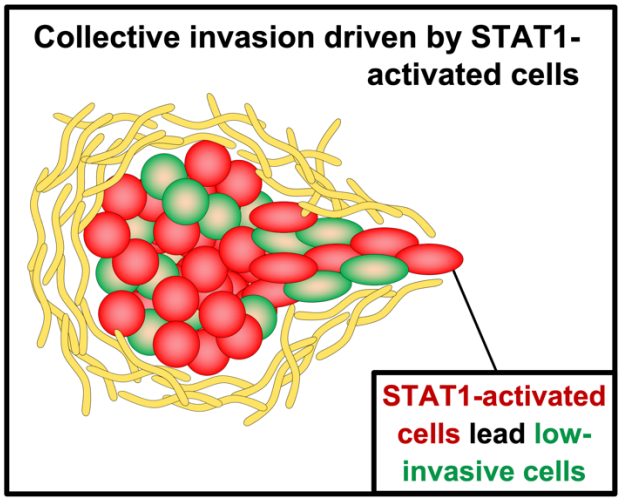

Fig. 4.62 STAT1 activated cells are located at the invasive front and drives collective invasion.

STAT1 activated cell are located at the invasive front of skin SCC group *in vivo* and *in vitro*. In co-culture system with direct contact, STAT1 activated 6-scarlet cells drives 7-emerald cells to collective invasion.

Chapter 5

Summary and Remaining Questions

In the present study, we have identified the contribution of integrin-ECM interaction and IFNB/STAT1 axis in collective invasion [102, 108]. Both mechanisms are in A431 cells, but the relationship between them is not clear. To confirm the consistency of the findings in this study, it is necessary to investigate STAT1 activity in integrin-β1 inhibited condition. We also reported that ECM proteins are present in intercellular sites, and it is possible that these are expressed in sealed intercellular spaces like IFNB. The nanolumina-like intercellular structure reported in this study are likely to be involved in the regulation of not only IFNB but also other soluble factors. In the future, we would like to investigate the possibility that disruption of intercellular structure would be a therapeutic target.

This study proposed STAT1 as a therapeutic target molecule to inhibit collective invasion: the contribution of STAT1 to collective invasion in vitro was significant, and STAT1 depletion by siRNA notably suppressed collective invasion. Furthermore, we demonstrate the intriguing finding that STAT1 is highly expressed in the invasion front of SCCs. The most significant value of this study is that by staining 76 skin SCC specimens for STAT1, we showed the rate of STAT1-positive and the rate of enriched STAT1 in the invasive front. Even in papers published in high-impact journals, there may be only a few or no patient specimens. Even when there are sufficient data of animal experiments, often only one animal model is used. In such cases, although the number of mice used in the analysis may be large, the mechanism of disease onset is uniform and does not adequately reflect the diversity of patients. On the other hand, although this study lacked animal experiments and used only one cell line, it was found that 70% were STAT1 positive and 40% were enriched STAT1 in the invasive front by analyzing 76 specimens. This 40% figure is sufficient to be a therapeutic target. HER2 is known as a representative target for molecular targeted therapy in breast cancer, but only about 20% of breast cancers are HER2-positive [109]. Of course, because the population numbers are different, it is not possible to simply compare breast cancer to skin cancer. However, the importance of the HER2 data in clinical practice means that the potential of the molecule as a target and the quality of the drug (Herceptin) are important. Therefore, the 40% figure indicates the possibility of STAT1 as a therapeutic target, and the contribution of STAT1 to *in vivo* cancers should be fully investigated in the future.

Skin squamous cell carcinoma would not be appropriate when considering not only collective invasion but also collective metastasis. Among skin cancers, melanoma frequently metastasizes, whereas skin SCC tends to be less aggressive and does not metastasize as frequently than other invasive cancers; therefore, there is less demand for drugs to inhibit the collective invasion and metastasis of skin SCC. From these things, it is necessary to investigate whether the findings of this study also occur in other cancers. Breast cancer should be examined first. Breast cancer is the most common type of cancer that metastasizes to distant organs [26, 33, 110]. Breast cancer has been shown to frequently invade as a cell cluster and there is a relationship between

increased CTC clusters in the blood and poor prognosis for patients [34]. Although there have been many previous studies on collective breast cancer invasion, no established therapeutic target molecules have been found. Furthermore, nanolumina formation promotes metastasis in TNBC, which may have a mechanism similar to that of A431 [96]. In addition, it is desirable to detect cancer at an early stage, considering the need to inhibit invasion. It is more effective to start treatment before the cancer spreads to surrounding normal tissues. Oral SCC would be also a target. Oral SCC is detected relatively early and cause distant metastasis and secondary tumor formation in cervical lymph nodes [111, 112]. It has also been suggested that integerin-β1 is also required for the collective invasion of oral SCC [50]; therefore, it is possible that phenomenon found in this study is replicated. Furthermore, even if lung and brain tumor do not progress distant metastasis, tissue destruction is directly related to poor patient prognosis [113-115]. The influence of collective invasion on tissue destruction have not been fully investigated. Thus, the contribution of collective invasion to other than distant metastases is also worth exploring.

Finally, I should discuss whether the phenomenon of collective invasion is an appropriate therapeutic target of cancer. Since inhibition of invasion alone does not eradicate cancer, if eradication of cancer is goal, the inhibitor of invasion should be prescribed in combination with other treatments (e.g., other cytotoxic drugs and radiation). In addition, since cell proliferation is essential for the formation of metastases, theoretically cytotoxic drugs will suppress metastases as a secondary effect. Then, is there no need to develop drugs and treatments intended for inhibition of collective invasion? My answer is No. First, directly inhibiting invasion is very different from secondarily inhibiting invasion by cytotoxic drugs. Side effects are a major problem with cancer drugs, and patients who are physically weak may not be able to take the medication due to side effects. On the other hand, drugs that directly inhibit invasion are expected to have fewer side effects because their goal is not to induce cell death but to suppress cancer cells to spread. Of course, there is concern that invasion inhibitors are less effective; however, it is very important to increase patient options of treatment. In addition, inhibition of collective invasion would be more effective than inhibition of individual invasion. Single cell migration is widely observed *in vivo*, and individual cancer invasion may be essentially similar to this. Therefore, inhibition of individual cancer invasion must take into account the influence of inhibiting the migration of immune cells and fibroblasts. On the other hand, there are few mechanisms that migrate in cell groups like cancer cells *in vivo*. Although collective migration is a major event during development of organisms, there are few reports of collective migration in mature individuals except for wound repair. These data indicate that inhibition of collective cancer invasion has superior specificity, therefore, it is expected to increase the dosage of the drug and to show high drug efficacy. However, it is unlikely that a pharmaceutical company would enter into a project as challenging as a collective invasion inhibitor. In fact, a clinical trials targeting

CTC clusters are performed as university led (ClinicalTrials.gov Identifier: NCT03928210, Location and Sponsor: Breast Cancer Center, University Hospital Basel, Principal Investigator: Marcus Vetter, PD Dr. med). In order to develop a drug targeting collective invasion, we must be prepared to do it ourselves.

I propose the following as a strategy, considering the practical issues in pharmaceutical process. First, because the development of new drugs is very hard, the replacement of existing drugs, known as drug repositioning, should be considered [116]. The experimental systems established in this study, collagen gel overlay condition and single cell-derived spheroid invasion assay, have good throughput and can be used for screening the efficacy of existing drugs. Also, if there is a hit in existing drugs, it may be possible to obtain cooperation from the pharmaceutical company that owns the rights if the remaining substance patent term is long enough. Since the cooperation of pharmaceutical companies is essential for clinical trials, it is also effective to screen only existing drugs for which the term of the substance patent remains sufficiently long. Even if the hit is an existing drug for which the substance patent has expired, it may be possible to obtain a patent for its application. Even if we do not receive cooperation from companies, this effort will certainly contribute to the development of therapies targeting collective invasion and to the advancement of science.

References

1 Howlader N, Noone A, Krapcho M, Miller D, Brest A, Yu M *et al.* SEER cancer statistics review, 1975–2017. *National Cancer Institute* 2020.

2 Sung H, Ferlay J, Siegel RL, Laversanne M, Soerjomataram I, Jemal A *et al.* Global Cancer Statistics 2020: GLOBOCAN Estimates of Incidence and Mortality Worldwide for 36 Cancers in 185 Countries. *CA Cancer J Clin* 2021; 71: 209-249.

3 Ishihara S, Inman DR, Li WJ, Ponik SM, Keely PJ. Mechano-Signal Transduction in Mesenchymal Stem Cells Induces Prosaposin Secretion to Drive the Proliferation of Breast Cancer Cells. *Cancer Res* 2017; 77: 6179-6189.

4 Ambrus JL, Ambrus CM, Mink IB, Pickren JW. Causes of death in cancer patients. *J Med* 1975; 6: 61-64.

5 Fidler IJ. Tumor heterogeneity and the biology of cancer invasion and metastasis. *Cancer Res* 1978; 38: 2651-2660.

6 Bielenberg DR, Zetter BR. The Contribution of Angiogenesis to the Process of Metastasis. *Cancer J* 2015; 21: 267-273.

7 Friedl P, Locker J, Sahai E, Segall JE. Classifying collective cancer cell invasion. *Nat Cell Biol* 2012; 14: 777-783.

8 Ferrara N. VEGF and the quest for tumour angiogenesis factors. *Nat Rev Cancer* 2002; 2: 795-803.

9 Carmeliet P. VEGF as a key mediator of angiogenesis in cancer. *Oncology* 2005; 69 Suppl 3: 4-10.

10 Cross MJ, Claesson-Welsh L. FGF and VEGF function in angiogenesis: signalling pathways, biological responses and therapeutic inhibition. *Trends Pharmacol Sci* 2001; 22: 201-207.

11 Tannock IF. The relation between cell proliferation and the vascular system in a

transplanted mouse mammary tumour. *Br J Cancer* 1968; 22: 258-273.

12 Folkman J. Tumor angiogenesis: therapeutic implications. *N Engl J Med* 1971; 285: 1182-1186.

13 Folkman J. Role of angiogenesis in tumor growth and metastasis. *Semin Oncol* 2002; 29: 15-18.

14 Zwaans BM, Bielenberg DR. Potential therapeutic strategies for lymphatic metastasis. *Microvasc Res* 2007; 74: 145-158.

15 Ward PM, Weiss L. Metachronous seeding of lymph node metastases in rats bearing the MT-100-TC mammary carcinoma: the effect of elective lymph node dissection. *Breast Cancer Res Treat* 1989; 14: 315-320.

16 Friedl P, Wolf K. Tumour-cell invasion and migration: diversity and escape mechanisms. *Nat Rev Cancer* 2003; 3: 362-374.

17 Odenthal J, Takes R, Friedl P. Plasticity of tumor cell invasion: governance by growth factors and cytokines. *Carcinogenesis* 2016; 37: 1117-1128.

18 Kalluri R, Weinberg RA. The basics of epithelial-mesenchymal transition. *J Clin Invest* 2009; 119: 1420-1428.

19 Yilmaz M, Christofori G. EMT, the cytoskeleton, and cancer cell invasion. *Cancer Metastasis Rev* 2009; 28: 15-33.

20 Friedl P, Wolf K. Tube travel: the role of proteases in individual and collective cancer cell invasion. *Cancer Res* 2008; 68: 7247-7249.

21 Wolf K, Wu YI, Liu Y, Geiger J, Tam E, Overall C *et al.* Multi-step pericellular proteolysis controls the transition from individual to collective cancer cell invasion. *Nat Cell Biol* 2007; 9: 893-904.

22 Reichert M, Bakir B, Moreira L, Pitarresi JR, Feldmann K, Simon L *et al.* Regulation of Epithelial Plasticity Determines Metastatic Organotropism in Pancreatic Cancer. *Dev*

Cell 2018; 45: 696-711.e698.

23 Del Pozo Martin Y, Park D, Ramachandran A, Ombrato L, Calvo F, Chakravarty P *et al.* Mesenchymal Cancer Cell-Stroma Crosstalk Promotes Niche Activation, Epithelial Reversion, and Metastatic Colonization. *Cell Rep* 2015; 13: 2456-2469.

24 Brabletz T, Kalluri R, Nieto MA, Weinberg RA. EMT in cancer. *Nat Rev Cancer*, vol. 18: England, 2018, pp 128-134.

25 Cheung KJ, Gabrielson E, Werb Z, Ewald AJ. Collective invasion in breast cancer requires a conserved basal epithelial program. *Cell* 2013; 155: 1639-1651.

26 Cheung KJ, Padmanaban V, Silvestri V, Schipper K, Cohen JD, Fairchild AN *et al.* Polyclonal breast cancer metastases arise from collective dissemination of keratin 14-expressing tumor cell clusters. *Proc Natl Acad Sci U S A* 2016; 113: E854-863.

27 Gaggioli C, Hooper S, Hidalgo-Carcedo C, Grosse R, Marshall JF, Harrington K *et al.* Fibroblast-led collective invasion of carcinoma cells with differing roles for RhoGTPases in leading and following cells. *Nat Cell Biol* 2007; 9: 1392-1400.

28 Wang X, Enomoto A, Asai N, Kato T, Takahashi M. Collective invasion of cancer: Perspectives from pathology and development. *Pathol Int* 2016; 66: 183-192.

29 Alexander S, Koehl GE, Hirschberg M, Geissler EK, Friedl P. Dynamic imaging of cancer growth and invasion: a modified skin-fold chamber model. *Histochem Cell Biol* 2008; 130: 1147-1154.

30 Padmanaban V, Krol I, Suhail Y, Szczerba BM, Aceto N, Bader JS *et al.* E-cadherin is required for metastasis in multiple models of breast cancer. *Nature* 2019; 573: 439-444.

31 Cheung KJ, Ewald AJ. A collective route to metastasis: Seeding by tumor cell clusters. *Science* 2016; 352: 167-169.

32 Aceto N, Bardia A, Miyamoto DT, Donaldson MC, Wittner BS, Spencer JA *et al.* Circulating tumor cell clusters are oligoclonal precursors of breast cancer metastasis. *Cell* 2014; 158: 1110-1122.

33 Khalil AA, Ilina O, Gritsenko PG, Bult P, Span PN, Friedl P. Collective invasion in ductal and lobular breast cancer associates with distant metastasis. *Clin Exp Metastasis* 2017; 34: 421-429.

34 Mu Z, Wang C, Ye Z, Austin L, Civan J, Hyslop T *et al*. Prospective assessment of the prognostic value of circulating tumor cells and their clusters in patients with advanced-stage breast cancer. *Breast Cancer Res Treat* 2015; 154: 563-571.

35 Ivashkiv LB, Donlin LT. Regulation of type I interferon responses. *Nat Rev Immunol* 2014; 14: 36-49.

36 Melnick JL, Dreesman GR, Adam E, Kaufman R. The role of herpes simplex virus in cervical and vulvar cancer. *Dev Biol Stand* 1982; 52: 87-94.

37 Hietanen S, Grénman S, Syrjänen K, Lappalainen K, Kauppinen J, Carey T *et al*. Human papillomavirus in vulvar and vaginal carcinoma cell lines. *Br J Cancer* 1995; 72: 134-139.

38 Tinevez JY, Perry N, Schindelin J, Hoopes GM, Reynolds GD, Laplantine E *et al*. TrackMate: An open and extensible platform for single-particle tracking. *Methods* 2017; 115: 80-90.

39 Nio J, Takahashi-Iwanaga H, Morimatsu M, Kon Y, Iwanaga T. Immunohistochemical and in situ hybridization analysis of galectin-3, a beta-galactoside binding lectin, in the urinary system of adult mice. *Histochem Cell Biol* 2006; 126: 45-56.

40 Hynes RO. Integrins: bidirectional, allosteric signaling machines. *Cell* 2002; 110: 673-687.

41 Plow EF, Haas TA, Zhang L, Loftus J, Smith JW. Ligand binding to integrins. *J Biol Chem* 2000; 275: 21785-21788.

42 Tadokoro S, Shattil SJ, Eto K, Tai V, Liddington RC, de Pereda JM *et al*. Talin binding to integrin beta tails: a final common step in integrin activation. *Science* 2003; 302: 103-106.

43 Ezzell RM, Goldmann WH, Wang N, Parashurama N, Ingber DE. Vinculin promotes cell spreading by mechanically coupling integrins to the cytoskeleton. *Exp Cell Res* 1997; 231:

14-26.

44 Holly SP, Larson MK, Parise LV. Multiple roles of integrins in cell motility. *Exp Cell Res* 2000; 261: 69-74.

45 Palecek SP, Loftus JC, Ginsberg MH, Lauffenburger DA, Horwitz AF. Integrin-ligand binding properties govern cell migration speed through cell-substratum adhesiveness. *Nature* 1997; 385: 537-540.

46 Howe A, Aplin AE, Alahari SK, Juliano RL. Integrin signaling and cell growth control. *Curr Opin Cell Biol* 1998; 10: 220-231.

47 Giancotti FG, Ruoslahti E. Integrin signaling. *Science* 1999; 285: 1028-1032.

48 Mitra SK, Schlaepfer DD. Integrin-regulated FAK-Src signaling in normal and cancer cells. *Curr Opin Cell Biol* 2006; 18: 516-523.

49 Hegerfeldt Y, Tusch M, Brocker EB, Friedl P. Collective cell movement in primary melanoma explants: plasticity of cell-cell interaction, beta1-integrin function, and migration strategies. *Cancer Res* 2002; 62: 2125-2130.

50 Kato T, Enomoto A, Watanabe T, Haga H, Ishida S, Kondo Y *et al.* TRIM27/MRTF-B-dependent integrin beta1 expression defines leading cells in cancer cell collectives. *Cell Rep* 2014; 7: 1156-1167.

51 Durbeej M. Laminins. *Cell Tissue Res* 2010; 339: 259-268.

52 Lu P, Weaver VM, Werb Z. The extracellular matrix: a dynamic niche in cancer progression. *J Cell Biol* 2012; 196: 395-406.

53 Kannus P. Structure of the tendon connective tissue. *Scand J Med Sci Sports* 2000; 10: 312-320.

54 Shoulders MD, Raines RT. Collagen structure and stability. *Annu Rev Biochem* 2009; 78: 929-958.

55 Loffek S, Hurskainen T, Jackow J, Sigloch FC, Schilling O, Tasanen K *et al*. Transmembrane collagen XVII modulates integrin dependent keratinocyte migration via PI3K/Rac1 signaling. *PLoS One* 2014; 9: e87263.

56 Borradori L, Sonnenberg A. Structure and function of hemidesmosomes: more than simple adhesion complexes. *J Invest Dermatol* 1999; 112: 411-418.

57 Watanabe M, Natsuga K, Nishie W, Kobayashi Y, Donati G, Suzuki S *et al*. Type XVII collagen coordinates proliferation in the interfollicular epidermis. *Elife* 2017; 6.

58 Nishimura M, Nishie W, Shirafuji Y, Shinkuma S, Natsuga K, Nakamura H *et al*. Extracellular cleavage of collagen XVII is essential for correct cutaneous basement membrane formation. *Hum Mol Genet* 2016; 25: 328-339.

59 Nishie W, Jackow J, Hofmann SC, Franzke CW, Bruckner-Tuderman L. Coiled coils ensure the physiological ectodomain shedding of collagen XVII. *J Biol Chem* 2012; 287: 29940-29948.

60 Nishie W, Natsuga K, Iwata H, Izumi K, Ujiie H, Toyonaga E *et al*. Context-Dependent Regulation of Collagen XVII Ectodomain Shedding in Skin. *Am J Pathol* 2015; 185: 1361-1371.

61 Qiao H, Shibaki A, Long HA, Wang G, Li Q, Nishie W *et al*. Collagen XVII participates in keratinocyte adhesion to collagen IV, and in p38MAPK-dependent migration and cell signaling. *J Invest Dermatol* 2009; 129: 2288-2295.

62 Moilanen JM, Loffek S, Kokkonen N, Salo S, Vayrynen JP, Hurskainen T *et al*. Significant Role of Collagen XVII And Integrin beta4 in Migration and Invasion of The Less Aggressive Squamous Cell Carcinoma Cells. *Sci Rep* 2017; 7: 45057.

63 Yodsurang V, Tanikawa C, Miyamoto T, Lo PHY, Hirata M, Matsuda K. Identification of a novel p53 target, COL17A1, that inhibits breast cancer cell migration and invasion. *Oncotarget* 2017; 8: 55790-55803.

64 Miyazaki K. Laminin-5 (laminin-332): Unique biological activity and role in tumor growth and invasion. *Cancer Sci* 2006; 97: 91-98.

65 Kim BG, An HJ, Kang S, Choi YP, Gao MQ, Park H *et al*. Laminin-332-rich tumor microenvironment for tumor invasion in the interface zone of breast cancer. *Am J Pathol* 2011; 178: 373-381.

66 Marinkovich MP. Tumour microenvironment: laminin 332 in squamous-cell carcinoma. *Nat Rev Cancer* 2007; 7: 370-380.

67 Zahir N, Lakins JN, Russell A, Ming W, Chatterjee C, Rozenberg GI *et al*. Autocrine laminin-5 ligates alpha6beta4 integrin and activates RAC and NFkappaB to mediate anchorage-independent survival of mammary tumors. *J Cell Biol* 2003; 163: 1397-1407.

68 Umeda T, Inouye K. Possible role of contact following in the generation of coherent motion of Dictyostelium cells. *J Theor Biol* 2002; 219: 301-308.

69 Haga H, Irahara C, Kobayashi R, Nakagaki T, Kawabata K. Collective movement of epithelial cells on a collagen gel substrate. *Biophys J* 2005; 88: 2250-2256.

70 Yamaguchi N, Mizutani T, Kawabata K, Haga H. Leader cells regulate collective cell migration via Rac activation in the downstream signaling of integrin beta1 and PI3K. *Sci Rep* 2015; 5: 7656.

71 Nystrom ML, Thomas GJ, Stone M, Mackenzie IC, Hart IR, Marshall JF. Development of a quantitative method to analyse tumour cell invasion in organotypic culture. *J Pathol* 2005; 205: 468-475.

72 Nykvist P, Tasanen K, Viitasalo T, Kapyla J, Jokinen J, Bruckner-Tuderman L *et al*. The cell adhesion domain of type XVII collagen promotes integrin-mediated cell spreading by a novel mechanism. *J Biol Chem* 2001; 276: 38673-38679.

73 Menyhart O, Nagy A, Gyorffy B. Determining consistent prognostic biomarkers of overall survival and vascular invasion in hepatocellular carcinoma. *R Soc Open Sci* 2018; 5: 181006.

74 Whittard JD, Akiyama SK. Activation of beta1 integrins induces cell-cell adhesion. *Exp Cell Res* 2001; 263: 65-76.

75 Serres E, Debarbieux F, Stanchi F, Maggiorella L, Grall D, Turchi L *et al*. Fibronectin expression in glioblastomas promotes cell cohesion, collective invasion of basement membrane in vitro and orthotopic tumor growth in mice. *Oncogene* 2014; 33: 3451-3462.

76 Nishie W, Kiritsi D, Nystrom A, Hofmann SC, Bruckner-Tuderman L. Dynamic interactions of epidermal collagen XVII with the extracellular matrix: laminin 332 as a major binding partner. *Am J Pathol* 2011; 179: 829-837.

77 Pestka S, Langer JA, Zoon KC, Samuel CE. Interferons and their actions. *Annu Rev Biochem* 1987; 56: 727-777.

78 Pestka S, Krause CD, Walter MR. Interferons, interferon-like cytokines, and their receptors. *Immunol Rev* 2004; 202: 8-32.

79 Li C, Chi S, He N, Zhang X, Guicherit O, Wagner R *et al*. IFNalpha induces Fas expression and apoptosis in hedgehog pathway activated BCC cells through inhibiting Ras-Erk signaling. *Oncogene* 2004; 23: 1608-1617.

80 Li G, Xiang Y, Sabapathy K, Silverman RH. An apoptotic signaling pathway in the interferon antiviral response mediated by RNase L and c-Jun NH2-terminal kinase. *J Biol Chem* 2004; 279: 1123-1131.

81 Pestka S. The human interferon-alpha species and hybrid proteins. *Semin Oncol* 1997; 24: S9-4-s9-17.

82 Pestka S, Kotenko SV, Muthukumaran G, Izotova LS, Cook JR, Garotta G. The interferon gamma (IFN-gamma) receptor: a paradigm for the multichain cytokine receptor. *Cytokine Growth Factor Rev* 1997; 8: 189-206.

83 Bernabei P, Coccia EM, Rigamonti L, Bosticardo M, Forni G, Pestka S *et al*. Interferon-gamma receptor 2 expression as the deciding factor in human T, B, and myeloid cell proliferation or death. *J Leukoc Biol* 2001; 70: 950-960.

84 Hattori M, Minato N. Rap1 GTPase: functions, regulation, and malignancy. *J Biochem* 2003; 134: 479-484.

85 Stark GR, Darnell JE, Jr. The JAK-STAT pathway at twenty. *Immunity* 2012; 36: 503-514.

86 Meissl K, Macho-Maschler S, Müller M, Strobl B. The good and the bad faces of STAT1 in solid tumours. *Cytokine* 2017; 89: 12-20.

87 Wong GS, Lee JS, Park YY, Klein-Szanto AJ, Waldron TJ, Cukierman E *et al*. Periostin cooperates with mutant p53 to mediate invasion through the induction of STAT1 signaling in the esophageal tumor microenvironment. *Oncogenesis* 2013; 2: e59.

88 Malilas W, Koh SS, Kim S, Srisuttee R, Cho IR, Moon J *et al*. Cancer upregulated gene 2, a novel oncogene, enhances migration and drug resistance of colon cancer cells via STAT1 activation. *Int J Oncol* 2013; 43: 1111-1116.

89 Khodarev NN, Beckett M, Labay E, Darga T, Roizman B, Weichselbaum RR. STAT1 is overexpressed in tumors selected for radioresistance and confers protection from radiation in transduced sensitive cells. *Proc Natl Acad Sci U S A* 2004; 101: 1714-1719.

90 Maddipati R, Stanger BZ. Pancreatic Cancer Metastases Harbor Evidence of Polyclonality. *Cancer Discov* 2015; 5: 1086-1097.

91 Hunter KW, Amin R, Deasy S, Ha NH, Wakefield L. Genetic insights into the morass of metastatic heterogeneity. *Nat Rev Cancer* 2018; 18: 211-223.

92 Kok SY, Oshima H, Takahashi K, Nakayama M, Murakami K, Ueda HR *et al*. Malignant subclone drives metastasis of genetically and phenotypically heterogenous cell clusters through fibrotic niche generation. *Nat Commun* 2021; 12: 863.

93 McGranahan N, Swanton C. Biological and therapeutic impact of intratumor heterogeneity in cancer evolution. *Cancer Cell* 2015; 27: 15-26.

94 Bozic I, Reiter JG, Allen B, Antal T, Chatterjee K, Shah P *et al*. Evolutionary dynamics of cancer in response to targeted combination therapy. *Elife* 2013; 2: e00747.

95 Au-Yeung N, Mandhana R, Horvath CM. Transcriptional regulation by STAT1 and STAT2 in the interferon JAK-STAT pathway. *Jakstat* 2013; 2: e23931.

96 Wrenn ED, Yamamoto A, Moore BM, Huang Y, McBirney M, Thomas AJ *et al.* Regulation of Collective Metastasis by Nanolumenal Signaling. *Cell* 2020; 183: 395-410.e319.

97 Coulombe PA, Fuchs E. Elucidating the early stages of keratin filament assembly. *J Cell Biol* 1990; 111: 153-169.

98 Kouklis PD, Hutton E, Fuchs E. Making a connection: direct binding between keratin intermediate filaments and desmosomal proteins. *J Cell Biol* 1994; 127: 1049-1060.

99 Konen J, Summerbell E, Dwivedi B, Galior K, Hou Y, Rusnak L *et al.* Image-guided genomics of phenotypically heterogeneous populations reveals vascular signalling during symbiotic collective cancer invasion. *Nat Commun* 2017; 8: 15078.

100 Schultz J, Koczan D, Schmitz U, Ibrahim SM, Pilch D, Landsberg J *et al.* Tumor-promoting role of signal transducer and activator of transcription (Stat)1 in late-stage melanoma growth. *Clin Exp Metastasis* 2010; 27: 133-140.

101 Xie B, Zhao J, Kitagawa M, Durbin J, Madri JA, Guan JL *et al.* Focal adhesion kinase activates Stat1 in integrin-mediated cell migration and adhesion. *J Biol Chem* 2001; 276: 19512-19523.

102 Kumagai Y, Nio-Kobayashi J, Ishida-Ishihara S, Tachibana H, Omori R, Enomoto A *et al.* The intercellular expression of type-XVII collagen, laminin-332, and integrin-β1 promote contact following during the collective invasion of a cancer cell population. *Biochem Biophys Res Commun* 2019; 514: 1115-1121.

103 Fawcett DW. Intercellular bridges. *Exp Cell Res* 1961; Suppl 8: 174-187.

104 Nguyen M, Mikita G, Hoda RS. "Intercellular bridges" in a case of well differentiated squamous carcinoma. *Diagn Cytopathol* 2016; 44: 121-123.

105 Ewald AJ, Huebner RJ, Palsdottir H, Lee JK, Perez MJ, Jorgens DM *et al.* Mammary collective cell migration involves transient loss of epithelial features and individual cell migration within the epithelium. *J Cell Sci* 2012; 125: 2638-2654.

106 Summerbell ER, Mouw JK, Bell JSK, Knippler CM, Pedro B, Arnst JL *et al*. Epigenetically heterogeneous tumor cells direct collective invasion through filopodia-driven fibronectin micropatterning. *Sci Adv* 2020; 6: eaaz6197.

107 Vilchez Mercedes SA, Bocci F, Levine H, Onuchic JN, Jolly MK, Wong PK. Decoding leader cells in collective cancer invasion. *Nat Rev Cancer* 2021.

108 Kumagai Y, Nio-Kobayashi J, Ishihara S, Enomoto A, Akiyama M, Ichihara R *et al*. The interferon-β/STAT1 axis drives the collective invasion of skin squamous cell carcinoma with sealed intercellular spaces. *Oncogenesis* 2022; 11: 27.

109 Ahn S, Woo JW, Lee K, Park SY. HER2 status in breast cancer: changes in guidelines and complicating factors for interpretation. *J Pathol Transl Med* 2020; 54: 34-44.

110 Wang Y, Klijn JG, Zhang Y, Sieuwerts AM, Look MP, Yang F *et al*. Gene-expression profiles to predict distant metastasis of lymph-node-negative primary breast cancer. *Lancet* 2005; 365: 671-679.

111 Shingaki S, Takada M, Sasai K, Bibi R, Kobayashi T, Nomura T *et al*. Impact of lymph node metastasis on the pattern of failure and survival in oral carcinomas. *Am J Surg* 2003; 185: 278-284.

112 Jerjes W, Upile T, Petrie A, Riskalla A, Hamdoon Z, Vourvachis M *et al*. Clinicopathological parameters, recurrence, locoregional and distant metastasis in 115 T1-T2 oral squamous cell carcinoma patients. *Head Neck Oncol* 2010; 2: 9.

113 Houghton AM. Mechanistic links between COPD and lung cancer. *Nat Rev Cancer* 2013; 13: 233-245.

114 Lund-Johansen M, Rucklidge GJ, Milne G, Bjerkvig R. A metalloproteinase, capable of destroying cultured brain tissue isolated from rat glioma cells. *Anticancer Res* 1991; 11: 1001-1006.

115 Mohanam S, Wang SW, Rayford A, Yamamoto M, Sawaya R, Nakajima M *et al*. Expression of tissue inhibitors of metalloproteinases: negative regulators of human glioblastoma invasion in vivo. *Clin Exp Metastasis* 1995; 13: 57-62.

116 Xue H, Li J, Xie H, Wang Y. Review of Drug Repositioning Approaches and Resources. *Int J Biol Sci* 2018; 14: 1232-1244.

Acknowledgment

First, I would like to thank Prof. Hisashi Haga for accepting me to Laboratory of Cell Dynamics. Your critical guidance on my research have led to success. I also appreciate for giving me a fruitful research environment. I was able to grow both as a researcher and as a person.

I appreciate Dr. Seiichiro Ishihara for kind and helpful support. I learned how to write a research grant application and how to present research from you. You have been a beacon to me as a researcher.

I would like to express my gratitude to Prof. Tomoyasu Aizawa and Prof. Kiminori Nakamura. All discussion with you helped me to improve my presentation in doctoral defense and this dissertation.

Special thanks go to Dr. Junko Nio-Kobayashi for our collaborative work. The histological experimental techniques and writing skills of paper I learned from you will certainly support my life as a researcher in the future. You have always been respectful of my opinion. Your dedication and cooperation are sincerely appreciated.

I would also like to Prof. Atsushi Enomoto, Dr. Ryosuke Ichihara, and Prof. Masashi Akiyama for discussion and analysis on clinical significance of my research. Patient tissue analysis generated great value for my research.

Huge thanks go to Prof. Hiroharu Kawahara, Prof. Yuichi Inoue, Dr. Akira Iwamoto, and Dr Masaharu Somiya for continuous support for me since I have graduated National Institute of Technology, Kitakyushu College. I aspired to be a researcher because I admired you all.

Thanks to the past/current members of Laboratory of Cell Dynamics. The time I spent with you all is a precious treasure for me. Thanks for the happy memories.

Finally, I would like to express my sincere gratitude to my family for the continuous support. They helped me a lot financially and mentally and always respected and encouraged me. I want to contribute to your future happier life from now on.